NATURAL RESOURCES

GEOLOGIC MAP OF THE MALTBY 7.5-MINUTE QUADRANGLE, SNOHOMISH AND KING COUNTIES, WASHINGTON

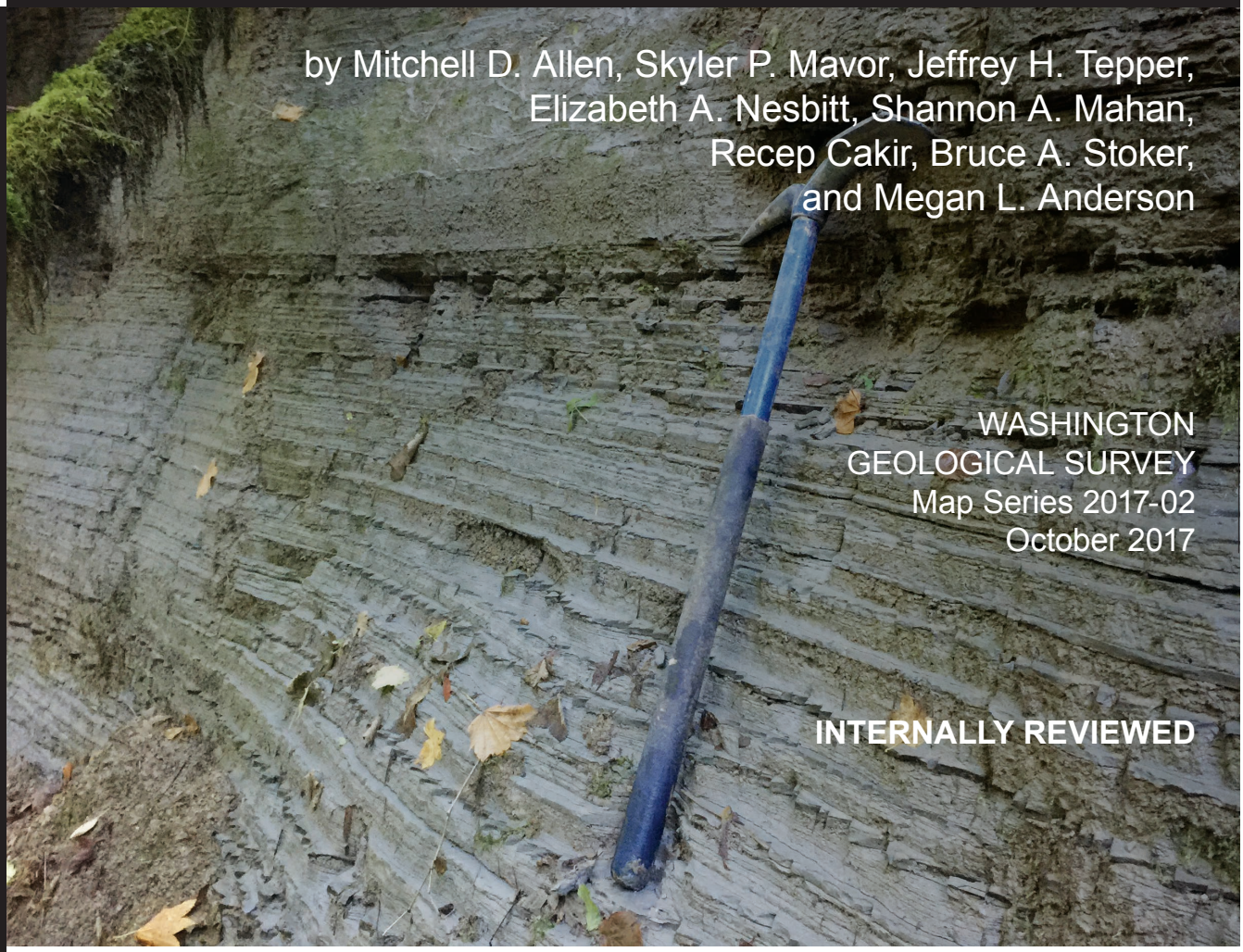

by Mitchell D. Allen, Skyler P. Mavor, Jeffrey H. Tepper, Elizabeth A. Nesbitt, Shannon A. Mahan, Recep Cakir, Bruce A. Stoker, and Megan L. Anderson

WASHINGTON
GEOLOGICAL SURVEY
Map Series 2017-02
October 2017

INTERNALLY REVIEWED

WASHINGTON STATE DEPARTMENT OF
NATURAL RESOURCES
WASHINGTON GEOLOGICAL SURVEY

GEOLOGIC MAP OF THE MALTBY 7.5-MINUTE QUADRANGLE, SNOHOMISH AND KING COUNTIES, WASHINGTON

by Mitchell D. Allen, Skyler P. Mavor, Jeffrey H. Tepper, Elizabeth A. Nesbitt, Shannon A. Mahan, Recep Cakir, Bruce A. Stoker, and Megan L. Anderson

WASHINGTON
GEOLOGICAL SURVEY
Map Series 2017-02
October 2017

This geologic map was funded in part by the USGS National Cooperative Geologic Mapping Program, award no. G16AC00286

This publication has been subject to an iterative technical review process by at least one Survey geologist who is not an author. This publication has also been subject to an iterative review process with Survey editors and cartographers and has been formatted by Survey staff.

WASHINGTON STATE DEPARTMENT OF
NATURAL RESOURCES
WASHINGTON GEOLOGICAL SURVEY

DISCLAIMER

Neither the State of Washington, nor any agency thereof, nor any of their employees, makes any warranty, express or implied, or assumes any legal liability or responsibility for the accuracy, completeness, or usefulness of any information, apparatus, product, or process disclosed, or represents that its use would not infringe privately owned rights. Reference herein to any specific commercial product, process, or service by trade name, trademark, manufacturer, or otherwise, does not necessarily constitute or imply its endorsement, recommendation, or favoring by the State of Washington or any agency thereof. The views and opinions of authors expressed herein do not necessarily state or reflect those of the State of Washington or any agency thereof.

INDEMNIFICATION

Research supported by the U.S. Geological Survey, National Cooperative Geologic Mapping Program, under USGS award number G16AC00286. The views and conclusions contained in this document are those of the authors and should not be interpreted as necessarily representing the official policies, either expressed or implied, of the U.S. Government.

WASHINGTON STATE DEPARTMENT OF NATURAL RESOURCES

Hilary S. Franz—*Commissioner of Public Lands*

WASHINGTON GEOLOGICAL SURVEY

David K. Norman—*State Geologist*
Timothy J. Walsh—*Assistant State Geologist*
John P. Bromley—*Assistant State Geologist*

Washington State Department of Natural Resources
Washington Geological Survey

Mailing Address:
MS 47007
Olympia, WA 98504-7007

Street Address:
Natural Resources Bldg, Rm 148
1111 Washington St SE
Olympia, WA 98501

Phone: 360-902-1450
Fax: 360-902-1785
Email: geology@dnr.wa.gov
Website: http://www.dnr.wa.gov/geology

Publications and Maps:
www.dnr.wa.gov/programs-and-services/geology/publications-and-data/publications-and-maps

Washington Geology Library Searchable Catalog:
www.dnr.wa.gov/programs-and-services/geology/washington-geology-library

Suggested Citation: Allen, M. D.; Mavor, S. P.; Tepper, J. H.; Nesbitt, E. A.; Mahan, S. A.; Cakir, Recep; Stoker, B. A.; Anderson, M. L., 2017, Geologic map of the Maltby 7.5-minute quadrangle, Snohomish and King Counties, Washington: Washington Geological Survey Map Series 2017-02, 1 sheet, scale 1:24,000, 43 p. text. [http://www.dnr.wa.gov/publications/ger_ms2017-02_geol_map_maltby_24k.zip]

Contents

FIGURES

TABLES

MAP SHEET

Geologic Map of the Maltby 7.5-minute Quadrangle, Snohomish and King Counties, Washington

by Mitchell D. Allen[1], Skyler P. Mavor[1,2], Jeffrey H. Tepper[3], Elizabeth A. Nesbitt[4], Shannon A. Mahan[5], Recep Cakir[1], Bruce A. Stoker[6], and Megan L. Anderson[7]

[1] Washington Geological Survey
1111 Washington St. SE
MS 47007
Olympia, WA 98504-7007

[2] Colorado State University
Department of Geosciences
1482 Campus Delivery
Fort Collins, CO 80523-1482

[3] University of Puget Sound
Geology Department
1500 N. Warner St.
Tacoma, WA 98416-1048

[4] Burke Museum of Natural History and Culture
University of Washington
Box 353010
Seattle, WA 98195-3010

[5] U.S. Geological Survey
Denver Federal Center
Box 25046, MS 974
Denver, CO 80225-5046

[6] Earth Systems
19729 207th Ave SE
Monroe, WA 98272

[7] Colorado College
Department of Geology
14 E. Cache La Poudre St.
Colorado Springs,
CO 80903

INTRODUCTION

The Maltby 7.5-minute quadrangle is located in Snohomish and King Counties, Washington, northeast of Seattle between the towns of Monroe, Snohomish, Duvall, and Woodinville (Fig. M1 on map sheet). New geologic mapping conducted during the 2016 field season is part of a multi-year effort to map bedrock, surficial, and structural geology at 1:24,000 scale across the eastern foothills of the Puget Lowland. Over the last decade, mapping has extended coverage in a continuous swath from North Bend to Granite Falls. The Maltby quadrangle is the westernmost extent of this effort and ties into existing and ongoing geologic mapping efforts by the USGS and the University of Washington.

The Maltby quadrangle features low, fluted hills (typically 400–600 ft elev.) that are truncated by a northwest-trending, low-elevation (<50 ft) river valley and incised by minor tributaries. The Skykomish and Snoqualmie Rivers converge in the quadrangle, forming the Snohomish River, which flows northwest and meets Puget Sound near the city of Everett. An ovoid topographic high called Lord Hill bounds these rivers to the north. In the northeast corner of the map area is a broad agricultural valley that we refer to as the 'Fryelands trough' (map sheet).

New technologies have been developed or improved since the most recent geologic mapping of the Maltby quadrangle (Minard, 1985a) that allow for more detailed and accurate mapping. Modern geochronologic techniques better constrain the ages of Quaternary and bedrock units, and lidar topographic imagery can be used for land-surface analysis, an invaluable tool for delineating glacial morphology and potentially active fault traces in the forested and developed landscape of the Puget Lowland.

We intend this map to assist in geologic hazard, geotechnical engineering, groundwater hydrology, earth resource management, academic research, and development planning investigations. Geologic hazards in the area include shallow- and deep-seated landslides, as well as earthquakes (both regional, subduction-zone scale and relatively local crustal-scale earthquakes). We propose several active regional structures in or near the Maltby quadrangle that are potential hazards to the region. This study seeks to characterize any features related to such hazards and to contribute to an improved geologic understanding of the Maltby quadrangle.

Geologic Setting

The Maltby quadrangle lies on the eastern side of the central Puget Lowland, where glacial deposits overlie Tertiary igneous and sedimentary bedrock. To the east of the quadrangle, rocks of the Cascade volcanic arc intrude through a Mesozoic accretionary belt. To the west, the Puget Lowland is bounded and underlain by Siletzia, an Eocene igneous province accreted onto North America about 50 Ma (Wells and others, 2014). Bedrock exposures in the quadrangle help define the structural uplifts between the Seattle and Everett basins (Fig. M1; Pratt and others, 1997), which are deep troughs filled with thick Tertiary sedimentary rocks overlain by glacial and nonglacial Quaternary sediment.

BEDROCK

Eocene volcanic bedrock in the northeastern part of the quadrangle is considered correlative with similar volcanic rocks exposed farther east (Danner, 1957; Rau and Johnson, 1999). Across the Snohomish River, fossiliferous Eocene to Oligocene terrestrial and marine sedimentary rocks are exposed along the western banks of the Snohomish and Snoqualmie Rivers. In the central

and southwestern parts of the quadrangle, bedrock is concealed by Quaternary cover. Geophysical data and subsurface boreholes that penetrate to sedimentary bedrock indicate that overlying unconsolidated deposits thicken to the southwest (Yount and others, 1985; Yount and Gower, 1991; Sherrod and others, 2008; Anderson and others, 2015)

SURFICIAL DEPOSITS

Continental ice-sheets have periodically occupied the Puget Lowland throughout the Quaternary. These repeated glaciations deposited a stratigraphically complex sequence of glacial and nonglacial deposits with unconformities separating as many as seven recognized glacial episodes (Troost, 2016). Cyclic episodes of glacial and nonglacial conditions have been correlated with marine oxygen-isotope stages (MIS[1])(Morrison, 1991; Troost, 2016). The most recent glaciation of the Puget Lowland occurred during MIS 2 and is termed the Vashon stade of the Fraser glaciation. The onset of MIS 2 in northern Washington was marked by a period of alpine glacial advance termed the Evans Creek stade, which preceded the arrival of the Vashon ice in the Puget Lowland (Armstrong and others, 1965). A period of nonglacial deposition during MIS 3 is regionally named the "Olympia nonglacial interval" (Hansen and Easterbrook, 1974, p. 587; Troost, 1999). In the quadrangle, nonglacial and glacial deposits predating the Vashon ice advance have been recognized by stratigraphic position (Newcomb, 1952; Capps and others, 1973; Minard, 1985a), but have not previously been tied to other regional pre-Vashon deposits with finite geochronology.

TECTONIC FRAMEWORK

Northeast-directed oblique convergence within the Cascadia subduction zone has resulted in a structurally complex forearc with discrete fault-bounded crustal blocks (Wells and others, 1998; Miller and others, 2001; McCaffrey and others, 2007, 2013). This convergence resulted in north-northeast-directed compression in the central Puget Lowland, which is partitioned by multiple active structures in the region. Some of these active structures project into or toward the Maltby quadrangle (Fig. M1), including the Monroe fault and strands of both the Southern Whidbey Island fault (SWIF) and the Rattlesnake Mountain fault zone (RMFZ). Attempts to trace and record paleoseismicity along these structures are complicated by extensive Quaternary glacial cover, vegetation, and urban development. Glaciotectonic deformation further confounds interpretations of deformed Quaternary exposures—most interpretations of these structures were made based on geophysical data.

Regional studies of the SWIF identified strands of this fault zone in the Maltby quadrangle and generalized a broad (~20 km [12.4 mi] in the Woodinville area) northwest-trending zone of complex, high-angle, oblique dextral strike-slip faults (Gower and others, 1985; Yount and Gower, 1991; Johnson and others, 1996, Pratt and others, 1997; Brocher and others, 2005; Sherrod and others, 2008). Strands of the SWIF were inferred to connect with faults of the RMFZ that were mapped south and east of the quadrangle (Liberty and Pape, 2006; Sherrod and others, 2008; Dragovich and others, 2010a, 2011a; Anderson and others, 2015). The SWIF and connecting structures may form a major, regionally extensive, seismogenic feature potentially as much as 385 km (239 mi) in length that crosses the Cascade Range (Blakely and others, 2011; WAEMD and others, 2012).

Many workers have documented evidence for Quaternary activity on the SWIF (Gower, 1978; Gower and others, 1985; Johnson and others, 1996; Kelsey and others, 2004), including investigations utilizing eight paleoseismic trenches (Sherrod and others, 2005a,b, 2008) near the map area. We plotted the locations of four of the trenches within the Maltby quadrangle as reported by Sherrod and others (2008). Two of these trenches (significant sites DNRFT1 and DNRFT2 on map sheet) recorded no observable tectonic activity, and the other two trenches (significant sites MBFT and FSFT on map sheet) showed evidence for Quaternary tectonic deformation. Hazard analysis modeling of a magnitude 7.4 earthquake on the SWIF using the HAZUS method places the potential for economic loss in the tens of billions of dollars, with thousands of injuries and hundreds of fatalities (WAEMD and others, 2012).

A concealed, high-angle reverse fault, named the Monroe fault, was mapped in the Monroe quadrangle to the east by Dragovich and others (2011a). This fault is accompanied by the partially concealed Monroe anticline in the hanging wall and Monroe syncline in the footwall and is considered potentially active on the basis of observations of folded Quaternary strata, although there are no known locations where the Monroe fault offsets Quaternary strata (Dragovich and others, 2011a, 2013, 2014b). Interpretations of isostatic gravity data by Dragovich and others (2015) project the Monroe fault and associated structures toward the Maltby quadrangle, where they hypothesized its junction with the SWIF.

METHODS

Geologic Mapping

We compiled surficial and bedrock geologic mapping by McKnight and Ward (1925), Newcomb (1952), Liesch and others (1963), Capps and others (1973), Minard (1985a), Yount and Gower (1991), and Booth and others (2007). We compared our surficial geologic mapping with aeromagnetic imagery and isostatic gravity contours (Fig. M2) derived from newly collected data to identify concealed geologic structures. These aeromagnetic data (including detailed methodology) have been previously published by Blakely and others (2004) and were provided electronically for this study by Richard Blakely (USGS, personal commun., 2016). Computer-generated max-spots[2] delineate the strongest magnetic and gravitational gradients and were used to decipher subsurface conditions. Geologic mapping was conducted from July to October of 2016.

[1] MIS: global *m*arine oxygen *i*sotope *s*tage curve, where even-numbered stages are used as proxy for timing and intensity of global glacial periods (Morrison, 1991). For discussion of corresponding Cordilleran ice sheet advances into the Puget Lowland, see Booth and others (2004), Troost and Booth (2008), Polenz and others (2013, 2015), and Troost (2016).

[2] Locations of anomalously large aeromagnetic field strength gradients, objectively identified by curvature analysis, which assumes that contacts are vertical and remanent magnetization is unimportant (Richard Blakely, written commun., 2013). See Blakely and others (2004) for a description of aeromagnetic max-spots methodology.

Lidar reconnaissance mapping of landslide features in the Maltby quadrangle was conducted by Washington Geological Survey (WGS) geologists using the SLIP protocol of Slaughter and others (2017, appendix B). Subsequent field investigation of lidar-identified features permitted detailed mapping of landslide deposits. We adopted some landslides mapped by King County along the Snoqualmie River corridor (King County, 2016) and modified that mapping with our direct field observations.

We reviewed 1,982 water wells and geotechnical borings (Jeschke and others, 2016; WGS internal records) in and within ~1 mi of the Maltby quadrangle, including several significant hydrogeologic investigations (Hart Crowser., 1993; Golder Associates, 1999, 2000, 2005, 2007). We could precisely locate 1,612 wells and borings and used them to inform our mapping. The locations of 68 wells and borings are shown on the map; these are wells we identified as best-located and most geologically informative inside the quadrangle. For these wells, we transcribed and interpreted driller's log information and assigned the likely geologic unit to depth. Geologic cross section A–A′ (map sheet) incorporates subsurface boring information in and near the map area, including regional geologic mapping and stratigraphic correlations from oil and gas exploration wells shown on Figure M1. Where no borehole constraints existed, we drew observations from site-specific bedrock depth estimates from Horizontal-to-Vertical Spectral Ratio analyses at seven sites (GP1–GP7, map sheet) within the quadrangle (see Data Supplement, DS1). Additionally, we referred to the seismic lines of Sherrod and others (2008) to infer Quaternary sediment thickness along cross section A–A′.

We used USGS Fact Sheet 2010-3059 for the geologic time scale (USGS Geologic Names Committee, 2010); where that scale lacked Epoch subdivisions, we referred to the International Chronostratigraphic Chart (v. 2015/01; Cohen and others, 2015) We followed the Udden-Wentworth scale (table 5 in Pettijohn, 1957) to classify unconsolidated sediment. We used the term 'northern source' to indicate polymict clast lithologies consistent with sediment transported by southward-flowing Pleistocene continental ice sheets.

Petrographic observations and modal percentage estimates were conducted in the WGS laboratory. Petrographic point counts and vitrinite reflectance estimates were conducted by Core Laboratories (Houston, Texas). Radiocarbon samples were analyzed by Beta Analytic, Inc. (Miami, Florida). Luminescence samples were prepared and analyzed at the USGS Luminescence Geochronology Lab in Denver, CO. U-Pb zircon analyses were conducted by S. Andrew DuFrane and staff (Univ. of Alberta). Erin Herring (Univ. of Oregon) provided insights into pre-Vashon climate conditions from pollen analyses of five sediment samples. Whole-rock major and trace element geochemical analyses were obtained from ALS Geochemistry (North Vancouver, B.C., Canada). Sedimentary paleontology samples were processed and analyzed at Burke Museum at the University of Washington. Analytical data for major-oxide and trace-element geochemistry, paleontological data, U-Pb zircon data, petrographic point counts, gravel clast counts, thin section descriptions, and earthquake focal mechanisms are presented in the Data Supplement (DS1–DS11).

DESCRIPTION OF MAP UNITS

Quaternary Unconsolidated Deposits

HOLOCENE NONGLACIAL DEPOSITS

af **Artificial fill**—Major road fill placed to elevate the land along road or railways; likely engineered; may include sand, cobbles, pebbles, boulders, silt, clay, organic matter, industrial or household waste, rip-rap, and concrete, in varied amounts; includes a Snohomish County landfill in the northwest portion of the quadrangle (sec. 36, T28N R5E) and a King County landfill near the southern map border (sec. 10, T26N R6W).

ml **Modified land**—Boulders, cobbles, pebbles, sand, silt, clay, diamicton, and organic matter, in varied amounts; locally derived but redistributed to modify topography; underlying units exposed in some areas; mapped where geographically extensive or thick enough (>2 m; >7 ft) to be geotechnically significant; excludes roads and pits where underlying units are readily identifiable, fill areas appear minor, or underlying units were more significant than surface modification.

LATEST PLEISTOCENE TO HOLOCENE NONGLACIAL DEPOSITS

Qp **Peat**—Organic and organic-rich sediment; includes peat, gyttja, muck, silt, and clay, with rare volcanic ash or pumicite; soft; dark brown or olive brown; typically wet and may include standing water. Many upland peat bogs formed in closed depressions in a relatively impermeable unit (for example, unit Qgt). Lowland peat bogs fill oxbow lakes and relict flood plains and thinly overlie unit Qa. Many of the peat areas in the Maltby quadrangle were described in detail by Rigg (1958), including cross sections of borehole transects. We adopted peat bodies mapped by that study with modifications from lidar, aerial photography, and field mapping. Rigg described thin pumicite layers, as much as 2.5 cm (1 in.) thick, in the Crystal Lake, Paradise Lake, Lake Leota, and lesser peat areas. Peat thickness is generally 2 to 8 m (7–26 ft), but may locally approach 15 m (50 ft) in the quadrangle (Rigg, 1958, p. 180). Some peat areas have been modified by agricultural or residential development. In these places, unit Qp was mapped where geotechnically significant peat deposits were historically recorded. We mapped a large body of unit Qp along the northeast boundary of the map area in the Fryelands trough, adapted from Rigg's (1958) detailed survey ("Frye Peat Area", p. 169). Collins and others (2003, fig. 13) indicated that this wetland may once have been even more extensive.

Qls **Landslide deposits**—Cobbles, pebbles, sand, silt, clay, boulders, and diamicton, in varied amounts, in slide bodies and toes; angular to rounded clasts and grains; unsorted; generally loose, jumbled, and unstratified, but locally retaining primary bedding and compaction. Characteristics of landslides include, but are not limited

to: headwall, lateral, or internal failure scarps; hummocky or lobate topography; leaning, fallen, or bent trees; enclosed depressions (sag ponds) with standing water or moisture-dependent vegetation; broken silts; rotated bedding planes; development of lateral drainages along deposit margins; and damage to roads or other infrastructure. In the map area, landslide slopes are often undercut by the modern or historical paths of major rivers; the landslide deposits were presumably removed by river erosion. Unit Qls contains only the deposits of landslide material; nondepositional landslide features are in other map units. The most landslide-prone area in the Maltby quadrangle (sec. 2, T26N R6E) is closely associated with the contact of dense silts and clays (units Qgaf and Qc_O) with overlying outwash (unit Qga) along an oversteepened slope undercut by the Snoqualmie River—we observed minor springs and seepage along this slope at and above the contact. Mass-wasting features not confidently distinguishable as landslides were mapped as unit Qmw. Absence of a mapped landslide or mass-wasting deposits does not imply an absence of hazard.

Qmw **Mass-wasting deposits**—Cobbles, pebbles, sand, silt, clay, boulders, and diamicton, in varied amounts; loose; often wet; generally unsorted, but locally stratified; shown along potentially or demonstrably unstable slopes; includes colluvium and landslides too small to map separately; locally includes compact and disturbed or undisturbed older deposits; often retains coloring of source material; generally saturated and hosting a concentration of moisture-dependent vegetation; commonly mantles slopes of steep creek valleys; especially extensive where stratigraphy consists of unconsolidated fine-grained deposits of units Qgaf and Qc_O; may host minor scarps associated with shallow slides. Unit Qmw was mapped where mass-wasting deposits were geotechnically significant (>2 m [7 ft] thick) or obscure underlying geology. Thickness varies across map area.

Qa **Alluvium**—Sand, pebbles, silt, clay, peat, cobbles, and organic material; dark brown to gray; loose; moderately to well sorted; stratified to massive; deposited in flood plains, stream channels, and on terraces; gravel subrounded to well rounded; clasts to large cobble size with rare boulders; clast supported and commonly imbricated; often concentrated in thin to medium planar beds and trough-shaped lenses; often micaceous; gravels predominantly equal parts plutonic, volcanic, and metamorphic rock (DS2), reflecting the geology in the greater Skykomish and Snoqualmie watersheds, as well as locally derived and imported glacial materials. Sands and silts show 6 in.-scale trough crossbeds, ripples, graded beds, and thin to laminated bedding. Fining-upward sequences are present and were interpreted as a repetition of channel, point bar, flood plain, and crevasse splay depositional environments typical of meandering-river sedimentary facies. We followed the mapping of Newcomb (1952, cross section A–A′) and inferred a thickness approaching 25 m (82 ft) of alluvium, supported by subsurface explorations (W3, W18) that encountered stratified gravel, sand, and silt in varied amounts. Upland bodies of unit Qa are deposited by small streams and derive material from local Quaternary and bedrock units. Unit Qa is a historically accessed unconfined aquifer for residential, agricultural, and municipal use (Newcomb, 1952, p. 44) and is hydraulically connected to recessional outwash in some locations, creating a composite aquifer (for example, the Skykomish River valley; Thomas and others, 1997, p. 40).

Qaf **Alluvial fan deposits**—Pebbles, sand, silt, cobbles, and boulders, in varied amounts; typically brown to gray; loose; moderately to poorly sorted; stratified. Unit Qaf forms gently dipping lobe-shaped surfaces where streams emerge from confining valleys. Sediment retains many lithological, compositional, and textural characteristics of local source material. Valleys that source unit Qaf deposits often have small streams with steep reaches that incise Quaternary glacial and nonglacial deposits. Surface-parallel stratified sand is deposited where sheet flow dominates; poorly sorted matrix-supported diamicton where debris flows dominate. Fan heights as tall as 6 m (20 ft) were measured following the methods of Slaughter and others (2017). The distal extent of alluvial fan morphology was mapped from lidar. Unit Qaf includes relict alluvial fan deposits that are too sparse to be broken out into an additional unit. Relict alluvial fan deposits were sourced from valleys that now lack an active channel and (or) have been incised too greatly to permit continued deposition across the fan surface.

PLEISTOCENE GLACIAL AND NONGLACIAL DEPOSITS

Deposits of the Vashon Stade of the Fraser Glaciation

Qgo **Vashon recessional outwash**—Sand and pebble to cobble gravel; some silt and clay; gray to tan where fresh; loose or soft to medium soft; polymict clasts subangular to well rounded; moderately to well sorted; may be stratified; fluvial deposits indicated by imbrication, crossbedding, rippled surfaces, and scour marks; lacustrine deposits by planar bedding, laminations, soft sediment deformation, and occasional dropstones. Moderately dipping, thin to medium planar beds characteristic of deltaic foreset bedding were observed at one upland locality (elev. 340 ft, sec. 18, T27N R6E), but were deemed spatially insufficient to map as a delta-facies subunit. Unit thickness, as indicated by subsurface exploration, is generally less than 10 m (33 ft), although Minard (1985a) suggested that it may be as much as 30 m (98 ft) in the quadrangle. The thickest unit Qgo deposits mapped occupy a broad valley floor in the northeast corner of the map

area; to the east, this broad topographic surface is graded to the underfit Woods Creek valley northeast of Monroe (Fig. M1, see *Vashon Glacial and Postglacial Conditions*). Other deposits are generally restricted to upland surfaces (180–400 ft elev.) southwest of the Snohomish River valley. Unit Qgo typically overlies Vashon till or ice-contact deposits (units Qgt and Qgic), but may cover older units. Landforms associated with recessional outwash deposits in the map area include, but are not limited to:

(1) Meandering channel incisions (10 m [33 ft]-scale) that dissect fluted topographic features. They commonly host fluvial deposits, typically transition to terraced landforms where the channels emerge into broad troughs between fluted landforms, and lack evidence for the source of sediment and erosional mechanism at the upper end (for example, sec. 30, T27N R6E). These features were interpreted as ice-proximal proglacial or subglacial drainage channels formed in a recessional setting.

(2) Perched terraces, convex valleyward on the southwest margin of the greater Snohomish River valley (elev. 340 ft [104 m]; sec. 7, T27 R6E).

(3) Broadly terraced and gently sloping regions that stem from the downslope termination of upland troughs near modern Cottage Lake (elev. ~260 ft [80 m]; secs. 1 and 12, T26N R5E, and sec. 7, T26N R6E).

Unit Qgo is a regional unconfined aquifer—it is an important source for drinking water and is susceptible to contamination (Newcomb, 1952). Where unit Qgo directly overlies Vashon advance outwash or pre-Vashon deposits, hydrologic connection may exist between aquifers (for example, Cottage Lake area, Golder Associates, 2007, fig. 2). Vashon recessional outwash deposits are the most widely mined source of sand and gravel in the Puget Lowland (Bethel, 2004). Undivided unit Qgo was mapped where deposits varied texturally or where exposure inhibited determination of dominant grain size. Subdivided into:

Qgos **Vashon recessional outwash, sand**—Sand with silt, rare pebbles, and clay; gray to pale brown where fresh, orange-brown where iron-stained from weathering; loose to medium dense; sand subangular to subrounded; moderately to well sorted; massive to poorly bedded. Field exposures provided a maximum observed thickness of 4 m (13 ft). Recessional sands were mapped in uplands west of the Snohomish River, but at lower elevations (45–61 m; 150–200 ft) than recessional lake landforms of unit Qgo. These sands may have been deposited in an ice-dammed recessional lake environment (see also *Vashon Glacial and Postglacial Conditions*).

Qgic **Vashon ice-contact deposits**—Diamicton (ablation till, flow till, or other melt-out till and supraglacial sediment); includes poorly compacted or patchy lodgment till; may include subglacial deposits, less commonly contains pebble and cobble gravel, sand, mud, and isolated boulders; pale gray, tan, or brown where fresh, orange-brown where oxidized or slightly weathered; compaction, sorting, and degree of stratification varied; gravels are polymict, typical of northern-sourced glacial deposits, and include locally sourced material. Unit Qgic was mapped where glacial diamicton lacked the competence and engineering properties of lodgment till; where diamicton had stratification or sorting that was insufficient to label as outwash; where hummocky, undulating, or irregular morphology suggested melt-out deposition of ice-bound sediment; or where lodgment till was of insufficient thickness, continuity, or areal extent to map separately from other Vashon deposits. Unit Qgic was most commonly observed in broad hummocky troughs bounded by kilometer-scale drumlins. Locally, sorted and rounded gravelly sands in 50 to 100 m (164–328 ft)-diameter mound features were interpreted as kame deposits (for example, along Fales Road, secs. 19 and 20, T27N R6E). Possible ice-marginal kame terraces were mapped in unit Qgic; such deposits have been mined as a source of sand and gravel in the quadrangle ('Pit' on the basemap in sec. 2, T26N R6E).

Locally, unit Qgic landforms may reflect topographic inversion of the Pleistocene ice surface. Depressions in the ice surface would have filled with sediment and stranded ice blocks during melt-out, preventing sedimentation—they are now modern lakes or closed depressions. Unsorted deposits may be crevasse- or moulin-infill sediment. Deposits of unit Qgic locally contain minor faults, folds, and oversteepened bedforms that may be related to settling of supra- or englacial sediment during ice melt-out, or deformation by ice-shove. Unit Qgic typically overlies units Qgt or Qga, but is also seen in contact with older glacial deposits and bedrock units. Thickness varies, but is often less than 10 m (33 ft). Variation in texture and thickness of deposits influences the unit's ability to host or confine aquifers. Where thin deposits of unit Qgic overlie unit Qga (common in map-scale glacial troughs in the southern half of the map area), surface water in unit Qgic may be hydraulically connected to aquifers hosted in the older unit. Hydraulic conductivity was not directly calculated and is expected to vary, but is generally inferred to be greater than for lodgment till and less than advance or recessional outwash deposits.

Qgt **Vashon lodgment till**—Diamicton; gray to brown; lightly to unweathered; unsorted; unstratified (local weak stratification); compact; stiff to very stiff; locally exhibits shear fabric; gravel to very large boulders are angular to subrounded and supported in a matrix of sand, silt, and clay. Clast casts are well developed with low surficial porosity, a glossy sheen, and little to no weathering rinds. Polymict clast lithologies are typical of northern-sourced glacial deposits and include locally sourced material. Localized exposures can be relatively

sand-rich, reflecting input from local sandstone bedrock and leading to reduced cohesive strength, increased porosity, and orange coloration from weathering-related iron-staining. Unit Qgt mantles topography and defines north-northwest-trending fluted uplands with sparse boulder-size glacial erratics. A greenstone glacial erratic of notable size, approximately 7 m (23 ft) on the long dimension, is located at significant site S2.

Regional average thickness of Vashon Till obtained from borehole records is about 10 m (33 ft), although deposition is irregular, discontinuous, and not reliably predictable from morphology (Troost and Booth, 2008). Greater thicknesses are inferred from subsurface records, but interpretations of these borehole logs are subject to error. The basal contact of unit Qgt is typically erosional; locally derived clasts are concentrated within unit Qgt above this contact. Unit Qgt is rarely seen in conformable contact with Vashon advance outwash deposits. Unit Qgt is deposited subglacially, largely by lodgment of glacial debris at the base of the overriding ice sheet, but may also include compacted subglacial melt-out deposits.

In the southern part of the map area, gently sinuous subparallel ridges, oriented roughly perpendicular to paleo ice-flow direction, traverse fluted topography. These are asymmetric ridges with steeply dipping southeast-facing slopes, gently dipping northwest-facing slopes, average wavelengths of approximately 100 m (328 ft), and amplitudes of as much as 8 m (26 ft)(secs. 8 and 9, T26N R6E). Most ridges are traceable for about 0.5 km (0.3 mi); some may exceed 1 km (0.6 mi), but are dissected by recessional outwash channels. These features resemble ribbed (Rogen) terrain (following the terminology of Benn and Evans, 2010) and appear to classify as minor ribbed moraine after Dunlop and Clark (2006) on the basis of size and relief. Haugerud (2009b) recognized comparable features on the Kitsap peninsula and made similar interpretations, with the caveat that such features in the literature are generally larger and more extensive. Field investigation of these ridges indicated that they are in part composed of compacted (lodgment) till; cross-sectional exposures were not accessible during this study, but may be available where recessional outwash has incised into transverse ridges. Haugerud (2009b) noted that: "A wide variety of mechanisms have been suggested for formation of such ribbed moraines, including subglacial thrust stacking of basal till and ice, as well as crevassing at the base of an ice sheet and injection of till upwards (or aqueous deposition of sorted material) into the ice fractures."

Unit Qgt has relatively low values of hydraulic conductivity and forms a regional hydrogeologic confining unit (Thomas and others, 1997; Vaccaro and others, 1998; Savoca and others, 2009) and, where present, restricts flow between aquifers hosted in recessional and advance outwash (or older) units. Perched water tables form on the surface of unit Qgt, and these unconfined aquifers are subject to strong seasonal variation (Newcomb, 1952; Liesch and others, 1963). Surface water collects in natural depressions that are underlain by lodgment till.

Qga **Vashon advance outwash, undivided**—Sand, pebble to cobble gravel, silt, and clay, in varied amounts; blueish gray, brown, or gray to tan; orange-staining where weathered; compact; commonly coarsens upsection; sand is medium dense to dense, mud is medium soft to very stiff; clasts typically rounded and moderately sorted; very thinly to thickly bedded; bedding generally planar and subhorizontal, but includes ripple-scale crossbeds, cut-and-fill structures, and graded bedding; beds locally distorted, faulted, or chaotically folded, which may result from soft-sediment deformation or Vashon ice compaction. Gravels are polymict with a mixture of northern and locally derived lithic fragments (DS2). Deposits resemble those of Vashon recessional outwash and are distinguished by ice-modified morphology and stratigraphic position beneath Vashon ice deposits. Relative degree of compaction is an additional distinguishing feature but may be difficult to ascertain in well-sorted or coarse-grained deposits. Exposures of advance outwash become more extensive in the southern portion of the map area and core some map-scale drumlins mantled by unit Qgt (secs. 9 and 10, T26N R6E). Unit Qga conformably overlies units Qc_O and Qcg_O. Sharp unconformable contacts are common where unit Qga overlies older pre-Vashon Quaternary units and bedrock. Undivided unit Qga was mapped where a range of grain sizes were exposed or limited exposure prohibited determination of dominant grain size. Unit Qga was deposited as proglacial outwash from a southward-advancing glacier in glaciolacustrine, fluvial, and deltaic depositional environments. Field exposures suggest a maximum unit thickness of as much as 34 m (112 ft). Interpreted subsurface data provided a maximum unit thickness approaching 50 m (164 ft) along cross section A–A′. Golder Associates (2000, fig. 2.7) found that unit thickness may exceed 100 m (328 ft) in the map area. We agree with Capps and others (1973) that advance outwash deposits thin northeastward as they pinch out against Tertiary bedrock in the subsurface (cross section A–A′).

Unit Qga has been mined in the map area and the region (Minard, 1985a,b). Historic gravel pits in the quadrangle (sec. 18, T27N R6E; sec. 10, T26N R6E) show development of unit Qga as an aggregate resource. Unit Qga is a regionally important aquifer for domestic and municipal use and is the principal aquifer for western Snohomish County (Thomas and others, 1997). Groundwater is generally unconfined in the aquifer, but may be confined locally in upland areas capped by lodgment till (Hart Crowser, 1993, fig. 3; Golder Associates, 2000, fig. 2.3). Artesian conditions are documented in wells near Cold Springs (sec. 12, T26N R5E; Golder Associates, 2007, p. 6). Unit Qga hosts the Cross Valley aquifer, which in 1987 was designated as a federally protected sole source

aquifer by the U.S. Environmental Protection Agency (Office of the Federal Register, 1987). In the Maltby quadrangle, Golder Associates (2000, p. 16) recognized a pattern of relatively higher horizontal hydraulic conductivity in the lower portion of Vashon advance outwash. They outlined a lower sub-unit that is relatively coarser-grained sand and gravelly sand and noted that water wells screened in this interval are generally more productive. Pivaroff-Ward (2015, table 4) presents a summary of published values of geotechnical and engineering parameters for Vashon advance outwash in the Lynnwood area. Subdivided into:

Qgas **Vashon advance outwash sand**—Sand and sparse gravel; pale gray to pale brown; orange-brown where mildly weathered; compact; loose to dense; subangular to subrounded gravel to small cobbles, compositionally polymict; well sorted; massive to planar-bedded; local thin, planar silt interbeds. Petrographically, the sand fraction largely consists of a diverse lithic assemblage with monocrystalline quartz as the most common crystal grain type. Textures indicative of grain compaction are preserved within intact sand clods. Outcrops have a disproportionate amount of small mammal burrows, owing to the easily excavated sorted sand (also noted in sandy glacial deposits elsewhere by Benn and Evans, 2010). Deposits are often drumlinized and mantled or capped by lodgment till (sec. 7, T26N R6E). Unit Qgas may be exposed in sub- or postglacial incisions. Field exposures along a roadcut provide a continuous thickness of 21 m (69 ft)(sec. 7, T26N R6E). The base of this unit was not exposed, though boreholes and regional studies (Troost and Booth, 2008) indicate that the unit conformably overlies Vashon proglacial lacustrine deposits or pre-Vashon units with localized erosional contacts and is broadly contemporaneous with the Esperance Sand Member of Vashon Drift of Mullineaux and others (1965). Unit Qgas was deposited by outwash from the advancing Vashon ice sheet, and we infer that the sediments may have been laid down in a glaciofluvial-deltaic to glaciolacustrine depositional environment.

Qgaf **Vashon advance outwash, silt and clay**—Silt and clay with sparse gravel; blue-gray to gray-brown where fresh, dark brown on weathered surfaces; stiff to hard; well sorted; predominantly clayey silt, but includes silty clay; locally sandy; typically contains randomly distributed, subangular pebbles to cobbles as dropstones; often micaceous; planar, locally wavy, thin beds and laminae; local convolute bedding and rhythmic interbeds of silt and clay (Fig. 1); subhorizontal, except where deformed by overburden or mass-wasting events; beds laterally continuous at outcrop-scale; distorted or chaotically folded in places, which may be from soft-sediment deformation or Vashon-ice compaction; meter-scale beds and lenses of diamicton locally present and may be related to iceberg-rafted deposition, flow till, or subaqueous debris-flow sedimentation; grain size and sedimentary structures suggest deposition in lacustrine environment; maximum thickness of 10 m (33 ft) observed in field exposures, but subsurface boreholes suggest thickness in excess of 22 m (72 ft) along High Bridge Road (W29, W31, sec. 22, T27N R6E); lower contact generally not observed but thought to be locally gradational with unit Qc_o (see description for unit Qc_o) consistent with prior mapping efforts (Minard 1985a; Booth, 1990); may be texturally indistinguishable from unit

Figure 1. Rhythmic, planar-bedded silt and clay of unit Qgaf representing cyclical lacustrine sedimentation (SE¼ sec. 10, T26N R6E; view to the south). Deformed, chaotic bedding is faintly visible in the 15 cm-thick set above the digging tool. This deformation is restricted to beds within the set. We interpret this deformation as primary, perhaps a subaqueous turbidity current or soft-sediment deformation. Absence of dropstones in this exposure suggest that there was no calving ice margin nearby. Dropstones and diamicton lenses are present elsewhere in unit Qgaf. These deposits are associated with extensive slope failure in this drainage (Bethel, 2004; this study) and elsewhere across the map area.

Qc_O; mapped where confidently glaciolacustrine, lacked organic debris, supported by stratigraphic relations, or delineated by radiocarbon ages. Where exposures are oversteepened in stream valleys, slopes are commonly mantled by loose, saturated debris derived from shallow landsliding or mass-wasting events (see unit Qls for more details). This unit correlates with unit Qgl_V in adjoining 1:24,000-scale geologic maps of Dragovich and others (2010b, 2011, 2015), finer-grained subdivisions of units Qtb (transitional beds) of Minard (1985a), the Pilchuck Clay Member of Newcomb (1952), and is broadly contemporaneous with the Lawton Clay Member of Mullineaux and others (1965)(see *Vashon Glacial and Postglacial Conditions*). Vashon proglacial fine-grained deposits have been identified as an intermittent confining layer at the base of aquifers hosted in younger units (Golder Associates, 1999).

Pre-Vashon Glacial and Nonglacial Deposits

Qc_O **Deposits of the Olympia nonglacial interval (MIS 2–3), sand and silt**—Sand and silt with minor clay and gravel; blue-gray to brown-gray where fresh, orange-brown where oxidized, dark brown where organic-rich; very stiff to hard; medium dense to dense; gravel to coarse pebbles; clasts subangular to subrounded; moderately to very well sorted; micaceous; gravel concentrated in thin to thick beds planar at outcrop scale; bedding generally subhorizontal; planar laminations to medium beds; occasional centimeter- to meter-scale trough-shaped sets of tangential, very thin crossbeds and laminae; meter-scale fining upwards sequences grade from medium sand to clay with sharp basal unconformities; locally abundant organic-rich sediment and centimeter-scale flattened wood fragments concentrated in medium to thick planar or wavy sets of thin beds and laminae. Sand and gravel compositions are predominantly lithic (DS2 and DS3); sand fraction is compositionally comparable to sand in unit Qcg_O, and quartz is largely monocrystalline. Petrographic textures indicative of grain compaction are preserved within intact sediment clods. Unit Qc_O is often texturally indistinguishable from unit Qgaf. It was mapped where organic material is present and where supported by stratigraphic relations or delineated by radiocarbon dates. Where it is overlain by unit Qga or Qgaf, the upper contact was drawn at the highest observed organic material or the lowest evidence of glacially influenced deposition (see description of unit Qgaf). The basal contact was not directly observed, but partial exposures suggest a gradational contact with unit Qcg_O (schematic columnar section CS1; sec. 22, T27N R6E). True thickness was difficult to determine because of the gradational nature of the upper and lower contacts. A maximum thickness of 30 m (98 ft) was observed in field exposures (secs. 11 and 14, T27N R6E). Unit Qc_O is exposed from 43 to 238 ft elevation and largely restricted to the northeast quadrant of the map area along the margins of broad valleys. Deposits of unit Qc_O are most indicative of a low-energy fluvial facies in a meandering river system similar to modern rivers in the map area. This unit is correlative with the organic-rich portions of unit Qtb of Minard (1985a). The relatively low-permeability, fine-grained portions of unit Qc_O and correlative units have been identified as local and regional confining layers (Golder

Figure 2. Luminescence age site GD8 in a 60 cm (24 in.)-thick interbed of well-sorted, fine to coarse sand, with sparse pebbles concentrated along bedding. Sinusoidal crossbedding dips to the northeast (view to the north). This sand lens is traceable for roughly 16 ft across the outcrop and exposed on the opposite bank of the drainage. The bounding gravel deposits are locally clast supported with a sandy matrix and are weakly imbricated. Occasional decimeter-scale sand and silt beds are present in unit Qcg_O, though coarse sandy gravel is the most characteristic lithology.

Associates, 1999; Newcomb 1952; Thomas and others, 1997), where discontinuous sand layers host local aquifers (Golder Associates, 2005). Five new radiocarbon and two luminescence ages between 20 and ~32 ka establish the age of this unit in late MIS 3 to early MIS 2 (Tables A1 and B1). Paleoenvironmental interpretations of pollen samples collected in unit Qc_o broadly indicate cooler than modern temperatures (see *Deposits of MIS 3 and early MIS 2*).

Qcg_o **Deposits of the Olympia nonglacial interval (MIS 2–3), gravel**—Pebble and cobble gravel, typically with a coarse sand matrix and rare small boulders; gray-brown to dark brown where fresh, orange-brown where weathered; moderately to well sorted; matrix to clast supported; clasts subrounded to rounded, typically oblate, weakly imbricated; polymict (DS2); clasts lightly weathered with rinds typically <0.5 mm thick; some highly weathered plutonic clasts; rare randomly oriented, flattened, angular cobble- to boulder-size, laminated silt and mud rip-up clasts found in most exposures. Sand portion is compositionally comparable to sands of unit Qc_o (DS3); predominantly lithic grains; largely monocrystalline sand-size quartz; petrographic textures indicative of grain compaction in preserved clods; weakly stratified or massive; bedding generally subhorizontal; where exposed, crossbeds in gravel form medium to very thick sets (Fig. 2); discontinuous thin to thick lenses of well-sorted sand and silt are common; laterally continuous at 1 m- to 10 m-scales; crossbeds are typically thin and sinusoidal or tangential; sparse pebbles (≤2 cm) along the base of some crossbeds; flattened twig radiocarbon dated (age site GD5; map sheet) in one such silt-dominated lens. Crossbeds in one locality are northeast-dipping and gravel imbrication orientations are roughly northwest-trending on average, suggestive of a northwest-trending paleocurrent direction. A maximum thickness of 15 m (49 ft) was estimated from field exposures; subsurface explorations indicate that unit thickness varies and may be as thick as 60 m (197 ft) in places (Hart Crowser, 1993). Exposures of unit Qcg_o range in elevation from 60 to 155 ft and are largely confined to exposures along the western Snoqualmie River valley at the east map boundary. The basal contact of this unit is sharp and erosional where overlying unit Qps (sec. 22, T27N R6E). Textures of unit Qcg_o are most consistent with a braided fluvial system. Unit Qcg_o has been historically mined for aggregate resource at a small quarry (High Bridge Gravel Pit, sec. 26, T27N R6E) and is a discontinuous but locally important aquifer (Hart Crowser, 1993). Unit Qcg_o is correlative with unit Qog (Olympia gravel) of Minard (1985a). One new radiocarbon and two luminescence ages place the unit between ~21 and ~35 ka (Tables A1 and B1).

Qps **Pre-Vashon sand**—Medium sand, but ranges from fine to coarse; pale brown to light gray where fresh, orange-brown to gray-brown on weathered faces; sparse cobbles recorded in subsurface exploration logs; well sorted; grains subangular to rounded; predominantly lithic; polycrystalline quartz more abundant than monocrystalline grains; medium dense to dense; massive or thin to medium planar bedded; discontinuous, thin lens-shaped beds of pebbly sand; centimeter-scale ripple bedforms. There are abundant northwest-striking, moderately to steeply dipping faults with both normal and reverse centimeter-scale separation of beds in roadcuts near age site GD9 and in nearby cutbanks of the Snoqualmie River between age sites GD7 and 10-28D (map sheet). Interpretation of subsurface boreholes suggests thicknesses of as much as 25 m (82 ft)(borehole B9, map sheet). The lower contact with unit Qpu is sharp and interpreted as erosional. Textures of unit Qps are most indicative of a fluvial-deltaic depositional environment. Locally, bedding measurements bounding the basal contact between age sites GD7 and 10-28D suggest a gently folded contact, but the poorly exposed contact prevented field confirmation. Two new luminescence ages at the top (site GD9) and bottom (site GD7) of the unit (Appendix B; schematic columnar section CS1) suggest that deposition occurred in early MIS 3 to late MIS 4 time between ~53 and ~65 ka. Unit Qps is correlative with portions of unit Qtu of Minard (1985).

Qpt **Pre-Vashon till**—Diamicton, locally sandy; gray, blue-gray, or brown where fresh, orange-brown on weathered faces; massive; compact, locally resembles concrete; local shear fabric; clasts are polymict, consistent with northern-sourced lithologies; maximum observed thickness 1.5 m (5 ft). We mapped unit Qpt in two locations along the Snoqualmie (near age site GD1) and Snohomish Rivers (significant site S3). In each case, the unit underlies pre-Vashon deposits and thus reflects a pre-Vashon glaciation in the Puget Lowland. The base of the unit was not observed due to limited exposure, but it is inferred to overlie, but may be contemporaneous with, unit Qpu along the Snoqualmie River (sec. 22, T27N R6E). Unit Qpt is correlative with portions of unit Qtu of Minard (1985).

Qpu **Pre-Vashon glacial and nonglacial deposits, undivided**—Pebble gravel, sand, silt, clay, diamicton, organic sediment, and boulders, in varied amounts; color, weathering, rounding, sorting, and bedding varied; compact. Unit Qpu is limited and mapped at or slightly above modern river elevations. Exposures along the Snoqualmie River (sec. 22, T27N R6E) range from blue-gray, well-sorted, laminated to thin planar-bedded silt and minor clay to exposures of similar lithology, but full of subrounded pebble-size dropstones and local wavy bedding. Between age sites GD7 and 10-28D, unit Qpu is mapped at the elevation of the Snoqualmie River and descends beneath the river's surface. Here, the deposits consist largely of sandy diamicton. The upper 1.5 m (4.9 ft) of exposure becomes increasingly

stratified and sorted, with thin beds and laminations of silt and sand with minor clay and pebble-size dropstones. Locally, bedding has tight to isoclinal, harmonic, northwest-trending folds intruded by a steeply dipping, northwest-striking, 2 cm (0.8 in.)-thick clastic dike. Outcrops in the Snohomish River (significant site S3), visible during seasonal low-water conditions, expose tan, well-sorted, compact silt; laminated to thin beds; extensive chaotically oriented, 10 cm (4 in.)-scale, tight and isoclinal folds; oversteepened bedding. We infer a lacustrine depositional environment at this site from the bedding and fine-grained nature of this deposit. We speculate a pre-Vashon age for this deposit on the basis of small differences in the amount of small-scale deformation and compaction at this site compared with that of unit Qgaf upslope. However, the upper contact between unit Qpu and overlying Qgaf was not observed. The basal contact of unit Qpu is sharp, and the unit overlies bedrock and unit Qpt at significant site S3. Maximum observed thickness was 2 m (7 ft), but the unit extends below the river surface, and therefore the total thickness is unknown. Sample 10-28D (Dragovich and others, 2011a,b) of unit Qpu was radiocarbon infinite.

Tertiary Bedrock

ΦEn **Nearshore sedimentary rocks (Oligocene to late Eocene)**—Siltstone to coarse-grained lithic sandstone, with rare pebble conglomerate; brown or gray to dark gray on fresh faces, orange-brown or tan to dark gray on weathered surfaces with hackly concentric weathering pattern; well lithified to friable (where weathered); typically tuffaceous and fossiliferous; locally glauconitic and pale green near fossiliferous exposures; locally micaceous; rare millimeter-scale carbonized detritus; largely calcitic, and effervescent with HCl; includes siliceous or hematite cement; pebble to small boulder-size calciferous concretions common and nucleate around marine macrofossils; bedding predominantly massive, which may be the result of bioturbation; where defined, bedding is thin to very thick, planar, with some poorly defined crossbedding. Rocks are typically tuffaceous (≤70%) with pumice fragments and glass shards. Lithic grains are largely composed of volcanic rock fragments (11.6–54%), but include plutonic, metamorphic, and sedimentary rock fragments. Accessory minerals (0.8–3.6%) include muscovite, biotite, hornblende (≤2%), and unidentified opaque grains. The accumulation of micro-scale bedding structures is indicative of a turbidite sequence, although a complete sequence was not observed. Point-count data (DS3) indicate sandstone lithologies are litharenite to feldspathic litharenite (Folk, 1980) with sparse, subrounded to subangular pebbles. Sparse conglomerates are found in discontinuous thin lenses and interbeds within sandstone. Weathered rock commonly displays spheroidal weathering, with concentric red-brown stained faces (Liesegang rings) as much as 40 cm (16 in.) in diameter (Fig. 3). Minor stream channels are often floored with fresh bedrock at the base of weathering profiles that are typically ~4 m (13 ft) thick, but locally exceed 10 m (33 ft)(sec. 7, T27N R6E). Resistant beds commonly define northwest-trending, strike-parallel topographic ridges visible in lidar where Quaternary cover is thin (secs. 8 and 17, T27N R6E). Inferred minimum thickness is ~600 m (1,968 ft) on the basis of semi-continuous exposure in stream channels, assuming there is no structural offset. Lithologic character and fossil

Figure 3. Typical weathered exposure of unit ΦEn siltstone and sandstone at age site GD15 (view to the southeast). Hackly, iron-stained weathering planes form concentrically around less-weathered enclaves. Weathered zone commonly permeates the upper 4 m (13 ft) of unit ΦEn, but locally exceeds 10 m (33 ft) thickness. Liesegang rings obscure bedding orientations and measurements were not possible in some exposures. Weathering may affect the engineering properties of bedrock; site-specific investigations are recommended to determine material characteristics. Note ovoid concretions in the upper left corner and the planar, gently dipping sandstone bed in the upper half of the photo.

assemblages indicate that deposition is submarine at inner to mid-shelf water depths. Rare carbonized detritus and leaf fossils were found near the upper reaches of unit ΦEn. Basal contact is inferred to be interfingering and gradational, vertically and horizontally, with unit ΦEc and is arbitrarily defined in this study as the uppermost exposure of pebble-bearing sandstone or conglomerate of unit ΦEc. Sparse benthic foraminifera suggest correlation with the Refugian stage in Washington State (Rau, 1981). Molluscan fossils indicate the middle Galvinian stage, which is approximately equivalent to the Refugian foraminiferal stage (Prothero and Armentrout, 1985), about 35–33 Ma (see *Paleontology of Sedimentary Bedrock*). The ~28 Ma U-Pb date on unit Φvt (age site GD27) interbedded high in the stratigraphic section indicates that most of unit ΦEn is early Oligocene or older; strata higher in the section may extend into the late Oligocene. Divided into:

Φvt **Tuff (Oligocene)**—Coarse rhyolitic crystal vitric (ash) tuff; white to light gray on fresh faces, tan to gray on weathered surfaces; consists of ash-size fragmented glass shards, subangular pumice fragments, and crystals; very strongly lithified; massive; local poorly defined bedding in northernmost exposure (sec. 36, T28N R5E); geochemically rhyolitic and peraluminous (see *Geochemistry*). The tuff in this area contains rocks that appear compositionally similar in thin section, but show a greater degree of reworking that partially defines bedding by the incorporation of subangular to subrounded, ash-size volcanic rock fragments. Maximum observed thickness of 3 m (10 ft). We observed concentrated float of unit Φvt at locations where this unit would be expected to crop out. We suspect that unit Φvt varies in thickness but is laterally extensive across the map area. On the basis of the lithologic character of this unit and surrounding strata, we speculate that this unit was deposited in a relatively quiet, subaqueous environment. Preservation of delicate glass shards suggests that this volcanic material experienced minimal reworking. Unit Φvt is found interbedded with siltstone and sandstone of unit ΦEn in the small drainage northwest of age site GD27—new U-Pb analyses of the tuff at this site suggest a maximum depositional age of 27.8 ±0.4 Ma (Appendix C).

ΦEc **Continental sedimentary rocks (early Oligocene to Eocene)**—Sandstone and pebble and cobble conglomerate, with minor siltstone to shale; tan to brown or gray-brown on fresh exposure, tan to red-brown on weathered exposures; typically well indurated but locally friable or altered to clay where weathered; variably calcite cemented; interbedded lithologies vary in thickness and lateral extent; internal lithologic contacts often sharp, but locally gradational; gravels subrounded on average, commonly oblate; bimodal compositional maturity (predominance of immature volcanic and mature quartzose lithologies, see below); texturally mature; little to no tuffaceous component beyond rare discontinuous centimeter-scale ash beds. Conglomerates variably clast or matrix supported; massive to weakly imbricated; poorly defined, thick to very thick sets of thin to medium tangential crossbeds; typically cliff forming; ≤20 m (66 ft) thick along west bank of Snohomish River south of SR522 (significant site S5). Conglomerate clast lithologies are polymict but predominantly volcanic (50%, abundant andesite), and include sedimentary (26%, abundant chert), metamorphic (19%, abundant quartzite), and plutonic (4%) rock fragments (DS2). Sandstones are typically crossbedded, best exposed in 9 m (30 ft)-thick roadcut (significant site S4) with thick, nonparallel planar sets of thin to medium, sinusoidal, southwest-dipping crossbeds; locally pebble-rich, pebbles often form lenses where concentrated at base of bedding planes; litharenite (DS3)(Folk, 1980); rare lithic wacke. Siltstone to shale exposures are locally wavy and laminated to medium planar bedded; observed thickness as much as 15 m

Figure 4. Deciduous and coniferous terrestrial plant fossils preserved in a detached boulder of unit ΦEc. Such fossil localities are often found in conjunction with centimeter-scale thickness subbituminous coal stringers. We interpret continental deposition for unit ΦEc in a fluvial or deltaic environment.

(49 ft); often contain leaf fossils, including deciduous stems and leaves (Fig. 4) and impressions resembling leaves of *Metasequoia* (dawn redwood); host sparse, thin, discontinuous stringers of coal traceable at 10 cm (4 in.)-scale; coal is subbituminous A to B rank with reflectance values from 0.44 to 0.51% (DS4). We estimate 550 to 790 m (1,804–2,592 ft) thickness for unit ΦEc in the Maltby quadrangle, although thickness is poorly constrained due to poorly constrained bounding contacts and discontinuous exposure. Lithologic characteristics of unit ΦEc are most consistent with a braided fluvial depositional environment. The coal-bearing, finer-grained strata may indicate a deltaic influence, but may be interpreted as flood-plain deposits of the fluvial system. The lower contact of unit ΦEc is concealed beneath alluvium; these rocks may have a disconformable contact with unit Evp (see *Nature of the Contacts between Tertiary Units*). We speculate that unit ΦEc may correlate with the oldest strata of the Blakeley Formation or the Renton Formation of the Puget Group (see *Oligocene–Eocene Sedimentation*).

Sedimentary rock outcropping in the southeast corner of the Maltby quadrangle (sec. 11, T26N R6E) is tentatively correlated with unit ΦEc on the basis of lithologic similarities and mapped as unit ΦEc?. Sandstone and pebble to cobble conglomerate with rare siltstone are locally tuffaceous with glass shards and pumice fragments; dark gray to brown where fresh, and red- to orange-brown where weathered; gravels to coarse cobbles are sub- to well rounded; poorly to well sorted; may be friable or hackly; massive to stratified; thin to thick planar bedded; typically matrix supported, ranges to clast supported; gravels commonly concentrated along base of bedding planes. Volcanic rock fragments make up an average of 82% of gravel-size lithics (DS2). Decomposition of clasts and poor induration suggest a relatively high degree of weathering. The lithologic character of unit ΦEc? is most indicative of a fluvial depositional environment. Assuming continuous bedding orientations between exposures, these rocks in the southeast corner of the quadrangle would project stratigraphically upsection from all bedrock exposures to the northwest, though concealed structures may complicate apparent stratigraphic relations. Dragovich and others (2010a) report a preliminary age of ~18 Ma from a lithic lapilli tuff (their unit Mvc) at age site 09-54Z (map sheet, Appendix C). However, statistical analysis (this study) of those data reveal a youngest zircon peak age at ~27 Ma (Appendix C)(see *Oligocene–Eocene Sedimentation*).

Evp **Volcanic rocks of Mount Persis of Tabor and others (1993), undivided (middle to late Eocene)**—Andesite and dacite flows, autoclastic breccia, block-and-ash flows, rare tuff, and volcaniclastic boulder breccia; predominant lithology is gray to dark gray, fine- to coarse-grained, porphyritic, orthopyroxene-bearing hornblende clinopyroxene andesite flows; typically massive with sparse pebble- to cobble-size breccia of similar lithology; competence varies with weathering, fresh rock is well indurated; local columnar jointing; subhorizontal to gently dipping; phenocrysts (10–50%) include plagioclase (50–99%), clinopyroxene (1–24%), hornblende (0–20%), orthopyroxene (0–3%), sparse opaques (0–5%), and rare zircon (<1%); cumulophyric texture common; rare seriate grain-size distribution; sparse to extensive alteration of phenocrysts and groundmass with replacement by calcite, biotite, and chlorite. Detailed petrographic observations are available in the Data Supplement (DS5).

While multiple lithologies are exposed across Lord Hill, they are all mapped as the undivided unit Evp due to extensive Quaternary cover and apparent lack of continuity. Exposures of autoclastic and pyroclastic breccia are common (Fig. 5) along the east and north flanks of Lord Hill. Epiclastic deposits are rare in the quadrangle. A block-and-ash flow deposit with meter-scale boulders was excavated in a small quarry on the

Figure 5. Clast-supported monomict andesitic boulder breccia of unit Evp exposed along the Snohomish River at geochemistry site G7. Pebble- to meter-scale boulder breccia in a porphyritic matrix of comparable lithology has only a slight variation in color and phenocryst abundance. Coarseness of these volcaniclastics suggests deposition proximal to a volcanic source. Glacial striations visible on polished faces of breccia indicate a Vashon ice flow azimuth of 171° (view to the east). Outcrop is best exposed during seasonal low-water conditions.

northeast side of Lord Hill (near geochemistry site G16). The deposit has a couple of 1 to 2 m (3–7 ft)-wide vertical columns of concentrated, irregularly shaped centimeter-scale vesicles. We speculate that these vertical columns may be gas chimneys related to a dome collapse. Tuff deposits are generally rich in lithic lapilli (with lesser amounts of pumice lapilli) and crystal ash, exhibiting similar alteration styles to those described above. Wood and terrestrial plant fossils have been reported in clastic interbeds within Mount Persis volcanic units to the east (Danner, 1957; Dragovich and others, 2010b, 2011a, 2013).

Unit Ev_p is not considered a planar stratigraphic unit. It is assumed to vary in thickness with distance from proximal facies. A thickness of 300 to 450 m (984–1,476 ft) was inferred from geophysical modeling in neighboring quadrangles by Dragovich and others (2010b, 2011a). We follow their interpretations in cross section A–A′. Unit Ev_p is correlative with unit Evs_p of Dragovich and others (2010b, 2011a), and farther south, the Tukwila Formation of the Puget Group (Tabor and others, 1993). We infer a conformable contact with unit Evs_{pg} in cross section A–A′. This stratigraphic relation has been described in the Socal Schroeder oil well to the west (Rau and Johnson, 1999) and inferred in neighboring 7.5-minute quadrangles to the east and southeast (Dragovich and others, 2010b, 2011a). A new U-Pb age sample was collected from a lithic lapilli crystal ash tuff (age site GD28, Appendix C) with a weighted mean age of 43.4 ±0.4 Ma. Divided into:

Ei_p **Volcanic rocks of Mount Persis of Tabor and others (1993), dikes (middle to late Eocene)**—Andesite and dacite dikes around the flanks of Lord Hill; similar in color to flows but slightly darker; steeply dipping with various orientations; planar to gently undulating; locally glassy with rare andesitic xenoliths; widths range from centimeter- to 10 meter (33 ft)-scale. Notable dike-like features (geochemistry site G18) are exposed in a large inactive quarry on the southwest end of Lord Hill.

Evs_{pg} **Puget Group, undivided (Eocene)(cross section only)**—Arkosic sandstone, tuffaceous sandstone, tuff, tuff breccia, andesitic conglomerate, and less common siltstone and coal; may include Renton, Tukwila, and Tiger Mountain Formations of the Puget Group, though several workers have suggested a possible correlation of the Tukwila Formation to the volcanic rocks of Mount Persis (for example, Tabor and others, 1993). Rau and Johnson (1999) evaluated the Socal Schroeder oil well and suggested that the volcanic rocks of Mount Persis (unit Ev_p) overlie at least part of the Puget Group. They posited that these sediments beneath likely correlate with Tiger Mountain Formation exposed to the southeast. Dragovich and others (2010b, 2011a) show the Puget Group sediment pinching out north and east of the Maltby quadrangle. We follow their interpretation, and on cross section A–A′, we show a ~65 m (213 ft) layer of unit Evs_{pg}—a thickness comparable to that shown on cross section A–A′ of Dragovich and others (2011a). Dragovich and others (2015) indicated that Puget Group strata do not continue north of Monroe. It is important to note that the apparent thickening of unit Evs_{pg} across the hinge of the Fiddlers Bluff anticline on cross section A–A′ is a product of vertical exaggeration; the unit is intended to be drawn with consistent thickness and no structural or stratigraphic thickening is implied.

KJm_w **Western mélange belt of Frizzell and others (1987), undivided (Cretaceous to Jurassic)(cross section only)**—Argillite, sandstone, chert, pebble conglomerate, tuff, and intermediate to mafic volcanic flows; less common gabbro, diabase, and tonalite; rare marble and variably serpentinized or carbonated ultramafic rocks; all metamorphosed to prenhite-pumpellyite facies and possibly to greenschist facies. Tabor and others (1993) recognized a northeastward trend of increasing metamorphic grade. It is thus possible that rocks of the Western mélange belt (WMB) in the Maltby quadrangle are lower metamorphic grade than any exposed at the surface to the east and north. We speculate that Tertiary sedimentary and igneous rocks overlie the WMB at depth in the Maltby area on the basis of geophysical inferences (Sherrod and others, 2008; Anderson and others, 2015; this study) and mapped surface and subsurface relationships to the east (Danner, 1957; Tabor and others, 1993; Dragovich and others, 2002, 2010, 2011). No direct surface or subsurface observations record the presence of the WMB in the Maltby quadrangle or farther west. Dragovich and others (2014a) report the youngest known maximum depositional age of metasedimentary rocks in the WMB at ~74 Ma; other geochronologic work indicates ages ranging into the Jurassic, including intrusive igneous ages of 150 to 170 Ma (Tabor and others, 2000).

RESULTS AND OBSERVATIONS

Geochemistry

Major and trace elements were measured on 18 samples of the Mount Persis volcanics and one sample of tuff from unit Qvt (age site GD27)(DS6 and DS7). The Mount Persis samples classify as andesites and dacites (Fig. 6A) and display limited chemical diversity (for example, 60–67 wt.% SiO_2, 3.8–0.8 wt.% MgO). On AFM (Fig. 6B; Irvine and Baragar, 1971) and FeOt/MgO vs. SiO_2 diagrams (Miyashiro, 1974), these rocks straddle the boundary between the calc-alkaline and tholeiitic series (Fig. 6B), and on spidergrams (Figs. 6C and D) they have Ta-Nb depletions characteristic of subduction-related magmas. All Mount Persis samples have similar rare earth element (REE) patterns with modest light rare earth (LREE) enrichment (La/YbN = 4.8–9.6) and negligible Eu anomalies (Fig. 6D).

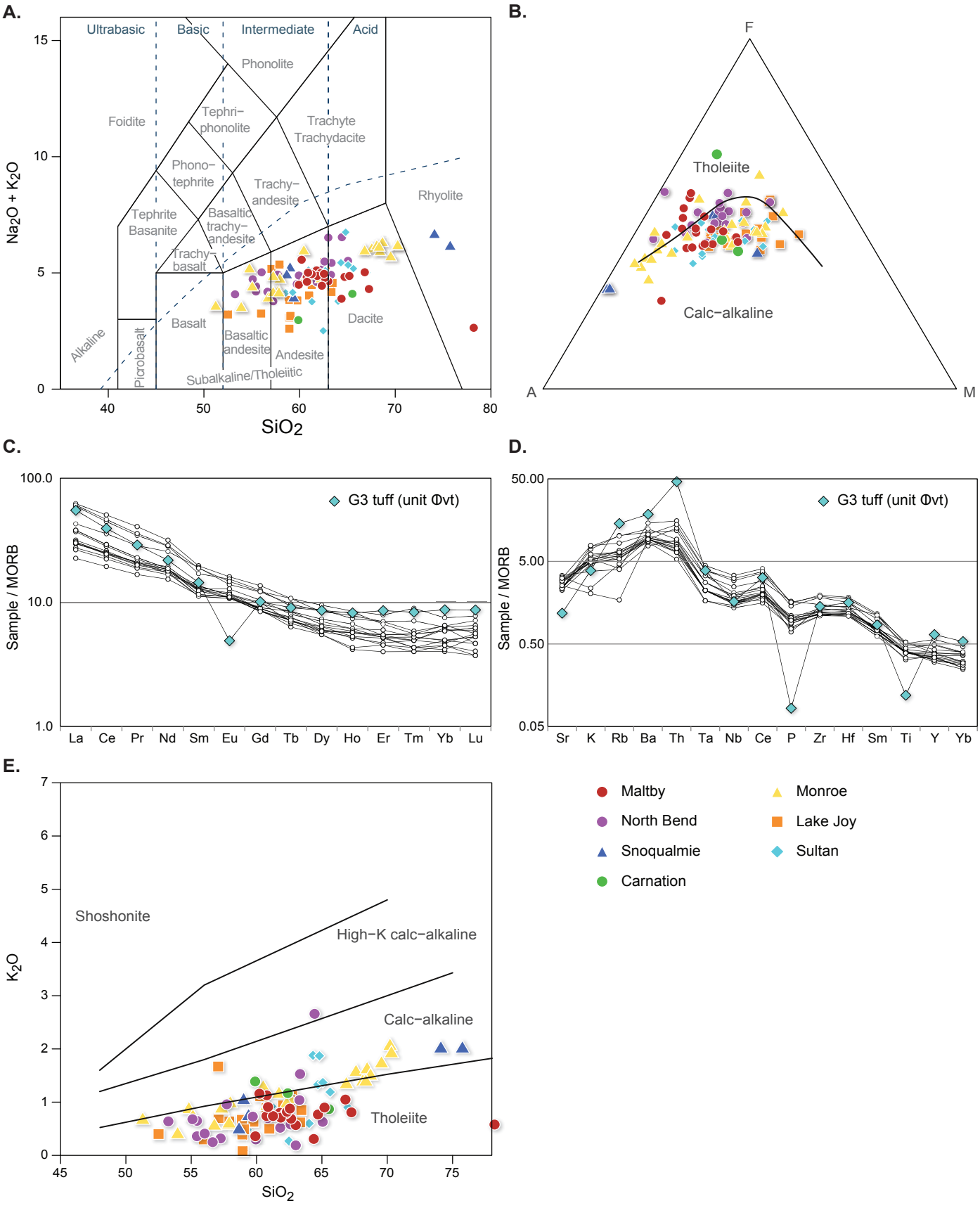
A.
Ultrabasic
Basic
Intermediate
Acid
Phonolite
Foidite
Tephri–phonolite
Trachyte
Trachydacite
Phono–tephrite
Trachy–andesite
Rhyolite
Tephrite
Basanite
Basaltic trachy–andesite
Trachy–basalt
Basalt
Basaltic andesite
Andesite
Dacite
Alkaline
Picrobasalt
Subalkaline/Tholeiitic
Na2O + K2O
SiO2
B.
F
Tholeiite
Calc–alkaline
A
M
C.
G3 tuff (unit Φvt)
Sample / MORB
La Ce Pr Nd Sm Eu Gd Tb Dy Ho Er Tm Yb Lu
D.
G3 tuff (unit Φvt)
Sample / MORB
Sr K Rb Ba Th Ta Nb Ce P Zr Hf Sm Ti Y Yb
E.
Shoshonite
High–K calc–alkaline
Calc–alkaline
Tholeiite
K2O
SiO2
Maltby
North Bend
Snoqualmie
Carnation
Monroe
Lake Joy
Sultan

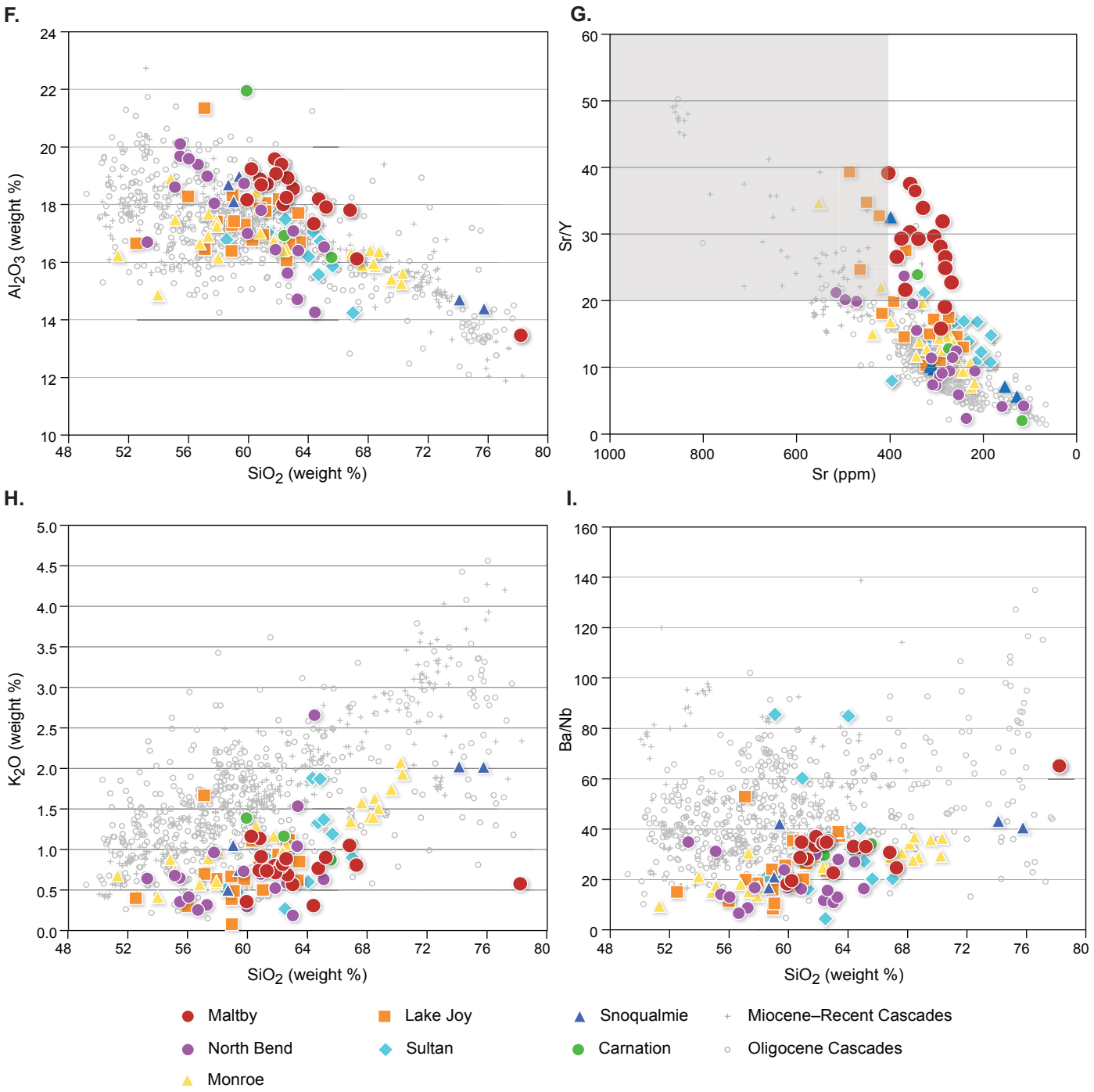

Figure 6. Geochemistry data illustrating the compositional diversity of the volcanic rocks of Mount Persis, including data from nearby Monroe, Carnation, Sultan, Lake Joy, Snoqualmie, and North Bend quadrangles. **A.** *(facing page)* Total alkali vs. silica diagram (Le Bas and others, 1986). Outlier point in the rhyolite field is the Oligocene tuff (unit Φvt) from the Maltby quadrangle. **B.** AFM diagram (Irvine and Baragar, 1971) showing that the volcanic rocks of Mount Persis straddle the boundary between calc-alkaline and tholeiitic series. Note that samples from the more easterly quadrangles (Sultan, Lake Joy, Snoqualmie, and North Bend) tend to be calc-alkaline. The Maltby quadrangle has the highest proportion of tholeiitic samples. **C.** MORB-normalized spider diagram showing K-Rb-Ba-Th enrichments and Ta-Nb depletions characteristic of subduction-related magmas. Teal-colored diamonds represent unit Φvt; all other data are for unit Ev_p sampled in this study. Data normalized to MORB values of Sun and McDonough (1989). **D.** Average REE contents of Eocene igneous units normalized to chondrite values of Boynton (1984). The Oligocene tuff (unit Φvt; teal diamonds) is the only sample with a pronounced Eu anomaly, indicative of feldspar fractionation. **E.** Plot of K_2O vs. SiO_2 (Peccerillo and Taylor, 1976) for the volcanic rocks of Mount Persis. Note that most Maltby samples plot as tholeiitic. **F.** *(above)* Harker diagram for alumina comparing the volcanic rocks of Mount Persis samples with 623 analyses of Oligocene to Holocene Cascade-arc rocks from Washington. The high-silica Maltby sample is unit Φvt. Note that some Mount Persis samples, particularly those from the Maltby and Lake Joy quadrangles, have distinctly high Al_2O_3. **G.** Plot of Sr/Y vs. Sr showing in gray, the field for adakites (Defant and Drummond, 1990). Note the unusually high Sr/Y of most samples from the Maltby quadrangle and some from the Lake Joy quadrangle. **H.** Harker diagram for K_2O comparing the volcanic rocks of Mount Persis samples with 623 analyses of Oligocene to Holocene Cascade-arc rocks from Washington. The high-silica Maltby sample is unit Φvt. Note that most Mount Persis samples have low K_2O compared to the younger arc rocks. **I.** Plot of Ba/Nb vs. SiO_2 comparing the volcanic rocks of Mount Persis samples with 623 analyses of Oligocene to Holocene arc rocks from the Washington Cascades. The high-silica Maltby sample is unit Φvt. Note that the Mount Persis samples have low Ba/Nb compared to most of the younger arc rocks.

Rocks assigned to the Mount Persis volcanics have also been mapped in six other nearby quadrangles, and a total of 104 samples have been chemically analyzed (Dragovich and others, 2008, 2009a,b, 2010a,b, 2011a,b, 2012, 2013). Collectively, these samples range from basalt to rhyolite, although the vast majority are basaltic andesites, andesites, and dacites (MacDonald and others, 2013; Fig. 6A). Most plot as low-K tholeiites (Fig. 6E), and as with the Maltby samples, straddle the boundary lines between calc-alkaline and tholeiitic (Fig. 6B). MacDonald and others (2013) recognized that some Mount Persis rocks have adakite affinities, which are indicative of derivation from an eclogitic source that is commonly assumed to be either the subducted slab or deep arc crust (Defant and Drummond, 1990; Martin and others, 2005). Distinctive chemical characteristics of adakites include high Sr (>400 ppm), low Y (<18 ppm), high Sr/Y (>20), low Yb (<1.8 ppm), high La/YbN (>10), high Al_2O_3 (>15 wt. %), and high Na_2O (>3.5 wt.%). None of the 104 Mount Persis samples have La/YbN > 10, but 25 of them (24% of total) have at least five of the other characteristics, and of these samples, most (22) are from either the Maltby or Lake Joy quadrangles. Almost 90 percent of the Mount Persis samples from the Maltby quadrangle have Al_2O_3 > 15, Sr/Y > 20, Y < 20 ppm, and Yb < 1.8 ppm, three of the most definitive adakite traits, but only one sample has >400 ppm Sr (Figs. 6F and C). Conversely, although adakites are less common among samples from the Lake Joy quadrangle (6 of 21 samples), these rocks have higher Sr (average 429 ppm), suggesting there are systematic geographic variations in the composition of Mount Persis rocks. Six U-Pb zircon dates for the Mount Persis volcanics span ~10 m.y. (~36–46 Ma) but provide no evidence of temporal changes in chemistry.

While the major and trace element compositions of the Mount Persis volcanics are typical of subduction-related magmatism, there are also subtle chemical distinctions between these rocks and the majority of Cascade-arc volcanics. The most notable of these are higher Al_2O_3 and Sr/Y and lower K_2O and Ba/Nb (Figs. 6F–I). The first two distinctions reflect the adakite affinities of the Mount Persis rocks and suggest slab melting could be involved in their genesis. Elevated Ba/Nb (>30) is characteristic of subduction-related magmas; the average ratio for 623 Oligocene to Holocene samples from the Washington Cascades is 49.2 (GeoRoc database at http://georoc.mpch-mainz.gwdg.de/georoc/ and Paul Hammond, written commun., 2003). Lower Ba/Nb among Mount Persis samples (average = 26.3), as well as their low K_2O contents, points to an immature arc setting (for example, newly established and [or] built on thin oceanic crust).

Unit Φvt tuff (site G3) is chemically distinct from the Mount Persis samples. It has higher SiO_2 (Fig. 6A), a more pronounced subduction signature (Figs. 6B and C), and a REE pattern with a large negative Eu anomaly (Fig. 6D). This tuff also lacks the adakite affinities that characterize the Mount Persis samples (see above).

Paleontology of Sedimentary Bedrock

Marine fossils collected from unit ΦEn from limited outcrops along Fiddlers Bluff and in the vicinity of Cathcart indicate a time period that spans the Eocene–Oligocene boundary. A sparse benthic foraminiferal species list from this study is shown in Table 1. The species *Cassidulina galvinensis* is temporally restricted, and other species are long ranging from the late Eocene through early Miocene or longer. The *Cassidulina galvinensis* biozone of western Washington (Rau, 1958, 1981) is correlated with the Refugian stage, defined in California (Mallory, 1959). In western Washington, this stage spans the Eocene–Oligocene boundary (Prothero and Armentrout, 1985) at 33.9 Ma. Marine molluscan fossils from unit ΦEn collected during and prior to this study from numerous localities along Fiddlers Bluff and in the vicinity of Cathcart are listed in Table 2 and the Data Supplement (DS8). The assemblage listed in Table 3 is characteristic of the *Echinophoria dalli* biozone of the

Table 1. Benthic foraminiferal species list from two localities in this study. Taxa with "sp." are identifiable only to the taxonomic level at which the label appears. Author citations with parentheses indicate that the respective taxon placements deviate from what was originally presented by the author.

Site ID	Genus and species	Taxonomy author
	Cassidulina galvinensis	Cushman and Frizzell, 1940
	Cassidulina pulchella	D'Orbigny, 1839
	Gyroidina condoni	Cushman and Schenck, 1928
	Haplophragmoides sp.	
GD21	*Melonis pompilioides*	(Fichtel and Moll, 1798)
	Pseudonodosaria obtusissima	(Reuss, 1863)
	Quinqueloculina imperialis	Hanna and Hanna, 1924
	Quinqueloculina weaveri	Rau, 1948
	Sigmoidella pacifica	Cushman and Ozawa, 1928
	Haplophragmoides sp.	
GD13	*Pseudonodosaria obtusissima*	(Reuss, 1863)
	Quinqueloculina weaveri	Rau, 1948

Table 2. Marine molluscan fossils from this study. Taxa with 'sp.' are identifiable only to the taxonomic level at which the label appears. Author citations with parentheses indicate that the respective taxon placements deviate from what was originally presented by the author.

Site ID	Genus and species	Taxonomy author
GD19	*Spisula packardi*	Dickerson, 1917
GD20	*Acharax dalli*	(Clark, 1925)
	Family Naticidae	Not identifiable to genus
GD21	*Bathymodiolus willapaensis*	
	Vulcanoides sp. *nov.*	
	Acharax dalli	(Clark, 1925)
	Lucinoma sp. *nov.*	
GD22	*Bathymodiolus willapaensis*	(Squires and Goedert, 1991)
	Lucinoma hannibali	(Clark, 1925)
	Conchecele bisecta	(Conrad, 1849)
	Pitar (Katherinella) arnoldi	(Weaver, 1916)
GD13 and GD16	*Martesia* in wood	

Table 3. Marine molluscan fossils from numerous localities with along Fiddlers Bluff and in the vicinity of Cathcart from previous studies. The assemblage is characteristic of the Echinophoria dalli biozone, Galvinian molluscan stage (Armentrout, 1975). Author citations with parentheses indicate that the respective taxon placements deviate from what was originally presented by the author.

Molluscan class	Genus and species	Taxonomy author
Gastropoda	*Molopophorus gabbi*	Dall, 1909
	Molopophorus stephensoni	Dickerson, 1917
	Priscofusus chehalisensis	(Weaver, 1912)
Bivalvia	*Nuculana washingtonensis*	(Weaver, 1916)
	Acila shumardi	(Dall, 1909)
	Nemocardium weaveri	(Anderson and Martin, 1914)
	Pitar dalli	(Weaver, 1916)
	Tellina townsendensis	Clark, 1925
	Thracia condoni	Dall, 1909
	Spisula packardi	Dickerson, 1917
	Mydesma dalli	Clark, 1922

Galvinian molluscan stage (Armentrout, 1975). The Galvinian stage is correlated with the Refugian benthic foraminiferal stage (Armentrout 1975; Prothero and Armentrout, 1985). Regionally, Unit ΦEn fauna in the Maltby quadrangle are similar to those of Lincoln Creek Formation type sections near Porter Bluff and Pe Ell in Mason and Lewis Counties, respectively (Armentrout, 1975), and outcrops of the Quimper Formation on the southeastern side of Discovery Bay in Jefferson County (Armentrout and Berta, 1977).

Molluscan and foraminiferal assemblages from unit ΦEn indicate that the depositional environment was inner to mid-shelf with cool water temperatures, in contrast to the shallow subtropical conditions described by Lindquist (1957). Most of the fossil localities have fauna indicative of an ecosystem created by seepage of cold methane from underlying sediment strata. Faunal and biochemical signatures of seeps are found in numerous late Eocene through Pliocene marine sedimentary units in western Washington (for example, Goedert and Squires, 1990; Peckmann and others, 2002; Kuechler and others, 2011). Only a few of these localities indicate prolonged fluid flow from the subsurface; most indicate diffuse and (or) intermittent seepage (Nesbitt and others, 2013). Cenozoic diffuse seeps in western Washington are characterized by the following bivalve mollusks: *Bathymodiolus willapaensis*, *Vulcanoides new species*, *Acharax dalli*, *Conchocele bisecta*, and *Lucinoma hannibali*. These fossils are not age-indicators. Fossilized wood that was bored by

'ship-worm' (clam genera *Martesia* and *Teredo*) and calcite-rich cemented concretions and nodules are common in these seep sites. Several areas along Fiddlers Bluff contain molluscan assemblages that do not indicate the presence of methane seeps (Table 3), and these assemblages are most similar to those of the lower Lincoln Creek Formation, Lewis County, Washington (Armentrout, 1975).

Geophysical Observations

We mapped two strong geophysical lineaments within the Maltby quadrangle on the basis of aeromagnetic and gravity anomalies (Fig. M2). Geophysical lineament A corresponds to an alignment of gravity max-spots defining a steep east–west-trending gravity gradient at the southern margin of a broad gravity low in the north end of the map area. This lineament highlights a marked northward decrease in subsurface densities and is spatially coincident with the southern edge of the Fryelands trough and the southern margin of the Everett basin (Fig. M1). Geophysical lineament B corresponds to the coincidence of max-spot-defined lineaments with both the aeromagnetic and gravity anomalies, yet anomalies individually extend beyond their collocation into neighboring quadrangles. Across geophysical lineament B, there is a pronounced decrease in subsurface densities and a strong increase in rock magnetism at depth toward the southwest.

Gravity values generally decrease from northeast to southwest across much of the quadrangle. Gravity contours across the center of the quadrangle roughly align with the measured strike of southwest-dipping sedimentary bedding in support of the thickening of Quaternary and Tertiary sedimentary strata toward the Seattle basin (Yount and others, 1985; Yount and Gower, 1991). Gravity contours form a northwest-trending gravity high under Lord Hill, where the relative densities diminish quickly to the northeast and southwest and gradually decrease in amplitude to the northwest. This ridge is broadly coincident with the location and orientation of the mapped Fiddlers Bluff anticline (see *Structure within the Map Area* below). To the west of the map area, this northwest-trending gravity ridge is roughly aligned with a broad east-trending gravity high termed the Kingston arch, described as an eastward-plunging anticlinal fold that delineates the northern margin of the Seattle basin (Gower and others, 1985; Yount, 1985; Johnson and others, 1994). To the east, this ridge broadens and is nearly coincident with previous geologic and geophysical mapping of the Monroe anticline (Dragovich and others, 2011a). A pronounced circular aeromagnetic high in the Snohomish River valley straddles the northern boundary of the Maltby quadrangle. This strong magnetic high does not coincide with a comparable gravity anomaly.

DISCUSSION

Tertiary Environments and Tectonics

Early Eocene deposition in the eastern Puget Lowland was dominated by nonmarine clastic extensional basins (Chuckanut Formation and correlatives) unconformably overlying the metamorphosed accretionary complex of the Mesozoic margin (Brown and Dragovich, 2003). From ~51 to 49 Ma, accretion of the Siletzia terrane disrupted these basins and re-organized the kinematic regime to that of regional strike-slip faulting, perhaps including the SWIF (Johnson and others, 1996; Brown and Dragovich, 2003) in western Washington (Wells and others, 2014; Eddy and others, 2015).

EOCENE MAGMATISM

A major magmatic and tectonic episode, known as the Challis event, is recorded between ~51 and 43 Ma across northwestern North America (Gaschnig and others, 2011). The Challis event was broadly contemporaneous with the accretion of Siletzia and the subsequent westward step of the subduction zone to its current location outboard of the accreted terrane. Several models have been postulated to explain this magmatism, including ridge subduction that produced a slab 'window' rollback, and (or) breakoff of the subducting slab, and potential interactions with the Yellowstone hotspot (Breitsprecher and others, 2003; Wells and others, 2014; Eddy and others, 2015; Tepper, 2016). Magmatism in western Washington during this time was compositionally diverse and likely reflects a rapidly changing tectonic framework, with melting of both mantle and crustal sources. Following reorganization of the subduction zone, the Cascade arc became active by about 42 Ma, generating more typical subduction-zone magmas characteristic of the modern arc (Tepper, 2016), although the timing of subduction-zone re-initiation is not tightly constrained. Eocene igneous rocks analyzed in this study have a subduction-zone signature, as well as elemental traits that suggest formation in a young arc. In particular, the adakite affinities are commonly associated with anomalously hot (young) subduction zones, and the low Ba/Nb ratios suggest an immature arc (see *Geochemistry*). We suggest that samples of the Mount Persis volcanics in the Maltby quadrangle (~44 Ma) represent some of the earliest known rocks of the nascent Cascade arc. More broadly, the temporal, petrologic, and geochemical diversity of the volcanic rocks of Mount Persis (47–36 Ma, MacDonald and others, 2013) may record the transition toward typical Cascades magmatism by mid- to late Eocene time. Although we could not discern any temporal geochemical trends within the existing Mount Persis dataset, future investigations with additional chronology may be able to identify compositional trends that document the evolution of the arc over time.

Geologic mapping of the volcanic rocks of Mount Persis to the east and southeast describes a broad southwestward thickening of clastic deposits, and a northeastward coarsening of clastic material, suggesting a volcanic source to the east (Dragovich and others, 2010a,b, 2011a; 2012; MacDonald and others, 2013). East of the Maltby quadrangle, a significant proportion of the clastic material interbedded with volcanic rocks is interpreted as fluvial flood-plain deposition contemporaneous with igneous activity (Danner, 1957; Dragovich and others, 2010a,b, 2011a). We classify flows and coarse clastic deposits in unit Ev_p within the Maltby quadrangle as volcanic core facies and proximal volcaniclastic facies, following Vessell and Davies (1981). Proximal volcanic facies indicate an additional volcanic source for the volcanic rocks of Mount Persis farther west than previously postulated.

NATURE OF THE CONTACTS BETWEEN TERTIARY UNITS

We infer that the unexposed contact between sedimentary rocks west of the Snohomish River (units ΦEc and ΦEn) and underlying volcanic rocks of Mount Persis (Evp) is disconformable on the basis of:

1. Relative ages of the two units.
2. Two water well logs (W21, W24) that appear to show penetration through overlying sedimentary rock into igneous bedrock below sea level just west of the Snohomish River. However, we note that water wells were not logged by trained geologists, and thus lithologic descriptions are not dependably accurate.
3. Interpretations of the Socal Schroeder oil well located west of the map area (Fig. M1). Rau and Johnson (1999) infer from drilling records that Oligocene and Eocene sedimentary rocks overly the volcanic rocks of Mount Persis.
4. Bedding orientations in the sedimentary rocks indicate that they are folded into a gently west-plunging, upright anticline such that bedding in sedimentary units consistently dips away from the upland exposures of unit Evp on Lord Hill in the core of the anticline. Sedimentary bedrock is exposed north and northeast of the current map area (~1.5 mi east of the town of Snohomish), and the closest bedding measurement dips to the north (Newcomb, 1952, plate 1; Minard, 1985b). We infer from these exposures that, within the Maltby quadrangle, north-dipping sedimentary strata floor the Fryelands trough. This notion is supported by geophysical inferences (see *The Monroe Fault and Anticline*). In unit Evp, volcaniclastic bedding and igneous flow layering are sparsely exposed and likely do not reflect true original horizontality; however, we infer that layering in unit Evp is broadly parallel to bedding in the overlying sedimentary rock. Without constraints of the orientation of the contact, we were unable to determine an angular relationship that would reflect either a paleotopographic onlap (buttress unconformity) or tectonic tilting prior to deposition of the sedimentary bedrock.

Our interpretation of a depositional contact is consistent with mapping and descriptions of McKnight and Ward (1925), Newcomb (1952), Danner (1957, p. 479), Capps and others (1973), Minard (1985a), Yount and Gower (1991), and Dragovich and others (2010b, 2011a) and geophysical inferences by Sherrod and others (2008) and Anderson and others (2015). We consider the possibility that the contact is conformable; such a relationship has been described for the contact between the Renton Formation and the underlying Tukwila Formation near Issaquah south of the current map area (Vine, 1962; Booth and others, 2012). These formations are potentially contemporaneous with units ΦEc and Evp, respectively. Without direct age control at the base of unit ΦEc, we were unable to quantify an age gap represented by the contact and instead relied on chronology from higher in the stratigraphic section. Alternatively, the contact between these two units may be a northwest-trending fault through the Snohomish River valley (as postulated by Sherrod and others (2008) and Dragovich and others (2011a), see *Structure Within the Map Area*, below). We defer to the simpler explanation of a depositional relationship as described above.

OLIGOCENE–EOCENE SEDIMENTATION

The mid-Tertiary sedimentary rocks of unit ΦEc and ΦEn exposed along the west bank of the Snohomish River record a transition from continental to marine sedimentation. The stratigraphically lowest known exposures of Oligocene to Eocene sedimentary rocks in the Maltby quadrangle contain terrestrial plant fossils and sparse, discontinuous coal stringers indicating a continental depositional environment. Sedimentary structures suggest fluvial deposition (see unit ΦEc in the *Description of Map Units*). No chronology exists for unit ΦEc, although we are able to bracket the age between the ~44 Ma U-Pb age of underlying unit Evp (site GD28) and the overlying Refugian stage marine strata of unit ΦEn. Rau and Johnson (1999) tentatively correlated fossil-barren strata beneath Eocene–Oligocene (Refugian, 35–33 Ma) horizons found in the Socal Schroeder No. 1 well to the Renton Formation of the Puget Group.

Sedimentary rocks of unit ΦEn bearing Refugian stage foraminifera and Galvinian stage mollusks within upper stratigraphy exposed in the Maltby quadrangle mark a transition to marine depositional environments. McKnight and Ward (1925) used these exposures to describe a marine transgression that they considered upper Oligocene. Our biostratigraphic interpretations refine this event to the late Eocene or earliest Oligocene. Rau and Johnson (1999) indicated that thick packages of coal interbedded with marine sandstone- and siltstone-bearing Refugian foraminifera in the Socal Schroeder No. 1 well suggest fluctuating nonmarine and shallow marine environments, with progressively deepening water recorded upsection into Zemorrian stage strata. From the poorly exposed contact relations, we speculate that deposition of unit ΦEn and upper portions of unit ΦEc in the quadrangle may have been contemporaneous and that their stratigraphic positions may largely be a function of lateral facies gradation at the margin of a Tertiary basin. The new U-Pb age of ~28 Ma for unit Φvt near the uppermost exposures of unit ΦEn roughly corresponds to the early–late Oligocene boundary. Thus, rocks stratigraphically below this sample are early Oligocene or older, and strata above this bed are late Oligocene or younger.

Abundant tuffaceous sediment in the Oligocene–Eocene section suggests deposition proximal to an active Cascade arc. Volcanic clasts of intermediate composition in units ΦEc and ΦEn appear to corroborate this interpretation, but could have been eroded from inactive volcanic deposits of unit Evp. Well-preserved glass shards within the vitric tuff of unit Φvt suggest minimal reworking in a low-energy, arc-proximal setting. Unit Φvt geochemistry is consistent with volcanic units typical of the Oligocene Cascade arc (Fig. 6).

In contrast to correlations drawn by previous workers (Weaver, 1912, 1916; Lindquist, 1957), we posit that much of the marine stratigraphic section in the Maltby quadrangle is older than marine strata of the Blakeley Formation at its type section on Bainbridge Island (Fulmer, 1975). At the type section, Fulmer assigned the Blakeley Formation to the Refugian and

Zemorrian benthic foraminiferal stages, but recent reassessment of these exposures assigns them to Zemorrian and Saucesian stages (Prothero and Nesbitt, 2013). The biostratigraphic correlation of our samples to the Refugian and Galvinian stages suggests that unit ΦEn is older than the marine portions of the Blakeley Formation. Overlap of a 31.6 ±2.1 Ma fission-track age near the base of the Blakeley type section (Sherrod and others, 2002) and our date of ~28 Ma from unit Φvt (GD27; stratigraphically above the fossiliferous exposures of unit ΦEn) suggests that the deposition of these sedimentary rocks was in part contemporaneous.

Dragovich and others (2010a,b) reported a 16 to 20 Ma age range for a sample from site 09-54Z, collected from poorly exposed outcrops in the southeast corner of the Maltby quadrangle (their unit Mvc). However, they considered this age interpretation tentative, and we suggest that a more statistically appropriate depositional age for the sample is several Ma older in the late Oligocene (Appendix C). If the sample is indeed Miocene, it would represent the youngest known exposed sedimentary rock on the northeast edge of the Seattle basin. We agree with Dragovich and others (2010a,b) in the interpretation of these outcrops as the product of subaerial continental deposition with significant volcanic input, likely in a fluvial or deltaic environment. Rare carbonized detritus and leaf fossils are found near the upper strata of unit ΦEn and, together with the outcrops mentioned above, may suggest a return to nonmarine conditions in the late Oligocene or early Miocene. Miocene rocks found elsewhere in the Puget Lowland record terrestrial sedimentation and volcanism, but exposures are few and far between (Dragovich and others, 2009a,b; 2010a,b; 2015; Fulmer, 1975; Yount and Gower, 1991; Sherrod and others, 2002; Booth and others, 2012).

Quaternary Deposits

Limited surface exposures and the relatively few sufficiently deep boreholes interpreted for this study provide poor constraints on the geometry of Vashon and pre-Vashon deposits. Elevation is not a good indicator of relative age (Troost, 2006), as we expect that younger deposits likely incise older material. Complex pre-Vashon paleotopography and lateral discontinuity complicates geotechnical and hydrogeologic investigations, and these deposits are often convoluted beyond the resolution of typical borehole studies. We refer the reader to a comprehensive discussion of paleotopography, unconformities, and spatial predictability of Vashon and pre-Vashon sedimentation in the region by Troost (2006).

POSSESSION-AGE (MIS 4) OR OLDER DEPOSITS

The oldest Quaternary deposits in the quadrangle are Possession-age or older glacial deposits, on the basis of stratigraphic position relative to dated material. The stratigraphically lowest deposit with a finite date is from a well-sorted sand (unit Qps) with luminescence ages of about 65 ka (site GD7, Appendix B) at the base of the unit and 53 ka (site GD9, Appendix B) at the top of the unit (schematic columnar section CS1, map sheet). At the base of unit Qps, we observed a sharp, undulating contact with a weakly stratified diamicton (unit Qpu) that has a radiocarbon-infinite age (>43,500 yr BP; site 10-28D). Dragovich and others (2011b) interpreted a nonglacial origin for unit Qpu at this location. However, we agree with the prior mapping of Capps and others (1973) and Minard (1985a) that the underlying diamicton (unit Qpu) is indicative of glacial conditions. With no finite date from units Qpt or Qpu, we are unable to determine if they are Possession-age deposits as tentatively suggested by Capps and others (1973) and Minard (1985) or if the deposits reflect an older glacial episode.

The overlying well-sorted sands of unit Qps we interpret as either recessional outwash or nonglacial fluvial deposits from the end of the Possession glaciation. In either case, it appears that the ~65 ka date obtained from the base of unit Qps (site GD7) provides a rough minimum age for the retreat of the Possession glaciation in the Maltby quadrangle. Error values (~3,700 yr) of the analysis place this minimum age roughly coincident with ages previously reported that bracket deposits of the Possession glaciation between 76 and 61 ka (Troost, 2016) and the global MIS 4 cooling stage from 71 to 57 ka (Lisiecki and Raymo, 2005). Recent geochronological work indicates that Possession-age glacial deposits extend as far as the latitude of Tacoma, well south of the Maltby quadrangle (Troost and others, 2003; Booth and others, 2015; Troost, 2016).

DEPOSITS OF MIS 3 AND EARLY MIS 2

The oldest dated deposits of the MIS 3 nonglacial period in the Maltby quadrangle are exposed in bluffs along the western boundary of the Snoqualmie River valley (schematic columnar section CS1, map sheet). The ~53 ka age from age site GD9 in unit Qps, collected about 1 m (3 ft) below the upper contact, indicates that this unit extends into early MIS 3. A new luminescence date of ~31 ka in the lower part of unit Qcg_o (site GD8, Appendix B) suggests a notable time gap between deposition of units Qcg_o and Qps, and the sharp lithologic contrast between units Qcg_o and Qps appears to mark an unconformity. A radiocarbon date from unit Qcg_o of 28.140–27.810 ka (age site GD5) supports its correlation with the latter half of MIS 3; a luminescence date of ~21 ka (age site GD10) indicates that the unit may extend into early MIS 2 (~25 ka according to Siddall and others, 2008).

Deposition of unit Qc_o broadly followed that of unit Qcg_o in the Maltby quadrangle as suggested by new radiocarbon ages (Appendix C), though a luminescence date from age site GD10 from unit Qcg_o indicates some temporal overlap. Relative to unit Qcg_o, exposures of unit Qc_o extend to much lower elevations (43 ft above modern sea level, see unit description), suggesting an incised stratigraphic relationship, but are locally gradational and interfingering (CS1, map sheet). However, poor exposure of stratigraphic relations between these units precludes a detailed interpretation of the contact between them. Contrast between the meandering-stream-dominated facies represented by unit Qc_o and the braided-fluvial deposits of unit Qcg_o suggests a temporal transition from a high- to low-gradient fluvial system.

We propose that the terraced stratigraphic relationship and temporal transition from high- to low-energy fluvial facies represented by these units reflects the deposition of an outwash plain emanating from the Cascades during the Evans Creek stade and records a transition from proximal-intermediate to distal facies as described by Benn and Evans (2010, section 11.5.1). Alpine glaciations marking the initiation of the Evans

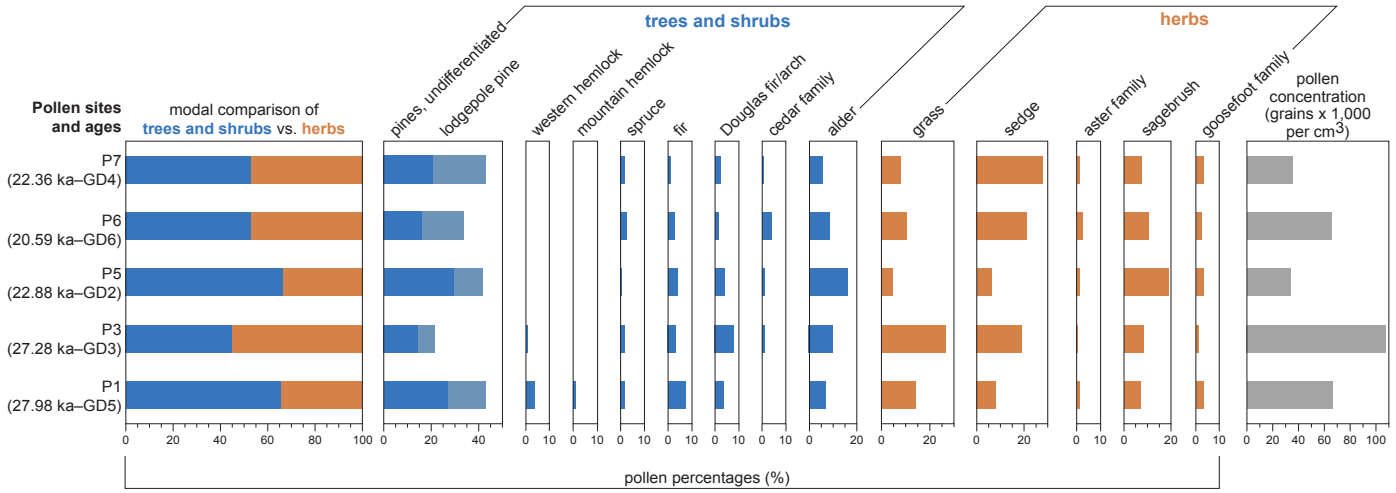

Figure 7. Pollen diagram for organic-rich sediment samples from the Maltby quadrangle. Two sites (P2 and P4) are not displayed on this figure due to insufficient pollen content. Ages for pollen sites are constrained by radiocarbon age sites from this study and are presented in calibrated calendar years. Pollen analysis by Erin Herring, University of Oregon.

Creek stade reached their maximum limits in the upper Skagit River valley to the north by 30 ka and remained there for nearly 10 ka, roughly coincident with similar events across mountain ranges in northern Washington and southern British Columbia as summarized by Riedel and others (2010, fig. 8).

These regional alpine glacial events are roughly contemporaneous with deposition of units Qco and Qcgo in the Maltby quadrangle and would be capable of providing the necessary sediment to the Puget Lowland. In surficial geologic mapping to the east, Booth (1990) correlated younger alpine drift in most drainages along the western front of the Cascades with the Evans Creek stade. Booth additionally noted that the western extent of these alpine glacial deposits is obscured, particularly by the subsequent incursion of Vashon ice. Low-energy fluvial and lacustrine deposits of similar age have been identified above modern sea level as far west as the Lofall area, where Contreras and others (2013) postulated a possible connection with Olympic alpine glaciations to explain the depositional elevations in light of sea levels being roughly 80 to 100 m (262–328 ft) lower during MIS 3 time (Yokoyama and Esat, 2011).

Pollen analyses (sites P1, P3, and P5–P7) generally suggest a cooler-than-modern climate during late MIS 3 and early MIS 2 time (Fig. 7; Erin Herring, Univ. of Oregon, written commun., 2016), as others have found in deposits of similar age (Riedel and others, 2010; Polenz and others, 2016). The ages of deposits hosting these pollens are roughly contemporaneous with dated alpine glaciations and associated deposits surrounding the Puget Lowland (Riedel and others, 2010; Polenz and others, 2016). Cooler climates in the Puget Lowland during late MIS 3 and early MIS 2 time likely initiated regional alpine ice advances, which may have increased the sediment supply to the Maltby quadrangle, contributing to the deposition of units Qco and Qcgo.

Although alpine glaciations are an attractive mechanism to explain the elevations, stratigraphic relations, and facies represented in units Qco and Qcgo, limited exposure inhibits confident correlation. Compilation of existing age control in similarly aged deposits and examination of the associated sedimentary sequences would be a great opportunity for future efforts to better understand the sequence of events surrounding the transition from MIS 3 to MIS 2 in the Puget Lowland.

VASHON GLACIAL AND POST-GLACIAL CONDITIONS

The transition from pre-Vashon nonglacial to Vashon advance outwash deposition in the map area is difficult to define and is locally considered a conformable contact between similar sedimentary facies (Minard, 1985a; Booth, 1990). All geochronologic ages collected for this study predate Vashon-age deposits, but glaciolacustrine deposits provide the earliest textural evidence for glacial sedimentation in the map area. As the ice sheet moved southward, it impounded drainage, both regionally and locally, resulting in proglacial lacustrine deposition of extensive layers of laminated silt and clay (Troost and Booth, 2008)—the Lawton Clay of Mullineaux and others (1965). We identified rhythmically bedded, sorted silt and clay deposits (unit Qgaf)—deposited in what we interpret as glacially dammed lakes that formed as Vashon ice advanced southward. Many outcrops in unit Qgaf contain evidence for iceberg-rafted debris, such as dropstones. Such observations suggest that these lakes were glacially dammed with a nearby ice margin in contrast to the Lawton Clay, where only rare evidence exists for ice-rafted debris (Troost and Booth, 2008). As the ice sheet continued to advance southward, deposits generally coarsened upward from distal lacustrine fines (units Qgaf and Qgas) to proximal sand-and-gravel-dominated fluvial outwash (unit Qga) emanating from the ice front.

Vashon ice reached the latitude of the Maltby quadrangle at roughly 18 to 17 ka during MIS 2 (Porter and Swanson, 1998, fig. 3a; Booth and others, 2004, fig. 9; Polenz and others, 2015, fig. 3). Ice arrival in the quadrangle is indicated by deposition of lodgment till often marked by a sharp erosional contact with the underlying deposits. Megascopic flute features and drumlins in the map area indicate that ice-flow directions ranged from azimuth 158° in the northeastern part of the map area to 171° in the southwest. Glacial till at or below the elevation of Fryelands trough and modern river valleys suggests that these troughs

existed subglacially, where meltwater would be a likely erosive mechanism as suggested by Booth (1994).

Geomorphic evidence in the map area suggests that ice melted in-situ rather than as a north-receding front of actively south-flowing ice, similar to suggestions made by Haugerud (2009a,b, 2010, 2014). Distinct recessional moraines are not found in the quadrangle, and geomorphic relations signify a melting ice front that was not actively south-flowing. Several meltwater channels appear to have formed from subglacial meltwater under stagnant ice. North of Cottage Lake, a deep U-shaped subglacial channel is sharply incised into drumlinized terrain. There is no modern stream sufficient to carve such a channel, and sharp channel margins indicate stationary ice. This channel grades southward into a broad, terraced plain at Cottage Lake. We posit that the broad surface of outwash deposits there precluded subglacial deposition of flowing ice. A similar sequence of deposits can be found north of this channel (secs. 19 and 30, T27N R6E). There, the outwash terrace transitions southeastward into a broad hummocky trough with kettled topography that hosts modern lakes and peat bogs.

Booth (1990) provides a comprehensive discussion of local evolution of recessional-lake drainage patterns as ice receded along the eastern margin of the Puget lobe, east and south of the map area. Similar to Booth's findings, we noted evidence of several recessional lake elevations across the map area. Convex terraced landforms, composed of recessional outwash, perched on the west bank of the Snohomish River valley at about 340 ft elevation, and on the north end of Lord Hill, sharp incisions terminate between 230 and 122 ft elevation, suggesting intersection with a body of water at those elevations. Evidence for the latest phase of glacial recessional sedimentation is in the Fryelands trough in the northeast corner of the Maltby quadrangle. Mapping by Dragovich and others (2011) to the east identified alluvial deposits sharing the same broad valley floor as deltaic recessional outwash (the 'Monroe fan'). Lidar shows the topographic continuity of this broad surface to the northeast across highway-modified land into Woods Creek valley (Fig. M1), which is filled with terraced recessional outwash (Dragovich and others, 2015). We suggest that the modern Woods Creek is an underfit stream occupying a valley that carried substantial glacial meltwater in the latest phase of ice recession. The gradational surface between recessional terrace elevations in Woods Creek and the Fryelands trough suggests that the modern topography is a relict recessional feature and that Holocene alluvial processes have had only a minor influence on this landscape.

Immediately following ice retreat, marine waters filled isostatically depressed lowlands of former subglacial meltwater pathways. Thorson (1989, fig. 6) postulated 100 to 110 m (328–361 ft) of net vertical uplift in the Redmond area. There is limited evidence that post-glacial marine incursion may have advanced up the Snohomish River as hypothesized by Thorson (1981, fig. 22). Although glaciomarine deposits were not directly recognized during the field investigation, "sea shells" in sediment (at elevations of -42 to -49 ft) beneath modern alluvium and directly over strata identified as "glacial till" were logged in a borehole record (B6) under the SR522 bridge at the center of the Snohomish River. Dethier and others (1995) described a stratigraphic section (≤56 ft elev.) of glaciomarine sediment in the Marysville area (Fig. M1) dated to 13,300 ±50 ^{14}C yr BP. By correlating regional elevations of marine deposits, they showed that the marine limit reached ~100 ft in the lower reaches of the Snohomish River valley near Everett. If recessional glaciomarine deposits exist in the Maltby quadrangle, they are covered by Holocene alluvium that has since filled the lowest-elevation river valleys.

Modern depositional and erosional processes in the major river valleys are affected by river modification and artificial levees along the lower reach of the Snohomish River that restrict meander paths and natural erosional patterns via rip-rap and other preventative measures. Much of unit Qa has been modified for agricultural use. We follow Bethel (2004) and infer that wetlands were much more extensive prior to human influences. Collins and Sheikh (2002) reported that in the year 2000, valley wetlands covered 19 percent of their pre-settlement extent. Oxbow lakes along the lower Snoqualmie River had disconnected from the main stem by the time of the first surveys in the 1870s (Collins and Sheikh, 2002).

Postglacial landslides and mass-wasting deposits in the quadrangle are concentrated on valley walls where rivers erode into the glacial stratigraphy. Many landslides in the quadrangle are spatially associated with the contact between relatively permeable Vashon advance outwash and less permeable deposits below, similar to trends described by Tubbs (1974) and Laprade and others (2000). Minor springs and groundwater seepage are often coincident with mapped landslides proximal to the aforementioned contact.

Structure within the Map Area

FIDDLERS BLUFF ANTICLINE

History, Location, and Geometry

In the northern half of the Maltby quadrangle, we mapped the informally named 'Fiddlers Bluff anticline', which deforms Oligocene to Eocene sedimentary units ΦEc and ΦEn and underlying volcanic rocks of Mount Persis (unit Evp). McKnight and Ward (1925) provided the first known description of folded sedimentary strata near Cathcart and noted a west-plunging anticline that they named the "Devil's Mountain anticline". Lindquist (1957) described in detail exposures along the railroad at Fiddlers Bluff, a name in use since the publication of Weaver (1912). Gower and others (1985) and Yount and Gower (1991, plate 1) also mapped an anticline that extended eastward through Bald Hill, projecting outside their map area near Monroe. We abandoned the name given by McKnight and Ward (1925) because: (1) there is possible confusion with the Darrington–Devils Mountain fault zone and associated structures to the north, (2) the name 'Devils Mountain' has fallen out of use and that landmark is now formally named Lord Hill, and (3) fold geometry is best constrained by outcrops in the railroad cuts along Fiddlers Bluff. To the east and west of these exposures, the mapped fold trace is poorly constrained.

The calculated hinge line and axial plane indicate that the Fiddlers bluff anticline is upright and gently west-northwest-plunging, with a subvertical axial surface and a gentle interlimb angle (Fig. 8; cross section A–A′). Bedding dip angles

are somewhat steeper on the north limb than the south and form a sharp hinge over a distance of ~5 m (~16 ft).

The northwest-trending isostatic gravity high (see *Geophysical Observations*) independently suggests the existence of a major antiformal bedrock structure in the subsurface of the quadrangle. The Fiddlers Bluff anticline hinge line is mapped to the north of this gravity ridge, and we suggest that this deviation could indicate a southern dip of the axial surface, as the gravity data represent geophysical conditions at depth, although other explanations are possible for the lack of spatial correlation. The strong gravity high implies that this fold is cored with dense bedrock. On cross section A–A′, we tentatively place the relatively dense rocks of the WMB (unit KJm$_W$) in the core of the Fiddlers Bluff anticline on the basis of mapping to the east that shows these rocks underlying the volcanic rocks of Mount Persis (Dragovich and others, 2010a). We suggest that future geophysical modeling with high-resolution gravity data could better constrain the subsurface geometry of this fold.

We agree with Yount and others (1985) and Sherrod and others (2008) that the strong magnetic high along the northern boundary of the quadrangle is most easily explained by the presence of concealed volcanic rocks of Mount Persis. We further suggest that this magnetized body lies at depth below low-density sedimentary rock on the basis of the low gravity values and thick sedimentary strata encountered in oil and gas wells to the northeast (Fig. M1).

Timing and Tectonic Interpretations

Stratigraphic relations constrain the age of the Fiddler's Bluff anticline from late Oligocene to the Pleistocene. Due to limited exposure, we were unable to assess changes in thickness of units ΦEc and ΦEn across the Fiddlers Bluff anticline. If sedimentary units thin across the fold hinge, that might suggest fold-related uplift of unit Evp and older units prior to the deposition of the younger sedimentary strata. There is some poorly exposed outcrop-scale folding in Quaternary strata overlying Tertiary bedrock in the area of Fiddlers Bluff (significant site S3). However, evidence for tectonic folding is equivocal, and we cannot rule out a glaciotectonic origin for the observed deformation.

The fold's orientation indicates a north-northeast subhorizontal direction of maximum shortening (Fig. 8). This direction is consistent with observed GPS-derived horizontal velocities in the Puget Sound region (McCaffrey and others, 2007, 2013). We postulate that this structure could be a surface expression of faulting at depth, either propagation folding above a blind reverse fault or a fault-bend fold above a detachment reverse fault, comparable with kinematic models proposed by Brocher and others (2005). We note that some earthquake epicenter locations are spatially associated with geophysical lineament A and the Fiddlers Bluff anticline (Fig. E1), though lack of a systematic orientation of focal mechanisms prevents a clear interpretation of kinematics (Appendix E; DS9).

Analogous structural features have been mapped elsewhere in the Puget Lowland, such as the Kingston arch, an east-plunging anticline directly west of the Maltby quadrangle (see *Geophysical Observations*). Isostatic gravity and seismic reflection imagery (Gower and others, 1985; Johnson and others, 1999) show that it crosses Puget Sound from Kingston to the Edmonds area (Fig. M1; Gower and others, 1985). The Kingston Arch is asymmetric, with a steeply south-southwest dipping axial surface (Pratt and others, 1997). Several workers have suggested Quaternary (Gower and others, 1985; Pratt and others, 1997; Brocher and others, 2001; ten Brink and others, 2002) or Neogene (Johnson and others, 1994) activity along the Kingston arch on the basis of patterns of young strata and microseismicity, although this inference is poorly constrained. Several geometric interpretations exist for the Kingston arch in the literature. A fault-bend fold model was put forth by Pratt and others (1997), where the Kingston arch reflected a bend in a deep thrust-sheet detachment. Alternatively, they thought that the arch could be the result of fault-propagation folding from a

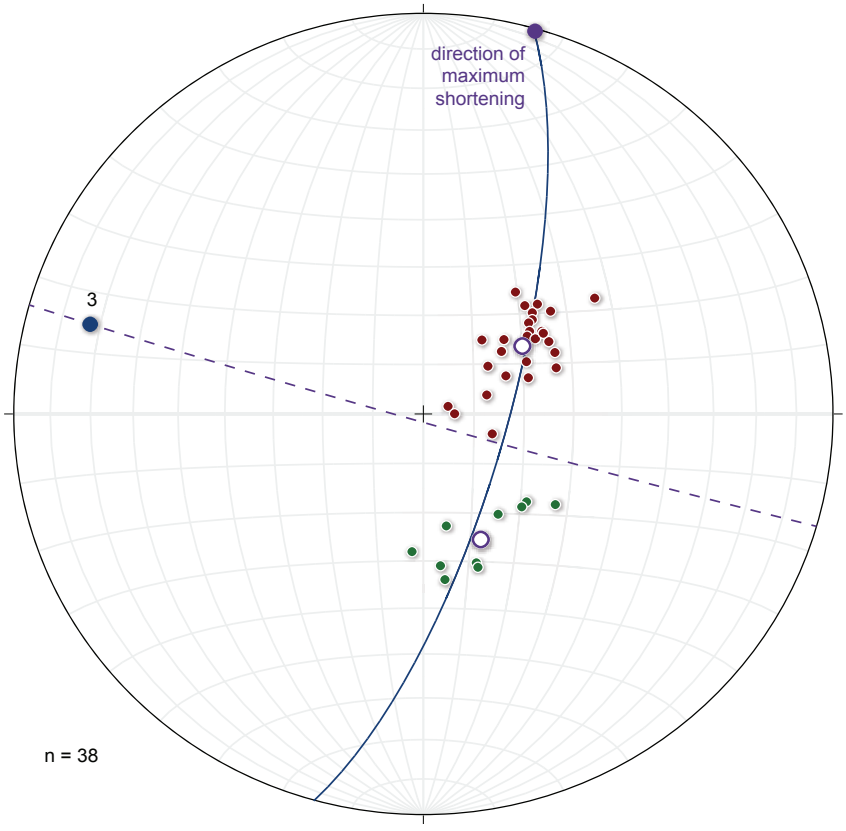

Figure 8. Stereonet of poles to bedding measurements from units ΦEc and ΦEn across the Fiddlers Bluff anticline (n = 38) plotted using Richard W. Allmendinger's 2011–2015 Stereonet © software (Allmendinger and others, 2013; Cardozo and Allmendinger, 2013; pdf file output per 2004© of Toby W. Rush). Exposures provided more measurements on the shallowly dipping south limb (red points) than on the steeper-dipping north limb (green points). A Bingham axial distribution analysis gives the cylindrical best-fit plane (solid navy line). Bingham axis 3 (navy point) suggests a fold hinge line trending 286° west-northwest and plunging 17°. Fischer mean vectors for each limb (hollow purple points) give an interlimb angle of 140°. Poor outcrop prevented direct measurement of the fold's axial plane. A calculated axial plane (dashed purple line) is oriented 106/89 SW and the pole to this plane plunges shallowly to an azimuth of 16° (purple point), our interpreted direction of maximum shortening.

blind thrust fault. More recent work (ten Brink and others, 2002) has supported this interpretation.

We note geometric and kinematic similarities between the Fiddlers Bluff anticline, Kingston arch, and Monroe anticline (discussed below)(Fig. M1), though we feel that existing data is insufficient to confidently correlate the structures. Between the seismic lines that constrain the Kingston arch and folded bedrock exposures in the Maltby quadrangle is a ~20 km (12 mi)-wide exposure gap of Quaternary cover (Fig. M1). Several studies have postulated that strands of the SWIF transect this area, although the amount of offset is unknown (see *The Southern Whidbey Island Fault Zone*, below). Future geophysical work could give insight to the complicated structural relations at the intersection zone of the Fiddlers Bluff anticline, SWIF, and Kingston arch.

THE MONROE FAULT AND ANTICLINE

The Monroe fault and anticline are a related set of east-west-trending structures mapped to the east by Dragovich and others (2011a, 2013) that project westward into the Maltby quadrangle. The existence of the Monroe fault was inferred because pre-Fraser nonglacial deposits are found at different elevations across the Skykomish River valley. Mapped traces of both these structures were largely defined by geophysical lineaments. Where traceable at the surface, the Monroe anticline and syncline are best described as gentle map-scale folds of bedding in Quaternary deposits (Dragovich and others, 2011).

Geophysical lineament A marks an east-west-trending gravity gradient that projects east of the Maltby quadrangle (Figs. M1, M2) toward similar geophysical lineaments that have been used by Dragovich and others (2011a, 2013) to map the surficial trace of the Monroe fault and anticline. In the Maltby quadrangle this gradient likely reflects density contrasts across a north-dipping contact between units ΦEc and Evp that may be either a depositional contact on the north limb of the Fiddlers Bluff anticline, a fault between the two units, or a combination of both. Following any of these interpretations, the Fiddlers Bluff anticline could merge eastward with the Monroe anticline, and we would expect sedimentary bedrock to underlie the Quaternary cover to the north of Lord Hill. Recent reinterpretation of geophysical data by Dragovich and others (2015, fig. 1) suggests that the trace of the Monroe anticline may be located significantly farther northwest than originally described by Dragovich and others (2011a, 2014b). However, no outcrops within the western part of the Monroe quadrangle support extending these structures into the Maltby quadrangle. Fewer than ten bedrock measurements constrain the Monroe anticline in the Monroe and Sultan quadrangles combined (Dragovich and others, 2011a, 2013). No dataset exists to compare our stereonet analysis of the Fiddlers Bluff anticline to the Monroe anticline. It is not possible to trace the structures with geologic mapping across the ~14 km (9 mi) gap between Fiddlers Bluff and the closest mapped exposures of the Monroe anticline southeast of Monroe. Additionally, many concealed cross-cutting faults have been postulated in the intervening area (Dragovich and others, 2011a, 2015) that may have offset the anticlines in unknown ways. For these reasons, we refrain from correlating the Fiddlers Bluff anticline and the Monroe anticline.

We use our mapping of the Fiddlers Bluff anticline, volcanic bedrock on Lord Hill, and geophysical lineament A to support the view of Dragovich and others (2015) that more evidence supports the possible western extension of the Monroe fault to the north of Lord Hill than to the southeast as was originally postulated by Dragovich and others (2011a). However, we do not map the Monroe fault north of Lord Hill because there are no map relations in the quadrangle that require the presence of a fault, and geophysical lineaments that could delineate a fault trace have alternative explanations.

THE SOUTHERN WHIDBEY ISLAND FAULT ZONE

We show strands of the SWIF within the Maltby quadrangle corresponding to Sherrod and others' (2008, figs. 12, 14) topographic and geophysical lineaments—the Grace, Little Bear Creek, and Cottage Lake lineaments. On the basis of paleoseismic trenching, they concluded that these lineaments are active fault strands. The southwesternmost strand of the SWIF in the Maltby quadrangle corresponds to the convergence of the Little Bear Creek and Grace lineaments. The Little Bear Creek topographic lineament projects southeastward to the western Maltby quadrangle boundary, though the partially collocated aeromagnetic lineament extends farther to the southeast into the Maltby quadrangle and merges with the Grace topographic lineament. New isostatic gravity data (Anderson and others, 2015) identified a weak anomaly that corresponds with the location of the Little Bear Creek lineament of Sherrod and others (2008), along with several lineaments they interpret as steeply dipping west-side-down faults. We agree that lower gravity to the southwest suggests west-side-down offset consistent with interpretations of Sherrod and others (2008) for the southwestern fault strand mapped in the Maltby quadrangle. The northeasternmost fault strand of the SWIF in the Maltby quadrangle corresponds to the Cottage Lake lineament. Field exposures in the Maltby quadrangle did not indicate the sense of offset of these strands of the SWIF beyond the interpretations of Sherrod and others (2008); thus we do not show relative offset across the mapped strands (cross section A–A′).

The topographic lineaments identified in the Maltby quadrangle are very subtle in comparison to other fault scarps in the Puget Lowland with demonstrated post-glacial activity (for example, Sherrod and others, 2003, 2004; Nelson and others, 2003). This could be a reflection of: (1) strike-slip deformation on the SWIF that does not create vertical topographic offset, (2) the broad, multi-strand nature of the SWIF, where each strand partitions a relatively small amount of strain, (3) low regional strain rates affecting the SWIF as a whole (McCaffrey and others, 2007, fig. 11), (4) human development activities that have obscured lineament traces, or (5) possible non-tectonic origins for these lineaments. We further note that Sherrod and others (2008) identified many other lineaments in aeromagnetic data that are not as well constrained by trenches, topographic scarps, or seismic lines.

Geophysical lineament B, where the collocated gravity and aeromagnetic data suggest a significant subsurface discontinuity, may be related to faulting along the SWIF. The much lower isostatic gravity values suggest that low-density deposits are thicker on the southwest side of this lineament. We believe that

geophysical lineament B potentially signifies a geologic structure that has offset lower-density sedimentary strata down to the southwest, consistent with modeling by Anderson and others (2015). Sherrod and others (2008) speculated that this magnetic lineament could mark a southwest-dipping blind reverse fault. Our interpretation of isostatic gravity data appears to indicate the opposite sense of slip. Detailed geophysical modeling is warranted to better constrain kinematics of this possible structure.

In stream exposures between fossil sites GD18 and GD19 at the northwestern termination of geophysical lineament B, unit ΦEn sedimentary bedrock is heavily jointed with closely spaced, steeply dipping joints striking subparallel to the trend of this geophysical lineament (map sheet). Additionally, there is a 5 m (16 ft)-tall vertical waterfall surface in the stream channel parallel to the strike of the heavily jointed bedrock at fossil site GD19. Roughly 150 m (492 ft) to the northwest, during road construction along Broadway Ave., heavily sheared bedrock with similarly striking fractures were temporarily exposed (Kathy Troost, Univ. of Washington, written commun., 2017). This deformation may be related to the SWIF, as the features described above are oriented similarly to what would be expected along this fault zone. Strong concentric weathering, along with the massive bedding texture typical of this unit obscure possible separation across jointed surfaces. A more detailed examination of these exposures may shed light on relating this bedrock deformation to strands of the SWIF.

Deformation based on subsurface information has been postulated along lineaments that project southeastward into the Maltby quadrangle from the northwest. Rau and Johnson (1999) described the location of the Alderwood No. 1 well as on a structural arch within the SWIF and reported fractured and sheared strata (Fig. M1). Blakely and others (2004) correlated deformation in this well with aeromagnetic and topographic lineaments they interpreted as strands of the SWIF. Review of the original 1947 detailed driller's bedrock core descriptions (WGS oil and gas records) detail many instances of gouge, fractures, and slickensides (often filled with calcite). Deformation was recorded throughout the available records (the WGS log records the 510–3,353 m [1,673–11,002 ft] depth interval), but there was a notable concentration of deformation features and gouge in the 2,040–2,430 m (6,693–7,972 ft) depth interval.

Northwest-striking structures mapped by Dragovich and others (2010b, 2011a) to the southeast are not continued into the Maltby quadrangle for lack of convincing geologic evidence. Dragovich and others (2010b, 2011a,b) used geophysical modeling to map concealed strands of the RMFZ, including the Snoqualmie Valley fault no. 1, Cherry Valley fault, and an intervening unnamed anticline and syncline that fold Quaternary strata (Fig. M1). Orientations of small faults and folds in well-exposed Quaternary strata near the projected trace of the Cherry Valley fault in the Maltby quadrangle between age sites GD7 and 10-28D (map sheet) are roughly consistent with structures mapped by Dragovich and others (2010b, 2011a), although they also could be tectonic, glaciogenic, or related to slope instability.

Dragovich and others (2010a,b, 2011a,b) considered the sedimentary bedrock exposed in the southeast corner of the Maltby quadrangle (unit ΦEc?, map sheet) to be Miocene and proposed a tectonic model where Miocene deposits were preserved in a strike-slip synclinal basin within the SWIF. We note that these exposures are lithologically similar to unit ΦEc exposed farther north and have similarly oriented bedding. Our statistical analysis of U-Pb zircon analytical data published by Dragovich and others (2011b, appendix 6) suggests that this bedrock may have formed earlier, closer to ages found for units ΦEc and ΦEn (Appendix C). If accurate, this new age interpretation appears to remove the necessity for a tectonic model to explain the origin of Miocene rocks. The simplest explanation of these exposures is that these younger rocks are merely upsection from the older rocks farther north, which is supported by the similar bedding orientations observed between exposures.

Most kinematic interpretations of the SWIF (for example, Brocher and others, 2005; Sherrod and others, 2008) do not describe potential interactions with the Fiddlers Bluff anticline, Kingston arch, or Monroe fault and fold structures. We recognize that the Fiddlers Bluff anticline appears to have formed in response to north-northeast-directed compression (Fig. 8), compatible with the kinematic models proposed for the SWIF (Brocher and others, 2005; Dragovich and others, 2014b). Dragovich and others (2014b) postulated that the Monroe fault merges with the SWIF and partitions the north-south compressional component of strain on the SWIF, whereas the RMFZ partitions the dextral component. Dragovich and others (2015) indicated that this merger could be located near the northwest corner of the Maltby quadrangle. We consider this plausible, but observations in this study did not provide evidence to confirm this hypothesis. Some earthquake epicenters are located near mapped strands of the SWIF and RMFZ (Fig. E1) and potentially reflect active tectonism along these structures. However, given the structural complexity of the area, relatively deep hypocenters, and the lack of a clear pattern of epicenters and orientations from focal mechanisms, we cannot confidently correlate seismicity with mapped fault traces (Appendix E; DS9).

ACKNOWLEDGMENTS

This geologic map was funded in part by the U.S. Geological Survey (USGS) National Cooperative Geologic Mapping Program under award no. G16AC00286. We wish to thank Michael Polenz, Timothy Walsh, and Alex Steely (all WGS) for excellent feedback throughout the life of this project. Jessica Czajkowski and Jari Roloff (both WGS) guided this project with much-needed editorial feedback. Richard Blakely (USGS) provided aeromagnetic data and stimulating discussions. Curtis Koger (Associated Earth Sciences, Inc.) provided reports of geotechnical investigations in the quadrangle. Tara Salzer (WGS) provided logistical support during the field season. Todd Lau, Spenser Scott, Alex Kover, and Robert Cove (all WGS) collected and processed geophysical data for this study. Ashley Cabibbo, Dylan Chase, Daniel Eungard, and Dylan Baldwin (all WGS) accurately located and cataloged subsurface data. We thank the Washington State Department of Transportation (WSDOT) for access to geotechnical records and Eric Dingeldein (WSDOT) for his assistance with those records. Kara Jacobacci and Trevor Contreras (WGS) did a preliminary review of the map area for landslide hazards and gave insightful feedback. Stephanie Earls (WGS) provided access to many useful references through the

Washington Geology Library. Dan Smith (King County) and Kathy Troost (Univ. of Wash.) assisted with field mapping and provided useful feedback for Quaternary mapping. Bruce Stoker (Earth Systems) facilitated trips along river exposures in his river boat. Zak Fiorito (AAA Monroe Rock Corp.) facilitated access to exposures in the AAA Quarry. Select members of the Snohomish Conservation District provided local insight and land access. Several landowners granted access to important outcrops; Bobbi Lindemulder, Mark Craven, and David Remlinger were particularly helpful.

REFERENCES

Allmendinger, R. W.; Cardozo, N. C.; Fisher, D., 2013, Structural geology algorithms: Vectors & Tensors: Cambridge University Press [Cambridge, U.K.], 289 p.

Anderson, F. M., 1914, Neocene record in the Temblor basin, California, and Neocene deposits of the San Juan district, San Luis Obispo County: Proceedings of the California Academy of Sciences, 4th Series, v. IV, p. 15-112. [https://babel.hathitrust.org/cgi/pt?id=hvd.32044107313108;view=1up;seq=13]

Anderson, M. L.; Waters, Katharine; Dragovich, J. D.; Blakely, R. J.; Wells, R. E., 2015, New determination of the shape of the Seattle basin, Washington from gravity and magnetic data—Implications for seismic ground motion and crustal faults [abstract]: American Geophysical Union (AGU) Fall Meeting [San Francisco, CA], webpage. [https://agu.confex.com/agu/fm15/meetingapp.cgi/Paper/58560]

Armentrout, J. M., 1975, Molluscan biostratigraphy of the Lincoln Creek Formation, southwest Washington. *In* Weaver, D. W.; Hornaday, G. R.; Tipton, Ann, editors, Paleogene symposium and selected technical papers—Conference on future energy horizons of the Pacific coast: American Association of Petroleum Geologists Pacific Section, 50th Annual Meeting, p. 14-18.

Armentrout, J. M.; Berta, Annalisa, 1977, Eocene–Oligocene foraminiferal sequence from the northeast Olympic Peninsula, Washington: Journal of Foraminiferal Research, v. 7, no. 3, p. 216-233.

Armstrong, J. E.; Crandell, D. R.; Easterbrook, D. J.; Noble, J. B., 1965, Late Pleistocene stratigraphy and chronology in southwestern British Columbia and northwestern Washington: Geological Society of America Bulletin, v. 76, no. 3, p. 321-330.

Arnold, Ralph, 1908, Descriptions of new Cretaceous and Tertiary fossils from the Santa Cruz Mountains, California: Proceedings of the United States National Museum, v. 34, no. 1617, p. 345–390.

Barnes, D. F.; Oliver, H. W.; Robbins, S. L., 1969, Standardization of gravimeter calibrations in the geological survey: Eos (American Geophysical Union Transactions), v. 50, no. 10, p. 526-527.

Benn, D. I.; Evans, D. J. A., 2010, Glaciers and glaciation: Oxford University Press, 802 p.

Bethel, John, 2004, An overview of the geology and geomorphology of the Snoqualmie River watershed: King County Department of Natural Resources and Parks, Water and Land Resources Division, 88 p. [http://your.kingcounty.gov/dnrp/library/2004/kcr1833.pdf].

Blakely, R. J.; Sherrod, B. L.; Weaver, C. S.; Wells, R. E.; Rohay, A. C.; Barnett, E. A.; Knepprath, N. E., 2011, Connecting the Yakima fold and thrust belt to active faults in the Puget Lowland, Washington: Journal of Geophysical Research—Solid Earth, v. 116, no. B07105, 33 p. [http://onlinelibrary.wiley.com/doi/10.1029/2010JB008091/abstract].

Blakely, R. J.; Sherrod, B. L.; Wells, R. E.; Weaver, C. S.; McCormack, D. H.; Troost, K. G.; Haugerud, R. A., 2004, The Cottage Lake aeromagnetic lineament—A possible onshore extension of the southern Whidbey Island fault, Washington: U.S. Geological Survey Open-File Report 2004-1204, 60 p. [http://pubs.er.usgs.gov/publication/ofr20041204]

Booth, D. B., 1990, Surficial geologic map of the Skykomish and Snoqualmie Rivers area, Snohomish and King counties, Washington: U.S. Geological Survey Miscellaneous Investigations Series Map I-1745, 2 sheets, scale 1:50,000, with 22 p. text. [https://pubs.er.usgs.gov/publication/i1745]

Booth, D. B., 1994, Glaciofluvial infilling and scour of the Puget Lowland, Washington, during ice-sheet glaciation: Geology, v. 22, no. 8, p. 695-698. [http://faculty.washington.edu/dbooth/Booth%20GEOLOGY%201994.pdf]

Booth, D. B.; Troost, K. G.; Clague, J. J.; Waitt, R. B., 2004, The Cordilleran ice sheet. *In* Gillespie, A. R.; Porter, S. C.; Atwater, B. F., editors, The Quaternary period in the United States: Elsevier, p. 17-43.

Booth, D. B.; Troost, K. G.; Tabor, R. W., 2015, Geologic map of the Vashon 7.5′ quadrangle and selected areas, King County, Washington: U.S. Geological Survey Scientific Investigations Map 3328, 1 sheet, scale 1:24,000, 11 p. text. [http://pubs.er.usgs.gov/publication/sim3328]

Booth, D. B.; Troost, K. G.; Wisher, A. P., 2007, Geologic map of the Redmond Bear Creek Area: Pacific Northwest Center for Geologic Mapping Studies, University of Washington, 1 sheet, scale 1:24,000. [http://your.kingcounty.gov/dnrp/library/water-and-land/groundwater/RBC-geomap2007.pdf]

Booth, D. B.; Walsh, T. J.; Troost, K. G.; Shimel, S. A., 2012, Geologic map of the east half of the Bellevue South 7.5′ x 15′ quadrangle, Issaquah area, King County, Washington: U.S. Geological Survey Scientific Investigations Map SIM-3211, 1 sheet, scale 1:24,000, and one GIS database. [http://pubs.usgs.gov/sim/3211/]

Boynton, W. V., 1984, Cosmochemistry of the rare earth elements—Meteorite studies. *In* Henderson, R., editor, Rare earth element geochemistry: Developments in Geochemistry 2, Elsevier, Ch. 3, p., 89-92.

Breitsprecher, K.; Thorkelson, D. J.; Groome, W. G.; Dostal, J., 2003, Geochemical confirmation of the Kula-Farallon slab window beneath the Pacific Northwest in Eocene time: Geology, v. 31, no. 4, p. 351-354. [http://www.geology.um.maine.edu/user/Wes_Groome/images/pdfs/breitsprecher_et_al_2003.pdf]

Brocher, T. M.; Blakely, R. J.; Wells, R. E.; Sherrod, B. L.; Ramachandran, Kumar, 2005, The transition between N-S and NE-SW directed crustal shortening in the central and northern Puget Lowland—New thoughts on the Southern Whidbey Island fault [abstract]: Eos (American Geophysical Union Transactions), v. 86, no. 52, p. F1459. [http://adsabs.harvard.edu/abs/2005AGUFM.S54A..06B]

Brocher, T. M.; Parsons, T. E.; Blakely, R. J.; Christensen, N. I.; Fisher, M. A.; Wells, R. E.; SHIPS Working Group, 2001, Upper crustal structure in Puget Lowland, Washington—Results from the 1998 seismic hazards investigations in Puget Sound: Journal of Geophysical Research, v. 106, no. B7, p. 13,541-13,564.

Brown, E. H.; Dragovich, J. D., 2003, Tectonic elements and evolution of northwest Washington: Washington Division of Geology and Earth Resources Geologic Map GM-52, 1 sheet, scale 1:625,000, with 12 p. text. [http://www.dnr.wa.gov/publications/ger_gm52_tectonic_evolution_nw_washington.zip]

Capps, Gerald; Simmons, J. D.; Videgar, F. D., 1973, Preliminary report on the geology of southern Snohomish County, Washington: Washington Division of Geology and Earth Resources Open File Report 73-1, 11 p., 8 plates, scale 1:24,000. [http://d92019.eos-intl.net/D92019/OPAC/Details/Record.aspx?BibCode=10655985]

Cardozo, Nestor, Allmendinger, R. W., 2013, Spherical projections with OSXStereonet: Computers & Geosciences, v. 51, p. 193-205. [https://doi.org/10.1016/j.cageo.2012.07.021]

Clark, B. L., 1918, The San Lorenzo series of middle California—A stratigraphic and palaeontologic study of the San Lorenzo Oligocene series of the general region of Mount Diablo, California: University of California Publications, Department of Geological Sciences Bulletin, v. 11, no. 2, p. 45-235.

Clark, B. L., 1922, A new family and new genus from the Tertiary of the Pacific Coast: University of California Publications, Department of Geological Sciences Bulletin, v. 14, no. 4, p. 115-122, 2 plates.

Clark, B. L., 1925, Pelecypoda from the marine Oligocene of western North America: University of California Publications, Department of Geological Sciences Bulletin, v. 15, no. 4, p. 69-136.

Clark, B. L.; Arnold, Ralph, 1923, Fauna of the Sooke Formation, Vancouver Island, with description of a new coral by T. Wayland Vaughan: University of California Publications, Department of Geological Sciences Bulletin, v. 14, no. 5, p. 123-234, 28 plates.

Cohen, K. M.; Finney, S. C.; Gibbard, P. L.; Fan, J. X., 2013 (updated 2015), The ICS international chronostratigraphic chart: International Commission on Stratigraphy, 1 p. [http://www.stratigraphy.org/ICSchart/ChronostratChart2015-01.pdf]

Collins, B. D.; Montgomery, D. R.; Sheikh, A. J., 2003, Reconstructing the historical riverine landscape of the Puget Lowland. *In* Montgomery, D. R.; Bolton, S. M.; Booth, D. B.; Wall, L., editors, Restoration of Puget Sound rivers: University of Washington Press, p. 79-128.

Collins, B. D.; Sheikh, A. J., 2002, Mapping historical conditions in the Snoqualmie River valley (RM 0 - RM 40): Report to King County Department of Natural Resources by the Department of Earth and Space Sciences, University of Washington, 30 p. [http://govlink.org/watersheds/7/pdf/Snoqualmie-historical-map-conditions.pdf]

Conrad, T. A., 1849, Fossils from northwestern America—Mollusca: *In* Dana, J. D., editor, Geology: U.S. Exploring Expedition during the year 1838–1842, under the Command of Charles Wilkes, U.S. Navy, v. 10, p. 723–728.

Conrad, T. A., 1850, Descriptions of new fresh water and marine shells: Journal of the Academy of Natural Sciences of Philadelphia, v. 2, no. 1, p. 275-280, 3 plates.

Contreras, T. A.; Stone, K. A.; Legorreta Paulin, Gabriel, 2013, Geologic map of the Lofall 7.5-minute quadrangle, Jefferson and Kitsap Counties, Washington: Washington Division of Geology and Earth Resources Map Series 2013-03, 1 sheet, scale 1:24,000, with 19 p. text. [http://www.dnr.wa.gov/publications/ger_ms2013-03_geol_map_lofall_24k.zip]

Cushman, J. A.; Frizzell, D. L., 1940, Two new species of foraminifera from the Oligocene Lincoln Formation of Washington: Cushman Laboratory Foraminiferal Research Contributions, v. 16, part 2, no. 220, p. 42-43.

Cushman, J. A.; Ozawa, Y., 1928, An outline of a revision of the Polymorphinidae: Cushman Laboratory Foraminiferal Research Contributions, v. 4, p. 13-21.

Cushman, J. A., Schenck, H. G., 1928. Two foraminiferal faunules from the Oregon Tertiary: University of California Publications, Department of Geological Sciences Bulletin v. 17, p. 305–324.

Dall, W. H., 1903, Contributions to the Tertiary fauna of Florida (Part 6): Transactions of the Wagner Free Institute of Science of Philadelphia, v. 3, p. 1219-1654.

Dall, W. H., 1909, Contributions to the Tertiary paleontology of the Pacific coast—I. The Miocene of Astoria and Coos Bay, Oregon: U.S. Geological Survey Professional Paper 59, 278 p. [https://pubs.er.usgs.gov/publication/pp59]

Danner, W. R., 1957, A stratigraphic reconnaissance in the northwestern Cascade mountains and San Juan Islands of Washington State: University of Washington Doctor of Philosophy thesis, 3 v., 562 p., 7 plates.

Defant, M. J.; Drummond, M. S., 1990, Derivation of some modern arc magmas by melting of young subducted lithosphere: Nature, v. 347, p. 662-665.

Deshayes, G. P., 1839, Nouvelles espèces de mollusques, provenant des côtes de la Californie, du Méxique, du Kamtschatka et de la Nouvelle-Zélande: Revue Zoologique per la Société Cuvierienne, v. 2, no. 12, p. 356-361.

Dethier, D. P.; Pessl, Fred, Jr.; Keuler, R. F.; Balzarini, M. A.; Pevear, D. R., 1995, Late Wisconsinan glaciomarine deposition and isostatic rebound, northern Puget Lowland, Washington: Geological Society of America Bulletin, v. 107, no. 11, p. 1288-1303.

Dickerson, R. E., 1916. Stratigraphy and fauna of the Tejon Eocene of California: University of California Publications, Department of Geological Sciences Bulletin, v. 9, no. 17, p. 363-524, 11 plates.

Dickerson, R. E., 1917, Climate and its influence upon the Oligocene faunas of the Pacific coast, with descriptions of some new species from the *Molopophorus lincolnensis* zone: California Academy of Sciences Proceedings, v. 7, p. 157-192.

Dickinson, W. R.; Gehrels, G. E., 2009, Use of U-Pb ages of detrital zircons to infer maximum depositional ages of strata—A test against a Colorado Plateau Mesozoic database: Earth and Planetary Science Letters, v. 288, no. 1, p. 115-125.

D'Orbigny, A., 1839, Foraminifères. *In* Bertrand, Arthus, editor: Histoire physique, politique et naturelle de l'île de Cuba, p. 1-224.

Dragovich, J. D.; Anderson, M. L.; MacDonald, J. H., Jr.; Mahan, S. A; DuFrane, S. A.; Littke, H. A.; Wessel, G. R.; Saltonstall, J. H.; Koger, C. J.; Cakir, Recep, 2010a, Supplement to the geologic map of the Carnation 7.5-minute quadrangle, King County, Washington—Geochronologic, geochemical, point count, geophysical, earthquake, fault, and neotectonic data: Washington Division of Geology and Earth Resources Open File Report 2010-2, 42 p., 8 digital appendices. [http://www.dnr.wa.gov/publications/ger_ofr2010–2_carnation_supplement.zip]

Dragovich, J. D.; Anderson, M. L.; Mahan, S. A.; Koger, C. J.; Saltonstall, J. H.; MacDonald, J. H., Jr.; Wessel, G. R.; Stoker, B. A.; Bethel, J. P.; Labadie, J. E.; Cakir, Recep; Bowman, J. D.; DuFrane, S. A., 2011a, Geologic map of the Monroe 7.5-minute quadrangle, King and Snohomish Counties, Washington: Washington Division of Geology and Earth Resources Open File Report 2011-1, 1 sheet, scale 1:24,000, with 24 p. text. [http://www.dnr.wa.gov/publications/ger_ofr2011–1_geol_map_monroe_24k.zip]

Dragovich, J. D.; Anderson, M. L.; Mahan, S. A.; MacDonald, J. H., Jr.; McCabe, C. P.; Cakir, Recep; Stoker, B. A.; Villeneuve, N. M.; Smith, D. T.; Bethel, J. P., 2012, Geologic map of the Lake Joy 7.5-minute quadrangle, King County, Washington: Washington Division of Geology and Earth Resources Map Series 2012-01, 2 sheets, scale 1:24,000, 79 p. text. [http://www.dnr.wa.gov/publications/ger_ms2012-01_geol_map_lake_joy_24k.zip]

Dragovich, J. D.; Anderson, M. L.; Walsh, T. J.; Johnson, B. L.; Adams, T. L., 2007, Geologic map of the Fall City 7.5-minute quadrangle, King County, Washington: Washington Division of Geology and Earth Resources Geologic Map GM-67, 1 sheet, scale 1:24,000. [http://www.dnr.wa.gov/publications/ger_gm67_geol_map_fallcity_24k.zip]

Dragovich, J. D.; Frattali, C. L.; Anderson, M. L.; Mahan, S. A.; MacDonald, J. H., Jr.; Stoker, B. A.; Smith, D. T.; Koger, C. J.; Cakir, Recep; DuFrane, S. A.; Sauer, K. B., 2014a, Geologic map of the Lake Chaplain 7.5-minute quadrangle, Snohomish County, Washington: Washington Division of Geology and Earth Resources Map Series 2014-01, 1 sheet, scale 1:24,000, with 51 p. text. [http://www.dnr.wa.gov/publications/ger_ms2014-01_geol_map_lake_chaplain_24k.zip]

Dragovich, J. D.; Littke, H. A.; Anderson, M. L.; Hartog, Renate; Wessel, G. R.; DuFrane, S. A.; Walsh, T. J.; MacDonald, J. H., Jr.; Mangano, J. F.; Cakir, Recep, 2009a, Geologic map of the Snoqualmie 7.5-minute quadrangle, King County, Washington: Washington Division of Geology and Earth Resources Geologic Map GM-75, 2 sheets, scale 1:24,000. [http://www.dnr.wa.gov/publications/ger_gm75_geol_map_snoqualmie_24k.zip]

Dragovich, J. D.; Littke, H. A.; Anderson, M. L.; Wessel, G. R.; Koger, C. J.; Saltonstall, J. H.; MacDonald, J. H., Jr.; Mahan, S. A.; DuFrane, S. A., 2010b, Geologic map of the Carnation 7.5-minute quadrangle, King County, Washington: Washington Division of Geology and Earth Resources Open File Report 2010–1, 1 sheet, scale 1:24,000, with 21 p. text. [http://www.dnr.wa.gov/publications/ger_ofr2010-1_geol_map_carnation_24k.zip]

Dragovich, J. D.; Littke, H. A.; MacDonald, J. H., Jr.; DuFrane, S. A.; Anderson, M. L.; Wessel, G. R.; Hartog, Renate, 2009b, Geochemistry, geochronology, and sand point count data for the Snoqualmie 7.5-minute quadrangle, King County, Washington: Washington Division of Geology and Earth Resources Open File Report 2009-4, 35 p. text, 3 Microsoft Excel files. [http://www.dnr.wa.gov/publications/ger_ofr2009-4_snoqualmie_suppl.zip]

Dragovich, J. D.; Littke, H. A.; Mahan, S. A.; Anderson, M. L.; MacDonald, J. H., Jr.; Cakir, Recep; Stoker, B. A.; Koger, C. J.; Bethel, J. P.; DuFrane, S. A.; Smith, D. T.; Villeneuve, N. M., 2013, Geologic map of the Sultan 7.5-minute quadrangle, King and Snohomish Counties, Washington: Washington Division of Geology and Earth Resources Map Series 2013-01, 1 sheet, scale 1:24,000, with 52 p. text. [http://www.dnr.wa.gov/publications/ger_ms2013–01_geol_map_sultan_24k.zip]

Dragovich, J. D.; Logan, R. L.; Schasse, H. W.; Walsh, T. J.; Lingley, W. S., Jr.; Norman, D. K.; Gerstel, W. J.; Lapen, T. J.; Schuster, J. E.; Meyers, K. D., 2002, Geologic map of Washington—Northwest quadrant: Washington Division of Geology and Earth Resources Geologic Map GM-50, 3 sheets, scale 1:250,000, with 72 p. text. [http://www.dnr.wa.gov/publications/ger_gm50_geol_map_nw_wa_250k.pdf]

Dragovich, J. D.; Mahan, S. A.; Anderson, M. L.; MacDonald, J. H., Jr.; Frattali, C. L.; Littke, H. A.; Stoker, B. A.; Koger, C. J.; Smith, D. T.; DuFrane, S. A., 2014b, The Monroe fault, anticline, and synclinal basin—A potentially active fault and fold system in the Skykomish River Valley, Snohomish County, Washington [abstract]: Geological Society of America Abstracts with Programs, v. 46, no. 6, p. 779.

Dragovich, J. D.; Mahan, S. A.; Anderson, M. L.; MacDonald, J. H., Jr; Schilter, J. F.; Frattali, C. L.; Koger, C. J.; Smith, D. T.; Stoker, B. A.; DuFrane, Andrew; Eddy, M. P.; Cakir, Recep; Sauer, K. B., 2015, Geologic map of the Lake Roesiger 7.5-minute quadrangle, Snohomish County, Washington: Washington Division of Geology and Earth Resources Map Series 2015-01, 1 sheet, scale 1:24,000, 47 p. text. [http://www.dnr.wa.gov/publications/ger_ms2015-01_geol_map_lake_roesiger_24k.zip]

Dragovich, J. D.; Mahan, S. A.; Anderson, M. L.; MacDonald, J. H., Jr.; Wessel, G. R.; DuFrane, S. A.; Cakir, Recep; Bowman, J. D.; Littke, H. A., 2011b, Analytical data from the Monroe 7.5-minute quadrangle, King and Snohomish Counties, Washington—Supplement to Open File Report 2011-1: Washington Division of Geology and Earth Resources Open File Report 2011-2, 58 p., 2 plates, 2 Microsoft Excel files. [http://www.dnr.wa.gov/publications/ger_ofr2011–2_monroe_supplement.zip]

Dragovich, J. D.; Mavor, S. P.; Anderson, M. L.; Mahan, S. A.; MacDonald, J. H., Jr.; Tepper, J. H.; Smith, D. T.; Stoker, B. A.; Koger, C. J.; Cakir, Recep; DuFrane, S. A.; Scott, S. P.; Justman, B. J., 2016, Geologic map of the Granite Falls 7.5-minute quadrangle, Snohomish County, Washington: Washington Division of Geology and Earth Resources Map Series 2016-03, 1 sheet, scale 1:24,000, 63 p. text. [http://www.dnr.wa.gov/publications/ger_ms2016-03_geol_map_granite_falls_24k.zip]

Dragovich, J. D.; Walsh, T. J., 2008, Geochemical sample analyses of Tertiary and pre-Tertiary volcanic rocks in and around the North Bend 7.5-minute quadrangle, King County, Washington: Washington Division of Geology and Earth Resources Open File Report 2008-4, 6 p. text with 1 Excel file on DVD. [http://www.dnr.wa.gov/publications/ger_ofr2008-4_northbend_geochem.zip]

Dunlop, Paul; Clark, C. D., 2006, The morphological characteristics of ribbed moraine: Quaternary Science Reviews 25, p. 1668-1691.

Eddy, M. P.; Bowring, S. A.; Umhoefer, P. J.; Miller, R. B.; McLean, N. M.; Donaghy, E. E., 2015, High-resolution temporal and stratigraphic record of Siletzia's accretion and triple junction migration from nonmarine sedimentary basins in central and western Washington: Geological Society of America Bulletin, v. 128, no. 3/4, p. 425-441.

Fichtel, L. V.; Moll, J. P. C., 1798, Testacea microscopica: Verlag Ferdinand Berger & Söhne, 143 p.

Finn, C. A.; Phillips, W. M.; Williams, D. L., 1991, Gravity anomaly and terrain maps of Washington: U.S. Geological Survey Geophysical Investigations Map GP-988, 5 sheets, scale 1:500,000. [http://pubs.er.usgs.gov/publication/gp988]

Folk, R. L., 1980, Petrology of sedimentary rocks: Hemphill Publishing Company, 182 p.

Frizzell, V. A., Jr.; Tabor, R. W.; Zartman, R. E.; Blome, C. D., 1987, Late Mesozoic or early Tertiary mélanges in the western Cascades of Washington. *In* Schuster, J. E., editor, Selected papers on the geology of Washington: Washington Division of Geology and Earth Resources Bulletin 77, p. 129-148. [http://www.dnr.wa.gov/publications/ger_b77_papers_on_wa_geology_pt2of3.pdf]

Fulmer, C. V., 1975, Stratigraphy and paleontology of the type Blakeley and Blakely Harbor Formations. *In* Weaver, D. W.; Hornaday, G. R.; Tipton, Ann, editors, Paleogene symposium and selected technical papers—Conference on future energy horizons of the Pacific coast: American Association of Petroleum Geologists Pacific Section, 50th Annual Meeting, p. 210-271.

Gabb, W. M., 1866, Tertiary invertebrate fossils: California Geological Survey, Palaeontology, v. 2, sec. 1, pt. 1, p. 1-38.

Gabb, W. M., 1869, Cretaceous and Tertiary fossils: California Geological Survey, Palaeontology, v. 2, 299 p., 36 plates.

Gaschnig, R. M.; Vervoort, J. D.; Lewis, R. S.; Tikoff, Basil, 2011, Isotopic evolution of the Idaho batholith and Challis intrusive province, northern U.S. Cordillera: Journal of Petrology, v. 52, no. 12, p. 2397-2429.

Gehrels, G. E., 2009, Age Pick program [Microsoft Excel plugin]: University of Arizona LaserChron Center.

Goedert, J. L.; Squires, R. L., 1990, Eocene deep-sea communities in localized limestones formed by subduction-related methane seeps, southwestern Washington: Geology, v. 18, no. 12, p. 1182-1185.

Golder Associates, Inc., 1999, Groundwater protections issues and risks within the Cross Valley sole-source aquifer area from proposed cross-Cascade pipeline: Golder Associates, Inc. [Redmond, WA] [under contract to] Cross Valley Water District [Snohomish, WA], 71 p. [http://www.efsec.wa.gov/oplarchive/oplpft/crossvalley/wjr-1.pdf]

Golder Associates, Inc., 2000, Cross Valley sole source aquifer wellhead protection plan: Golder Associates, Inc., [Redmond, WA] [under contract to] Cross Valley Water District [Snohomish, WA], 247 p.

Golder Associates, Inc., 2005, Little Bear Creek hydrogeologic overview: Golder Associates, Inc., [Redmond, WA] [under contract to] Jones & Stokes [Bellevue, WA], 12 p., 4 plates. [https://snohomishcountywa.gov/DocumentCenter/View/8674]

Golder Associates, Inc., 2007, Final report—Hydrogeologic and geotechnical analysis for City of Woodinville sustainable development program. *In* Jones & Stokes; City of Woodinville Community Development Department, Sustainable development study—R-1 Zone: Jones & Stokes Environmental Report, Appendix A-1. [http://www.ci.woodinville.wa.us/Documents/News/SustainableDevelopment/Final_Repor_10_2008/Ch1A_Enviro%20Report%20Appendices.pdf]

Gower, H. D., 1978, Tectonic map of the Puget Sound region, Washington, showing locations of faults, principal folds, and large-scale Quaternary deformation: U.S. Geological Survey Open-File Report 78-426, 22 p., 1 plate, scale 1:250,000. [http://pubs.er.usgs.gov/usgspubs/ofr/ofr78426]

Gower, H. D.; Yount, J. C.; Crosson, R. S., 1985, Seismotectonic map of the Puget Sound region, Washington: U.S. Geological Survey Miscellaneous Investigations Series Map I-1613, 1 sheet, scale 1:250,000, with 15 p. text. [http://pubs.er.usgs.gov/publication/i1613]

Guynn, Jerome; Gehrels, George, 2010, Comparison of detrital zircon age distributions in the K-S test: University of Arizona LaserChron Center, 16 p.

Hanna, G. D.; Hanna, M. A., 1924, Foraminifera from the Eocene of Cowlitz River, Lewis County, Washington: University of Washington Publications in Geology, v. 1, no. 4, p. 57-63.

Hansen, B. S.; Easterbrook, D. J., 1974, Stratigraphy and palynology of late Quaternary sediments in the Puget Lowland, Washington: Geological Society of America Bulletin, v. 85, no. 4, p. 587-602.

Hart Crowser, Inc., 1993, Groundwater explorations, Woodinville Water District, Woodinville, Washington: Hart Crowser, Inc., 1 v.

Haugerud, R. A., 2009a, Stagnation of the Puget lobe of the Cordilleran ice sheet, northwest Washington [abstract]: Geological Society of America Abstracts with Programs, v. 41, no. 7, p. 432-433.

Haugerud, R. A., 2009b, Preliminary geomorphic map of the Kitsap Peninsula, Washington; version 1.0: U.S. Geological Survey Open-File Report 2009-1033, 2 sheets, scale 1:36,000. [http://pubs.usgs.gov/of/2009/1033/]

Haugerud, R. A., 2010, Retreat of the Puget lobe of the Cordilleran ice sheet [abstract]: Eos (American Geophysical Union Transactions), 2010 Fall Meeting, V11C-2295.

Haugerud, R. A., 2014, Maximum extent and retreat of the Puget lobe of the Cordilleran ice sheet, northwest Washington [abstract]: Geological Society of America Abstracts with Programs, v. 46, no. 6, p. 655.

Heiskanen, W. A.; Vening-Meinesz, F. A., 1958, The Earth and its gravity field: McGraw-Hill Book Company, Inc., 470 p.

International Union of Geodesy and Geophysics, 1971, Geodetic Reference System 1967: International Association of Geodesy Special Publication no. 3, 116 p.

Irvine, T. N.; Baragar, W. R. A., 1971, A guide to the chemical classification of the common volcanic rocks: Canadian Journal of Earth Sciences, v. 8, no. 5, p. 523-548.

Jachens, R. C.; Roberts, C. R., 1981, Documentation of a FORTRAN program, 'isocomp', for computing isostatic residual gravity: U.S. Geological Survey Open-File Report 81-574, 26 p.

Jackson, S. E.; Pearson, N. J.; Griffin, W. L.; Belousova, E. A., 2004, The application of laser ablation-inductively coupled plasma-mass spectrometry to in situ U-Pb zircon geochronology: Chemical Geology, v. 211, no.1, p. 47-69.

Jeschke, D. A.; Eungard, D. W.; Troost, K. G.; Wisher, A. P., 2016, Subsurface database of Washington State—GIS data: Washington Division of Geology and Earth Resources Digital Data Series 11, version 1.2, previously released October, 2015. [http://www.dnr.wa.gov/publications/ger_portal_subsurface_database.zip]

Johnson, S. Y.; Dadisman, S. V.; Childs, J. R.; Stanley, W. D., 1999, Active tectonics of the Seattle fault and central Puget Sound, Washington—Implications for earthquake hazards: Geological Society of America Bulletin, v. 111, no. 7, p. 1042-1053, 1 plate.

Johnson, S. Y.; Potter, C. J.; Armentrout, J. M., 1994, Origin and evolution of the Seattle fault and Seattle basin, Washington: Geology, v. 22, no. 1, p. 71-74, 1 plate.

Johnson, S. Y.; Potter, C. J.; Armentrout, J. M.; Miller, J. J.; Finn, C. A.; Weaver, C. S., 1996, The southern Whidbey Island fault—An active structure in the Puget Lowland, Washington: Geological Society of America Bulletin, v. 108, no. 3, p. 334-354, 1 plate.

Kelsey, H. M.; Sherrod, Brian; Johnson, S. Y.; Dadisman, S. V., 2004, Land-level changes from a late Holocene earthquake in the northern Puget Lowland, Washington: Geology, v. 32, no. 6, p. 469-472.

King County, 2016, Mapping of potential landslide hazards along the river corridors of King County, Washington—Technical report August 2016: King County Department of Natural Resources and Parks, Water and Land Resources Division, River and Floodplain Management Section, 1 v., 1 plate. [http://your.kingcounty.gov/dnrp/library/2016/kcr2783.pdf]

Klepeis, K. A.; Crawford, M. L.; Gehrels, George, 1998, Structural history of the crustal-scale Coast shear zone north of Portland Canal, southeast Alaska and British Columbia: Journal of Structural Geology, v. 20, no. 7, p. 883-904.

Kuechler, R. R.; Birgel, Daniel; Kiel, Steffen, Freiwald, Andre; Goedert, J. L.; Thiel, Volker; Peckmann, Joern, 2011, Miocene methane-derived carbonates from southwestern Washington, USA and a model for silicification at seeps: Lethaia, v. 45, no. 2, p. 259-273.

Laprade, W. T.; Kirkland, T. E.; Nashem, W. D.; Robertson, C. A., 2000, Seattle landslide study: Shannon & Wilson internal report W-7992-01 [Seattle, WA], 164 p.

Le Bas, M. J.; Le Maitre, R. W.; Streckeisen, A. L.; Zanettin, Bruno, 1986, A chemical classification of volcanic rocks based on the total alkali-silica diagram: Journal of Petrology, v. 27, part 3, p. 745-750.

Lees, J. M., 1999, Geotouch—Software for three and four dimensional GIS in the earth sciences: Computers & Geosciences, v. 26, no. 7, p. 751-761.

Lees, J. M., 2007, RFOC—Graphics for spherical distributions and earthquake focal mechanisms, graphics for statistics on a sphere, as applied to geological fault data, crystallography, earthquake focal mechanisms, radiation patterns, ternary plots and geographical/geological maps: Comprehensive R Archive Network (CRAN). [accessed May 31, 2011, at http://streaming.stat.iastate.edu/CRAN/web/packages/RFOC/index.html].

Lees, J. M., 2008, GEOmap—Topographic and geologic mapping: Comprehensive R Archive Network (CRAN) [accessed May 31, 2011, at http://streaming.stat.iastate.edu/CRAN/web/packages/GEOmap/index.html].

Liberty, L. M.; Pape, K. M., 2006, Seismic characterization of the Seattle and southern Whidbey Island fault zones in the Snoqualmie River valley, Washington—Final technical report: U.S. Geological Survey Earthquake Hazards Program, External Research Support, Funded Research Final Technical Reports, 17 p.

Liesch, B. A.; Price, C. E.; Walters, K. L., 1963, Geology and ground-water resources of northwestern King County, Washington: Washington Division of Water Resources Water-Supply Bulletin 20, 241 p., 3 plates, scale 1:48,000. [https://fortress.wa.gov/ecy/publications/summarypages/wsb20.html]

Lindquist, J. W., 1957, Molluscan paleontology of Fiddlers Bluff, Washington: University of Washington undergraduate research thesis, 38 p.

Lisiecki, L. E.; Raymo, M. E., 2005, A Plio-Pleistocene stack of 57 globally distributed benthic $\delta^{18}O$ records: Paleoceanography, v. 20, no.1, 17 p. [https://doi.org/10.1029/2004PA001071]

Ludwig, K. R., 2003, User's manual for Isoplot 3.00—A geochronological toolkit for Microsoft Excel: Berkeley Geochronology Center Special Publication No. 4a, 1 v.

MacDonald, J. H., Jr.; Dragovich, J. D.; Littke, H. A.; Anderson, Megan; DuFrane, S. A., 2013, The volcanic rocks of Mount Persis—An Eocene continental arc that contains adakitic magmas [abstract]: Geological Society of America Abstracts with Programs, v. 45, no. 7, p. 392.

Mallory, V. S., 1959, Lower Tertiary biostratigraphy of the California coast ranges: American Association of Petroleum Geologists, 416 p.

Martin, H.; Smithies, R. H.; Rapp, R.; Moyen, J. F.; Champion, D., 2005, An overview of adakite, tonalite-trondhjemite-granodiorite (TTG), and sanukitoid—Relationships and some implications for crustal evolution: Lithos, v. 79, p. 1-24.

McCaffrey, Robert; King, R. W.; Payne, S. J.; Lancaster, Matthew, 2013, Active tectonics of northwestern U.S. inferred from GPS-derived surface velocities: Journal of Geophysical Research—Solid Earth, v. 118, p. 709-723. [https://doi.org/10.1029/2012JB009473]

McCaffrey, Robert; Qamar, A. I.; King, R. W.; Wells, Ray; Khazaradze, Giorgi; Williams, C. A.; Stevens, C. W.; Vollick, J. J.; Zwick, P. C., 2007, Fault locking, block rotation and crustal deformation in the Pacific Northwest: Geophysical Journal International, v. 169, no. 3, p. 1315-1340.

McKnight, E. T.; Ward, A. H., 1925, Geology of the Snohomish quadrangle: University of Washington Master of Science thesis, 95 p., 5 plates.

Miller, M. M.; Johnson, D. J.; Rubin, C. M.; Dragert, Herb; Wang, Kelin; Qamar, Anthony; Goldfinger, Chris, 2001, GPS-determination of along-strike variation in Cascadia margin kinematics—Implications for relative plate motion, subduction zone coupling, and permanent deformation: Tectonics, v. 20, no. 2, p. 161-176.

Minard, J. P., 1985a, Geologic map of the Maltby quadrangle, Snohomish and King Counties, Washington: U.S. Geological Survey Miscellaneous Field Studies Map MF-1746, 1 sheet, scale 1:24,000. [http://ngmdb.usgs.gov/Prodesc/proddesc_7475.htm]

Minard, J. P., 1985b, Geologic map of the Snohomish quadrangle, Snohomish County, Washington: U.S. Geological Survey Miscellaneous Field Studies Map MF-1745, 1 sheet, scale 1:24,000. [http://ngmdb.usgs.gov/Prodesc/proddesc_7499.htm]

Miyashiro, Akiho, 1974, Volcanic rock series in island arcs and active continental margins: American Journal of Science, v. 274, no. 4, p. 321-355.

Morelli, C., editor, 1974, The International Gravity Standardization Net, 1971: International Association of Geodesy Special Publication no. 4, 194 p.

Morrison, R. B., editor, 1991, Quaternary nonglacial geology—Conterminous U.S.: Geological Society of America DNAG Geology of North America, v. K-2, 672 p., 8 plates in accompanying case.

Mullineaux, D. R.; Waldron, H. H.; Rubin, Meyer, 1965, Stratigraphy and chronology of late interglacial and early Vashon glacial time in the Seattle area, Washington: U.S. Geological Survey Bulletin 1194-O, 10 p. [http://pubs.er.usgs.gov/publication/b1194O]

Nelson, A. R.; Johnson, S. Y.; Kelsey, H. M.; Wells, R. E.; Sherrod, B. L.; Pezzopane, S. K.; Bradley, Lee-Ann; Koehler, R. D., III; Bucknam, R. C., 2003, Late Holocene earthquakes on the Toe Jam Hill fault, Seattle fault zone, Bainbridge Island, Washington: Geological Society of America Bulletin, v. 115, no. 11, p. 1388-1403.

Nesbitt, E. A.; Martin, R. A.; Campbell, K. A., 2013, New records of Oligocene diffuse hydrocarbon seeps, northern Cascadia margin: Palaeogeography, Palaeoclimatology, Palaeoecology, v. 390, p. 116-129.

Newcomb, R. C., 1952, Ground-water resources of Snohomish County, Washington: U.S. Geological Survey Water-Supply Paper 1135, 133 p., 2 plates, 1:62,500 scale. [http://pubs.er.usgs.gov/usgspubs/wsp/wsp1135]

Office of the Federal Register, 1987, Sole source designation of the Cross Valley aquifer, Snohomish County and King County, Washington: Federal Register, v. 52, no. 95, p. 18,606.

Peccerillo, Angelo; Taylor, S. R., 1976, Geochemistry of Eocene calc-alkaline volcanic rocks from the Kastamonu area, northern Turkey: Contributions to Mineralogy and Petrology, v. 58, no. 1, p. 63-81.

Peckmann, J.; Goedert, J. L.; Theil, V.; Michaelis, W.; Reitner, J., 2002, A comprehensive approach to the study of methane-seep deposits from the Lincoln Creek Formation, western Washington USA: Sedimentology v. 49, no. 4, p. 855-873.

Pettijohn, F. J., 1957, Sedimentary rocks: Harper and Brothers, 718 p.

Phillips, J. D.; Hansen, R. O.; Blakely, R. J., 2007, The use of curvature in potential-field interpretation, Exploration Geophysics, v. 38, p. 111–119. [https://doi.org/10.1071/EG07014].

Pivaroff-Ward, Kendra, 2015, Determining spatial distribution and physical properties of the Vashon advance outwash near Mountlake Terrace, Washington: University of Washington Master of Science thesis, 267 p.

Plouff, Donald, 1977, Preliminary documentation for a FORTRAN program to compute gravity terrain corrections based on topography digitized on a geographic grid: U.S. Geological Survey Open-File Report 77-535, 45 p. [https://pubs.usgs.gov/of/1977/0535/report.pdf]

Plouff, Donald, 2000, Field estimates of gravity terrain corrections and Y2K-compatible method to convert from gravity readings with multiple base stations to tide- and long-term drift-corrected observations: U.S. Geological Survey Open-File Report 2000-140, 35 p.[https://pubs.er.usgs.gov/publication/ofr00140]

Polenz, Michael; Allen, M. D.; Legorreta Paulín, Gabriel; Eungard, D. W.; Cakir, Recep; Scott, S. P.; Mahan, S. A., 2016, Geologic map of the Shelton Valley 7.5-minute quadrangle, Mason County, Washington: Washington Division of Geology and Earth Resources Map Series 2016-02, 1 sheet, scale 1:24,000, 45 p. text. [http://www.dnr.wa.gov/publications/ger_ms2016-02_geol_map_shelton_valley_24k.zip]

Polenz, Michael; Favia, J. G.; Hubert, I. J.; Legorreta Paulín, Gabriel; Cakir, Recep, 2015, Geologic map of the Port Ludlow and southern half of the Hansville 7.5-minute quadrangles, Kitsap and Jefferson Counties, Washington: Washington Division of Geology and Earth Resources Map Series 2015-02, 1 sheet, scale 1:24,000, 40 p. text. [http://www.dnr.wa.gov/publications/ger_ms2015-02_geol_map_port_ludlow_hansville_24k.zip]

Polenz, Michael; Petro, G. T.; Contreras, T. A.; Stone, K. A.; Legorreta Paulin, Gabriel; Cakir, Recep, 2013, Geologic map of the Seabeck and Poulsbo 7.5-minute quadrangles, Kitsap and Jefferson Counties, Washington: Washington Division of Geology and Earth Resources Map Series 2013-02, 1 sheet, scale 1:24,000, with 39 p. text. [http://www.dnr.wa.gov/publications/ger_ms2013-02_geol_map_seabeck-poulsbo_24k.zip]

Porter, S. C.; Swanson, T. W., 1998, Radiocarbon age constraints on rates of advance and retreat of the Puget lobe of the Cordilleran ice sheet during the last glaciation: Quaternary Research, v. 50, no. 3, p. 205-213.

Pratt, T. L.; Johnson, S. Y.; Potter, C. J.; Stephenson, W. J.; Finn, C. A., 1997, Seismic reflection images beneath Puget Sound, western Washington State—The Puget Lowland thrust sheet hypothesis: Journal of Geophysical Research, v. 102, no. B12, p. 27,469-27,489.

Prothero, D. R.; Armentrout, J. M., 1985, Magnetostratigraphic correlation of the Lincoln Creek Formation, Washington—Implications for the age of the Eocene/Oligocene boundary: Geology, v. 13, no. 3, p. 208-211.

Prothero, D. R.; Nesbitt, E. A., 2008, Paleomagnetism and tectonic rotation of the Restoration Point member of the Blakeley Formation (type Blakeley stage), Bainbridge Island, Washington, and the Pacific coast Oligocene–Miocene boundary: New Mexico Museum of Natural History and Science Bulletin 44, p. 315-311.

Rau, W. W., 1948, Foraminifera from the Porter shale (Lincoln Formation), Grays Harbor County, Washington: Journal of Paleontology, v. 22, no. 2, p. 152-174.

Rau, W. W., 1958, Stratigraphy and foraminiferal zonation in some of the Tertiary rocks of southwestern Washington: U.S. Geological Survey Oil and Gas Investigations Chart OC-57, 2 sheets. [https://pubs.er.usgs.gov/publication/oc57]

Rau, W. W., 1981, Pacific Northwest Tertiary benthic foraminiferal biostratigraphic framework—An overview. *In* Armentrout, J. M., editor, Pacific Northwest Cenozoic biostratigraphy: Geological Society of America Special Paper 184, p. 67-84.

Rau, W. W.; Johnson, S. Y., 1999, Well stratigraphy and correlations, western Washington and northwestern Oregon: U.S. Geological Survey Geologic Investigations Series Map I-2621, 3 sheets, with 31 p. text. [http://pubs.er.usgs.gov/publication/i2621]

Reuss, A. E., 1863, Die foraminiferen Familie der Lageniden: Sitzungsberichte der Kaiserlichen Akademie der Wissenschafen in Wien, Matematisch-Naturwissenschaftliche Classe, v. 46, p. 308-342.

Riedel, J. L.; Clague, J. J.; Ward, B. C., 2010, Timing and extent of early marine oxygen isotope stage 2 alpine glaciation in Skagit Valley, Washington: Quaternary Research, v. 73, no. 2, p. 313-323.

Rigg, G. B., 1958, Peat resources of Washington: Washington Division of Mines and Geology Bulletin 44, 272 p. [https://docs.google.com/file/d/0B9N-SFELuvxONy1EU3M1cTFMQWc/edit]

Savage, W. Z.; Morrissey, M. M.; Baum, R. L., 2000, Geotechnical properties for landslide-prone Seattle—Area glacial deposits: U.S. Geological Survey Open-File Report 00-228, 5 p. [http://pubs.er.usgs.gov/usgspubs/ofr/ofr00228/]

Savoca, M. E.; Johnson, K. H.; Sumioka, S. S.; Olsen, T. D.; Fasser, E. T.; Huffman, R. L., 2009, Hydrogeologic framework, groundwater movement, and water budget in tributary subbasins and vicinity, lower Skagit River basin, Skagit and Snohomish Counties, Washington: U.S. Geological Survey Scientific Investigations Report 2009-5270, 46 p., 2 plates, scale 1:46,080. [http://pubs.usgs.gov/sir/2009/5270/]

Sherrod, B. L.; Barnett, Elizabeth; Kelsey, H. M., 2005a, Excavation logs of two trenches across a strand of the southern Whidbey Island fault zone near Grace, Washington: U.S. Geological Survey Open-File Report 2005-1013, version 1.0, 1 sheet. [http://pubs.usgs.gov/of/2005/1013/]

Sherrod, B. L.; Blakely, R. J.; Weaver, C. S.; Kelsey, H. M.; Barnett, Elizabeth; Liberty, Lee; Meagher, K. L.; Pape, Kristin, 2008, Finding concealed active faults—Extending the southern Whidbey Island fault across the Puget Lowland, Washington: Journal of Geophysical Research, v. 113. [https://doi.org/10.1029/2007JB005060]

Sherrod, B. L.; Blakely, R. J.; Weaver, Craig; Kelsey, Harvey; Barnett, Elizabeth; Wells, Ray, 2005b, Holocene fault scarps and shallow magnetic anomalies along the southern Whidbey Island fault zone near Woodinville, Washington: U.S. Geological Survey Open-File Report 2005-1136, 35 p. [http://pubs.usgs.gov/of/2005/1136/]

Sherrod, B. L.; Brocher, T. M.; Weaver, C. S.; Bucknam, R. C.; Blakely, R. J.; Kelsey, H. M.; Nelson, A. R.; Haugerud, Ralph, 2004, Holocene fault scarps near Tacoma, Washington, USA: Geology, v. 32, no. 1, p. 9-12.

Sherrod, B. L.; Nelson, A. R.; Kelsey, H. M.; Brocher, T. M.; Blakely, R. J.; Weaver, C. S.; Rountree, N. K.; Rhea, B. S.; Jackson, B. S., 2003, The Catfish Lake scarp, Allyn, Washington—Preliminary field data and implications for earthquake hazards posed by the Tacoma fault: U.S. Geological Survey Open-File Report 03-455, 1 sheet, with 12 p. text. [http://pubs.usgs.gov/of/2003/of03-455/]

Sherrod, B. L.; Vance, J. A.; Leopold, E. B., 2002, Fission track ages of Tertiary bedrock in the hanging wall of the Seattle fault zone [abstract]: Geological Society of America Abstracts with Programs, v. 34, no. 5, p. A-108.

Siddall, M.; Rohling, E. J.; Thompson, W. G.; Waelbroeck, C., 2008, Marine isotope stage 3 sea level fluctuations—Data synthesis and new outlook: Reviews of Geophysics, v. 46, issue 4, p. [https://doi.org/10.1029/2007RG000226]

Simonetti, A.; Heaman, L. M.; Hartlaub, R. P.; Creaser, R. A.; MacHattie, T. G.; Bohm, Christian, 2005, U-Pb zircon dating by laser ablation-MC-ICP-MS using a new multiple ion counting Faraday collector array: Journal of Analytical Atomic Spectrometry, v. 20, no. 8, p. 677-686.

Slaughter, S. L.; Burns, W. J.; Mickelson, K. A.; Jacobacci, K. E.; Biel, Alyssa; Contreras, T. A., 2017, Protocol for landslide inventory mapping from lidar data in Washington State: Washington Geological Survey Bulletin 82, 27 p. text, with 2 accompanying ESRI file geodatabases and 1 Microsoft Excel file. [http://www.dnr.wa.gov/publications/ger_b82_landslide_inventory_mapping_protocol.zip]

Squires, R. L.; Goedert, J. L., 1991, New late Eocene mollusks from localized limestone deposits formed by subduction-related methane seeps, southwestern Washington: Journal of Paleontology, v. 65, no. 3, p. 412-416.

Stach, E.; Mackowsky, M.-Th.; Teichmueller, M.; Taylor, G. H.; Chandra, D.; Teichmueller, R., 1982, Stach's textbook of coal petrology; 3rd revised edition: Gebrueder Borntraeger, 535 p.

Sun, S.; McDonough, W. F., 1989, Chemical and isotopic systematic of oceanic basalts—Implications for mantle composition and processes. *In* Saunders, A. D.; Norry, M. J., editors, Magmatism in the ocean basins: Geological Society of London Special Publication 42, p. 313-345.

Swick, C. A., 1942, Pendulum gravity measurements and isostatic reductions: U.S. Coast and Geodetic Survey Special Publication 232, 82 p. [https://docs.lib.noaa.gov/rescue/cgs_specpubs/QB275U35no2321942.pdf]

Tabor, R. W.; Booth, D. B.; Vance, J. A.; Ford, A. B., 2002, Geologic map of the Sauk River 30- by 60-minute quadrangle, Washington: U.S. Geological Survey Geologic Investigations Series Map I-2592, 2 sheets, scale 1:100,000, with 67 p. text. [http://pubs.er.usgs.gov/usgspubs/i/i2592]

Tabor, R. W.; Frizzell, V. A., Jr.; Booth, D. B.; Waitt, R. B., 2000, Geologic map of the Snoqualmie Pass 30- by 60-minute quadrangle, Washington: U.S. Geological Survey Geologic Investigations Series Map I-2538, 1 sheet, scale 1:100,000, 57 p. text. [http://pubs.usgs.gov/imap/i2538]

Tabor, R. W.; Frizzell, V. A., Jr.; Booth, D. B.; Waitt, R. B.; Whetten, J. T.; Zartman, R. E., 1993, Geologic map of the Skykomish River 30- by 60-minute quadrangle, Washington: U.S. Geological Survey Miscellaneous Investigations Series Map I-1963, 1 sheet, scale 1:100,000, 42 p. text. [http://pubs.usgs.gov/imap/i1963/]

Tegland, N. M., 1933, The fauna of the type Blakeley, upper Oligocene of Washington: University of California Publications, Department of Geological Sciences Bulletin, v. 23, no. 3, p. 81-174.

Telford, W. M.; Geldart, L. P.; Sheriff, R. E., 1990, Applied geophysics; 2nd ed.: Cambridge University Press, 770 p.

ten Brink, U. S.; Molzer, P. C.; Fisher, M. A.; Blakely, R. J.; Bucknam, R. C.; Parsons, T. E.; Crosson, R. S.; Creager, K. C., 2002, Subsurface geometry and evolution of the Seattle fault zone and the Seattle basin, Washington: Seismological Society of America Bulletin, v. 92, no. 5, p. 1737-1753.

Tepper, J. H., 2016, Eocene breakoff and rollback of the Farallon slab—An explanation for the "Challis Event"? [abstract]: Geological Society of America Abstracts with Programs, v. 48, no. 4. [https://gsa.confex.com/gsa/2016CD/webprogram/Paper274512.html]

Thomas, B. E.; Wilkinson, J. M.; Embrey, S. S., 1997, The groundwater system and ground-water quality in western Snohomish County, Washington: U.S. Geological Survey Water-Resources Investigations Report 96-4312, 218 p., 9 plates. [http://pubs.er.usgs.gov/djvu/WRI/wrir_96_4312.djvu]

Thorson, R. M., 1981, Isostatic effects of the last glaciation in the Puget Lowland, Washington: U.S. Geological Survey Open-File Report 81-370, 100 p., 1 plate. [http://pubs.er.usgs.gov/publication/ofr81370]

Thorson, R. M., 1989, Glacio-isostatic response of the Puget Sound area, Washington: Geological Society of America Bulletin, v. 101, no. 9, p. 1163-1174.

Troost, K. G., 1999, The Olympia nonglacial interval in the southcentral Puget Lowland, Washington: University of Washington Master of Science thesis, 123 p. [https://fortress.wa.gov/dnr/geologydata/library/thesis/Troost1999_Olym_nonglacial.pdf]

Troost, K. G., 2006, Spatial predictability of Quaternary deposits in the central Puget Lowland. *In* SAGEEP 2006 Proceedings, Geophysical applications for environmental and engineering hazards—Advances and constraints: Environmental and Engineering Society, p. 260-273.

Troost, K. G., 2016, Chronology, lithology and paleoenvironmental interpretations of the penultimate ice-sheet advance into the Puget Lowland, Washington State: University of Washington Doctor of Philosophy thesis, 239 p.

Troost, K. G.; Booth, D. B., 2008, Geology of Seattle and the Seattle area, Washington. *In* Baum, R. L.; Godt, J. W.; Highland, L. M., editors, Landslides and engineering geology of the Seattle, Washington, area: Geological Society of America Reviews in Engineering Geology XX, p. 1-35.

Troost, K. G.; Booth, D. B.; Mahan, S. A.; Hagstrum, J. T., 2003, Presence of mid-Pleistocene deposits (MIS 4 through 8) in the Tacoma area—Did the Possession glacier make it to Tacoma? [abstract]: Geological Society of America Abstracts with Programs, v. 35, no. 6, p. 215.

Tubbs, D. W., 1974, Landslides in Seattle: Washington Division of Geology and Earth Resources Information Circular 52, 15 p., 1 plate. [http://www.dnr.wa.gov/publications/ger_ic52_landslides_in_seattle.pdf]

USGS Geologic Names Committee, 2010, Divisions of geologic time—Major chronostratigraphic and geochronologic units: U.S. Geological Survey Fact Sheet 2010–3059, 2 p. [https://pubs.usgs.gov/fs/2010/3059/]

Vaccaro, J. J.; Hansen, A. J., Jr.; Jones, M. A., 1998, Hydrogeologic framework of the Puget Sound aquifer system, Washington and British Columbia: U.S. Geological Survey Professional Paper 1424-D, 77 p., 1 plate. [https://pubs.er.usgs.gov/publication/pp1424D]

Van Winkle, K. E. H., 1918, Paleontology of the Oligocene of the Chehalis Valley, Washington: University of Washington Publications in Geology, v. 1, no. 2, p. 69-97, 2 plates.

Vermeesch, Pieter, 2012, On the visualisation of detrital age distributions: Chemical Geology, v. 312, p. 190-194.

Vessell, R. K.; Davies, D. K., 1981 Nonmarine sedimentation in an active fore arc basin. *In* Ethridge, F. G.; Flores, R. M., editors, Recent and ancient nonmarine depositional environments: models for exploration: Society of Economic Paleontologists and Mineralogists Special Publication 31, p. 31-45.

Vine, J. D., 1962, Stratigraphy of Eocene rocks in a part of King County, Washington: Washington Division of Mines and Geology Report of Investigations 21, 20 p. [http://www.dnr.wa.gov/publications/ger_ri21_strat_eocene_king_co.pdf]

Washington Division of Geology and Earth Resources (WADGER), 2010, Surface geology, 1:250,000—GIS data, June 2010: Washington Division of Geology and Earth Resources, 29.75MB. [http://www.dnr.wa.gov/publications/ger_portal_surface_geology_250k.zip]

Washington Division of Geology and Earth Resources (WADGER), 2016, Surface geology, 1:100,000—GIS data, November 2016: Washington Division of Geology and Earth Resources Digital Data Series DS-18, version 3.1, previously released June 2010.

Washington Emergency Management Division (WEMD); Washington Department of Natural Resources; U.S. Geological Survey; Federal Emergency Management Agency, 2012, Understanding earthquake hazards in Washington State—Modeling a magnitude 7.4 earthquake on the southern Whidbey Island fault zone: Washington Division of Geology and Earth Resources, 4 p. [http://www.dnr.wa.gov/publications/ger_seismic_scenario_swif.pdf]

Weaver, C. E., 1912, A preliminary report on the Tertiary paleontology of western Washington: Washington Geological Survey Bulletin 15, 80 p. [http://www.dnr.wa.gov/publications/ger_b15_prelim_rep_teriary_paleo_western_wa.pdf].

Weaver, C. E., 1916, The Tertiary formations of western Washington: Washington Geological Survey Bulletin 13, 327 p., 6 plates. [http://www.dnr.wa.gov/publications/ger_b13_teriary_form_western_wa_2.pdf]

Weaver, C. E., 1937, Tertiary stratigraphy of western Washington and northwestern Oregon: University of Washington Publications in Geology, v. 4, 266 p.

Wells, R. E.; Weaver, C. S.; Blakely, R. J., 1998, Fore-arc migration in Cascadia and its neotectonic significance: Geology, v. 26, no. 8, p. 759-762.

Wells, Ray; Bukry, David; Friedman, Richard; Pyle, Doug; Duncan, Robert; Haeussler, Peter; Wooden, Joe, 2014, Geologic history of Siletzia, a large igneous province in the Oregon and Washington Coast Range—Correlation to the geomagnetic polarity time scale and implications for a long-lived Yellowstone hotspot: Geosphere, v. 10, no. 4, 28 p.

Williams, H. F. L.; Hutchinson, Ian, 2000, Stratigraphic and microfossil evidence for late Holocene tsunamis at Swantown Marsh, Whidbey Island, Washington: Quaternary Research, v. 54, no. 2, p. 218-227.

Yokoyama, Yusuke; Esat, T. M., 2011, Global climate and sea level—Enduring variability and rapid fluctuations over the past 150,000 years: Oceanography, v. 24, no. 2, p. 54-69. [http://tos.org/oceanography/assets/docs/24-2_yokoyama.pdf]

Yount, J. C.; Dembroff, G. R.; Barats, G. M., 1985, Map showing depth to bedrock in the Seattle 30′ by 60′ quadrangle, Washington: U.S. Geological Survey Miscellaneous Field Studies Map MF-1692, 1 sheet, scale 1:100,000. [http://pubs.er.usgs.gov/publication/mf1692]

Yount, J. C.; Gower, H. D., 1991, Bedrock geologic map of the Seattle 30′ by 60′ quadrangle, Washington: U.S. Geological Survey Open-File Report 91-147, 37 p., 4 plates, scale 1:100,000. [http://pubs.er.usgs.gov/publication/ofr91147]

Yount, J. C.; Minard, J. P.; Dembroff, G. R., 1993, Geologic map of surficial deposits in the Seattle 30′ x 60′ quadrangle, Washington: U.S. Geological Survey Open-File Report 93-233, 2 sheets, scale 1:100,000. [http://pubs.er.usgs.gov/publication/ofr93233]

Appendix A. Radiocarbon Age Analyses

Table A1. Radiocarbon data from age sites. ^{14}C yr BP age estimate is in radiocarbon years before 1950, and uncertainty estimates are reported at 1σ (68% confidence). Age in ka is in calendar years before 1950 divided by 1,000 and has a 2σ uncertainty range. An age range is preferred because uncertainties are unequally distributed as a result of the calibration curves used to convert between radiocarbon and calendar years. Uncertainty statements reflect random and lab errors; errors from unrecognized sample characteristics or flawed methodological assumptions (for example, ^{14}C sample contamination from younger carbon flux) are not known. Age is adjusted for measured $^{13}C/^{12}C$ ratio (a 'conventional' age).

^{14}C site ID (geologic unit)		Reference	Material	Method	$^{13}C/^{12}C$ (o/oo)	Age estimate
GD1 (Qc_o)		this study	plant matter	^{14}C AMS	-27.6	17,960 ±60 ^{14}C yr BP (21.885–21.615 ka)
Lab ID[a]	Beta-450756	Delicate plant matter from brown, peaty base of a 1 to 2 cm (0.4–0.8 in.)-thick planar bed of organic-rich silt. Silt bed was within a deposit of stiff to very stiff, blue-gray and brown, interbedded clay, silt, and sand.				
TRS	sec. 22, T27N R6E					
Lat/long. (degrees)	47.810019 -122.014505					
Elev. (ft)	140					
GD2 (Qc_o)		this study	flattened wood fragment	^{14}C AMS	-28.2	19,010 ±60 ^{14}C yr BP (23.015–22.750 ka)
Lab ID[a]	Beta-450757	Flattened wood fragment from 75 cm (30 in.)-thick horizon of laminated to thin bedded, very organic and wood-rich fine sand and silt. Bedding within this horizon consisted of gently undulating very thin laminations to thin planar beds. This brown organic-rich horizon has a conformable contact with the underlying very stiff blue-gray mica-rich, fine sand and silt with planar laminations to thin beds.				
TRS	sec. 33, T28N R6E					
Lat/long. (degrees)	47.872363 -122.0429					
Elev. (ft)	64					
GD3 (Qc_o)		this study	flattened wood fragment	^{14}C AMS	-25.5	22,920 ±90 ^{14}C yr BP (27.410–27.140 ka)
Lab ID[a]	Beta-450755	Flattened wood fragment from brown wood-rich lamination within blue-gray to brown interbedded clay, silt, and very fine sand. Interbeds are planar to gently undulating laminations to thin beds. Sample was collected from a brown organic-rich, 2 cm (0.8 in.)-thick planar bed with abundant wood fragments as much as 5 cm (2 in.) in length.				
TRS	sec. 34, T28N R6E					
Lat/long. (degrees)	47.875474 -122.012813					
Elev. (ft)	85					
GD4 (Qc_o)		this study	flattened wood fragment	^{14}C AMS	-27.4	18,480 ±80 ^{14}C yr BP (22.457–22.245 ka)
Lab ID[a]	Beta-450758.	Flattened wood fragment from 50 cm (20 in.)-thick horizon of brown laminated to thin planar bedded, organic and wood-rich, well-sorted silt. Sampled from a very stiff, brown, 50 cm (20 in.)-thick horizon of organic and wood-rich well-sorted silt. Bedding within this horizon consists of laminations to thin planar beds interbedded with a package of silt to medium sand with bedding that ranges from planar laminae to medium beds to trough cross sets of laminae and thin beds of a low-energy fluvial deposit.				
TRS	sec. 11, T27N R6E					
Lat/long. (degrees)	47.83642 -122.007808					
Elev. (ft)	109					
GD5 (Qcg_o)		this study	flattened wood fragment	^{14}C AMS	-26.7	23,950 ±90 ^{14}C yr BP (28.140–27.810 ka)
Lab ID[a]	Beta -453264	Flattened twig in 50 cm (20 in.)-thick lens of gray, well-sorted, very fine sandy silt with sparse organic debris that pinches out on a 10 m (33 ft) scale. Surrounding deposit composed largely of dark brown, sandy, rounded pebble to cobble gravel that ranges from clast to matrix supported, with weak imbrication and poorly defined 10 cm (4 in.)-scale sets of thin to medium tangential crossbeds with sparse lenses (at a scale similar to sample horizon described above) that are predominantly fine to coarse sand and often crossbedded.				
TRS	sec. 23, T27N R6E					
Lat/long. (degrees)	47.808964 -122.00723					
Elev. (ft)	115					

^{14}C site ID (geologic unit)		Reference	Material	Method	^{13}C/^{12}C (o/oo)	Age estimate
GD6 (Qc_o)		this study	flattened wood fragment	^{14}C AMS	-26.7	17,070 ±60 ^{14}C yr BP (20.715–20.465 ka)
Lab ID[a]	Beta -456155	Flattened wood fragment from alternating laminations to thin beds of blue-gray and dark brown, organic-rich, fine sandy silt to silty fine sand. Faint bedding suggests subparallel, gently wavy laminations with alternating layers of dark brown organic sediment with centimeter-scale flattened wood debris and blue-gray micaceous sediment.				
TRS	sec. 32, T28N R6E					
Lat/long. (degrees)	47.871503 -122.068659					
Elev. (ft)	103					
10-28D (Qpu)		Dragovich and others (2011b)	charred organics	^{14}C AMS	-24	>43,500 ^{14}C yr BP
Lab ID[a]	Beta	"Site 28D is from a 2–4 m-high river cutbank along the Snoqualmie River in the Maltby quadrangle. AMS sample microscopically cleaned of many fine modern rootlets prior to sending to Beta Analytic, Inc. Petrographically, sands at the site contain significant monocrystalline quartz with lesser but significant plagioclase, hornblende, granitic lithic grains, and potassium feldspar; also contain other variable lithic grains; distinct SP composition. The silts and sands at this site are intensely liquefied, folded as well as fractured. We suspect these deposits were deformed by Quaternary offset along the Cherry Creek fault, which projects to near this site and appears to align with fault scarps and lineaments mapped by Sherrod and others (2008) along the southwestern slopes of Lords Hill in the western Maltby 7.5-minute quadrangle. Latitude and longitude are. See photo for site 25A on p. 48." (Dragovich and others, 2011, supplement appendix 1)				
TRS	sec. 23, T27N R6E					
Lat/long. (degrees)	47.805664 -121.003901					
Elev. (ft)	~30					

[a] Beta Analytic.

Appendix B. Luminescence Age Analyses

Table B1. Infrared-stimulated luminescence (IRSL) and optically stimulated luminescence (OSL) results from age site GD2. Analyses were performed on fine-grained feldspar (IRSL) and quartz (OSL). Ages and errors are rounded, and uncertainty estimates are 1σ (68% confidence), as reported by the lab. Uncertainty statements reflect random and lab errors; errors from unrecognized sample characteristics or flawed methodological assumptions (for example, incomplete predepositional resetting of luminescence samples) are not known.

Luminescence site ID (geologic unit)		Water content (%)[a]	K (%)[b]	U (ppm)[b]	Th (ppm)[b]	Total dose rate (Gy/ka)[c]	Equivalent dose (Gy)	Method	Age (ka)
GD7 (Qps)		6 (49)	0.90 ±0.03	0.53 ±0.08	2.48 ±0.14	1.47 ±0.05[d]	98.6 ±3.30[d]	IRSL	67,100 ±3,700[d]
						1.15 ±0.04[e]	71.3 ±3.21[e]	OSL	62,000 ±3,720[e]
Lab ID	IR039B	Sample collected from a pale brownish-tan, dense, well-sorted, medium sand that ranges from fine to coarse. Sand generally appears massive but includes faint, thin to medium planar beds locally truncated along steeply to moderately dipping planes with centimeter-scale separation. Bedding at this site is oriented 318/46.							
TRS	sec. 23, T27N R6E								
Lat/long. (degrees)	47.806341/ -122.004179								
Elev. (ft)	26								
Material	sand								
GD8 (Qcg_o)		9 (32)	0.98 ±0.02	0.92 ±0.13	3.21 ±0.14	1.86 ±0.10[d]	64.7 ±2.58[d]	IRSL	34,890 ±2,790[d]
						1.38 ±0.08[e]	37.8 ±3.03[e]	OSL	27,430 ±2,750[e]
Lab ID	E040C	Sampled from a lens 50 to 60 cm (20–24 in.)-thick, extending laterally for 5+ m (16+ ft) and traceable across the drainage. The lens was brown to gray-brown, medium dense to dense, well-sorted, fine to coarse sand (mode of medium sand) with sparse <2 cm (<0.8 in.) subrounded pebbles and has thin sinusoidal crossbeds (oriented 295/22) defined by subtle grain-size changes and sparse pebbles.							
TRS	sec. 23, T27N R6E								
Lat/long. (degrees)	47.808991/ -122.007133								
Elev. (ft)	95								
Material	sand								
GD9 (Qps)		11 (36)	1.01 ±0.05	0.99 ±0.18	2.92 ±0.29	1.86 ±0.11[d]	98.1 ±3.92[d]	IRSL	53,030 ±4,510[d]
						1.37 ±0.08[e]	71.4 ±2.14[e]	OSL	52,120 ±3,910[e]
Lab ID	E039A	Sample was collected in an orange-brown/tan, well-sorted, medium-dense, medium sand. Sand generally appears massive, but includes some faint, thin to medium planar beds. Some exposures (including the sampled exposure) have steeply to moderately dipping planes that truncate beds with centimeter-scale separation.							
TRS	sec. 26, T27N R6E								
Lat/long. (degrees)	47.804291/ -122.004119								
Elev. (ft)	81								
Material	sand								
GD10 (Qcg_o)		16 (35)	1.20 ±0.06	1.03 ±0.14	4.04 ±0.24	2.23 ±0.09[d]	48.4 ±2.42[d]	IRSL	21,700 ±1,520[d]
						1.65 ±0.06[e]	34.5 ±2.24[e]	OSL	20,890 ±1,775[e]
Lab ID	R351	Deposit is a 2 m (7 ft)-thick, brown, dense, sorted medium sand that ranges from fine to coarse and includes rare subrounded pebbles. The sand has faint, thin planar beds. There are sparse, 6 cm (2 in.)-thick, gently undulating, discontinuous at meter-scale lenses (or blocks?) of stiff silt with minor clay. The upper contact seems gradational, consisting of roughly 1 m (3 ft) of alternating thin planar to gently undulating beds of sand and the overlying silt and clay. The lower contact is also gradational over roughly 15 cm (6 in.), distinguished by an upward loss of pebbles from the underlying gravelly sand.							
TRS	sec. 26, T27N, R6E								
Lat/long. (degrees)	47.802962/ -122.004762								
Elev. (ft)	133								
Material	sand								

Luminescence site ID (geologic unit)		Water content (%)[a]	K (%)[b]	U (ppm)[b]	Th (ppm)[b]	Total dose rate (Gy/ka)[c]	Equivalent dose (Gy)	Method	Age (ka)
GD11 (Qc_o)		18 (36)	1.21 ±0.05	1.46 ±0.21	5.02 ±0.26	2.55 ±0.10[d]	31.1 ±0.93[d]	IRSL	12,150 ±550[d]
						1.81 ±0.07[e]	21.2 ±1.70[e]	OSL	11,720 ±1,230[e]
Lab ID	R353A	Sample was collected in a gray to pale brownish-gray, dense, moderately sorted, fining-upward ~1.5–2 m (5–7 in.)-thick (bottom not seen) sequence ranging from coarse sand to clay. Sandy deposits in this sequence have several centimeters-thick trough crossbed sets composed of planar thin to laminated beds. Thickness of crossbeds decreases with grain size in sandy portions of deposit. The upper ~20 cm (8 in.) of the sequence grades into well-sorted, very stiff to hard, gray to blueish-gray, planar thin beds and laminations of silt and clay. A sharp, planar contact defines the top of this sequence and is overlain by well-sorted, gray, thin planar bedded medium to coarse sand. Age is anomalously young and conflicts with radiocarbon age estimate from the same unit (site GD4).							
TRS	sec. 11, T27N, R6E								
Lat/long. (degrees)	47.836446/ -122.007854								
Elev. (ft)	131								
Material	sand/silt								
GD12 (Qc_o)		3 (29)	1.41 ±0.03	1.19 ±0.15	4.11 ±0.21	2.59 ±0.10[d]	83.4 ±2.50[d]	IRSL	32,220 ±2,090[d]
Lab ID	R353A	Sample was collected in a medium dense, light brownish-gray with localized orange-staining, well-sorted (very clean), medium to coarse sand with sparse fine sand layers and subrounded pebbles (<1 cm [<0.4 in.] diameter). There are 15 to 20 cm (6–8 in)-thick trough (some may be wedge?) crossbeds of thin tangential beds and laminations. Sets of crossbeds pinch out laterally at meter-scale. Average dip of crossbeds is to the northeast.							
TRS	sec. 11, T27N, R6E								
Lat/long. (degrees)	47.836446/ -122.007854								
Elev. (ft)	131								
Material	sand/silt								

[a] Field moisture, with values in parentheses indicating the complete sample saturation percentage. Ages calculated using ~50% of saturation values.

[b] Analyses obtained using high-resolution gamma spectrometry (HPGe detector).

[c] Cosmic doses and attenuation with depth were calculated using the methods of Prescott and Hutton (1994). See text for details. Cosmic doses varied from 0.18–0.12 Gy/ka.

[d] Dose rate and IRSL age for fine-grained 250 to180 microns K-feldspar, post IR230C; fade of 3.4%/decade. Exponential + linear fit used on equivalent dose.

[e] Dose rate and OSL age for fine-grained 250 to 180 micron size quartz. Exponential + linear fit used on single aliquot regeneration equivalent doses.

Appendix C. U-Pb Methods and Results

METHODS

Each sample (~5 kg) was crushed to fine sand-size particles. Heavy minerals were then concentrated using a Wilfley table. Between each sample great care was taken to clean crushing plates and the Wilfley table to reduce the risk of contamination. The zircon concentrate was then passed through a 220 µm sieve and the <220 µm fraction was sorted by magnetic separation using a Frantz LB1 to remove undesirable magnetic minerals. Zircons were then separated by density from the nonmagnetic fraction using di-methylene iodide heavy liquid. From the zircon separate, ~50 to 100 individual zircon grains were hand selected from each sample and mounted in epoxy. The grain mount was polished to expose the grain centers and regions suitable for analysis were identified from cathodoluminescence imaging.

U-Pb zircon data were collected at the Canadian Center for Isotopic Micro-analysis (CCIM) at the University of Alberta using procedures modified from Simonetti and others (2005). The analytical setup consists of a New Wave UP-213 laser ablation system interfaced with a Nu plasma MC-ICPMS equipped with three ion counters for static collection of Pb isotopes. We operated the laser at 4 Hz pulse rate with a beam diameter of 30 µm at a fluence of ~3 J/cm^2. Ablations were conducted in a He atmosphere at a flow rate of 1 L/min through the cell. Output from the cell was joined to the output from a standard Nu plasma desolvating nebulizer (DSN-100). On peak, gas + acid blanks (30s) were measured prior to a set of 10 to 20 analyses. Data were collected statically, consisting of 30 one-second integrations. Before and after each set of analyses, we analyzed zircon reference materials, GJ-1 (Jackson and others, 2004; L. M. Heaman, Univ. of Alberta, unpub. data), and 94–35 (Klepeis and others, 1998) to monitor U-Pb fractionation, reproducibility, and instrument drift. Mass bias for Pb isotopes was corrected by simultaneously measuring $^{205}Tl/^{203}Tl$ from an aspirated 0.5 ppb Tl solution (NIST SRM 997) using an exponential mass fractionation law and assuming a natural $^{205}Tl/^{203}Tl$ of 2.3871.

All data were reduced offline using an Excel©-based spreadsheet. Unknowns were normalized to the zircon reference material GJ-1 and the uncertainties reported are a quadratic combination of: (1) the standard error of the measured isotope ratio (internal precision) and (2) the standard deviation of the standard means (external precision). The external precision of the GJ-1 zircon reference material is estimated at ~1 percent at 2σ for $^{207}Pb/^{206}Pb$ and 2 percent at 2σ for $^{206}Pb/^{238}U$ during these analytical sessions. The secondary standard 94-35 treated as an unknown yielded a lower Tera-Wasserberg concordia intercept age of 55.61 ±0.39 Ma (2σ, MSWD, 0.65, n = 18), in excellent agreement with the 55.5 Ma ID-TIMS age of Klepeis and others (1998). Data points were discarded if it was obvious that an inclusion contributed to analysis, there was an extreme common Pb component, or the grain was in fact not zircon. All plots were generated using the Isoplot software of Ludwig (2003). Given the relatively broad range of zircon ages in samples GD27 and 09-54Z, we analyzed zircon spectra using kernal density estimate plots to assess the populations of zircon ages after Vermeesch (2012). Population peak ages were calculated using the *Age Pick* software of Gehrels (2009).

SAMPLE GD28

We obtained a sample of unit Evp from active workings of the Monroe AAA quarry on Lord Hill (sec. 10, T27N R6E). This quarry exposes complexly juxtaposed tuff, breccia, lava flows, and a 10 m (33 ft)-scale, steeply dipping, porphyritic andesite dike (map sheet). Clasts in breccia show slight variations of phenocryst proportions, though all clasts are petrographically classified as andesite. Multiply oriented and slickensided fault planes cut exposures with centimeter- to meter-scale offset. Petrographically, this sample is a lithic lapilli crystal ash tuff with fragmented and angular pyroclasts. Fine- to medium-grained crystals (40%) consist of euhedral plagioclase, subhedral chloritized equant (originally orthopyroxene?) grains, and unidentified anhedral opaque minerals. Lithic pyroclasts (5%) are predominantly altered porphyritic andesite with minor pumice clasts. These pyroclasts rest in a microlitic matrix of largely acicular plagioclase that appears locally devitrified. Geochemically, this sample plots in the dacite field of the TAS diagram (Fig. 6A).

With a single exception, all crystals analyzed (n = 55, Fig. C1; DS10) fell within the 43 to 46 Ma range, with a weighted mean age of 43.4 ±0.4 Ma. A single crystal was dated to ~115 Ma. We think this may be a xenocryst, perhaps incorporated from country rock during magma ascension. From the pyroclastic textures, we believe that this sample formed subaerially, and thus this date provides timing of extrusive volcanism.

SAMPLE GD27

We collected a sample of crystal vitric coarse (ash) tuff (unit Ovt) exposed in a roadcut along Fales Road (sec. 17, T27N R6E). This tuff conforms to bedding in unit OEn and could serve as a stratigraphic marker bed, though poor exposure of Tertiary bedrock confounded attempts to trace the unit for much distance. Geochemically, this sample is rhyolitic, and petrographic textures indicate minimal sedimentary reworking of igneous material.

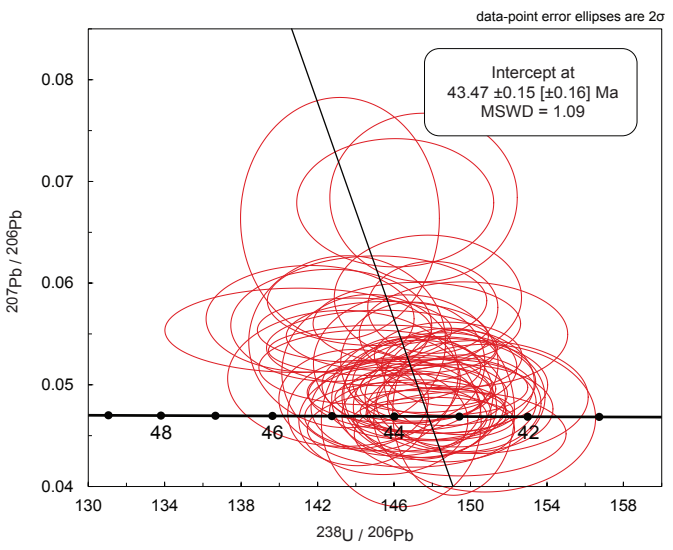

Figure C1. Concordia diagram for site GD28, a lithic lapilli crystal ash tuff of unit Evp. Data ellipses show 2σ analytical uncertainty for each measured zircon.

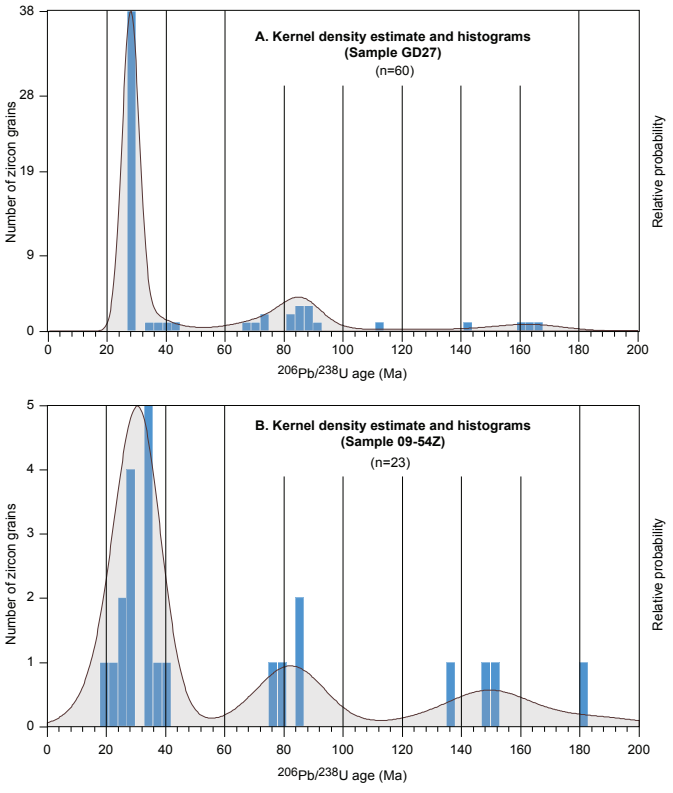

Figure C2. Histograms and kernal density estimate (Vermeesh, 2012) plots comparing samples from sites GD29 (this study) and 09-54Z (Dragovich and others, 2010b; note different vertical scale for crystal count). The youngest statistical age populations have peaks at ~28 Ma in GD27 and ~27 Ma in sample 09-54Z as determined by the Age Pick software of Gehrels (2009). Between the two samples we note similar age peaks in the late Cretaceous and some similar zircon ages in the early Cretaceous and Jurassic. Two grains with Proterozoic and Archean ages were omitted from the plot for sample GD27 due to their effects on the scale of this plot.

U-Pb zircon analyses reveal a spread of ages for this sample, with significant peak ages at 28 Ma (n = 38), 72 Ma (n = 3), 86 Ma (n = 9), and 166 Ma (n = 3) (DS11). The weighted mean age of the youngest peak is 27.8 ±0.4 Ma. We follow the assertion of Dickenson and Gehrels (2009) that this method is the most statistically valid estimate of maximum depositional age.

SAMPLE 09-54Z

Dragovich and others (2010a) sampled a lithic vitric lapilli tuff in the southwest corner of the Maltby quadrangle and reported:

> "We obtained a tentative $^{206}Pb/^{238}U$ zircon age of 16 to 20 Ma (~18 Ma) from sample 09-54Z (appendix 6). The age is considered preliminary because of the analytical uncertainty associated with Pb^{207}/Pb^{206} ratios due to low counts on Pb^{207}, often resulting in negative numbers. This uncertainty is a direct result of the young age of the deposit. The age is derived from the youngest zircon (18 Ma) in the zircon age population and is interpreted to reflect the deposition of this pyroclastic deposit."

Analytical data supplied in Dragovich and others (2010a, appendix 6) show that 23 individual zircons were analyzed, with repeat measurements of some crystals to total 61 analyses. Considering the context of the published zircon data for that sample and the small sample size of individual zircon crystals, we agree with the authors that the interpreted age is subject to scrutiny. We note that only two individual grains are dated to the Miocene, though repeated analyses on grain no. 12 seem to firmly establish the age of that crystal at ~21 Ma. We recognize the possibility of crystal contamination during sample collection or mineral separation. Dickinson and Gehrels (2009) tested methodology for determining maximum depositional ages (MDA) of detrital zircon samples and concluded that the youngest single-grain age method was the least statistically robust of all methods tested and often leads to erroneously young age interpretations. Peak ages using the Age Pick software (Gehrels, 2009) on sample 09-54Z are 27 Ma (n = 5), 34 Ma (n = 6) and 84 Ma (n = 4). (A weighted mean age was not calculated due to insufficient individual grain analyses for the software.) We suggest that the MDA may fall somewhere between the youngest age peak and the ages of younger individual grains. Given this possible older age and the uncertainties reported by the authors, we suggest that a Miocene interpretation for this sample is tenuous, and the sample may instead represent late Oligocene sedimentation. Further analyses are warranted for a statistically viable MDA determination of this sample.

COMPARISON OF SAMPLES GD27 AND 09-54Z

Comparison of detrital zircon kernal density estimate (KDE) spectra from samples from age sites GD27 and 09-54Z (Fig. C2) reveals similar populations of zircon ages. Strong peaks in both samples at 27 and 28 Ma may represent MDA at the beginning of the late Oligocene. Similar peaks exist in both samples in the late Cretaceous (the Age Pick software identifies two populations in sample GD27 that may not be reflected by the small sample

size of 09-54Z). Both samples contain grains dated to the late Jurassic or early Cretaceous, though in insufficient quantities to draw similarities between these populations with any degree of certainty. An Excel©-based Kolmogrov-Smirnoff test (Guynn and Gehrels, 2010) allows statistical analyses between zircon population distributions. When applied to samples GD27 and 09-54Z, this test indicates with 95 percent confidence level that zircon distributions are not statistically different. This finding, in conjunction with the similar calculated peak ages and visual comparisons of KDE spectra, indicate that the two samples had similar sediment sources.

Appendix D. Isostatic Gravity Data Collection Methods

In 2005 and 2014, we collected new gravity stations with two Lacoste & Romberg model G gravity meters within and surrounding the Maltby quadrangle. Combining this new data with older datasets compiled by Finn and others (1991) approximately halved the station spacing of that study resulting in a rather even distribution of ~1.5 km (0.9 mi)-spaced stations. Our base station was a temporary site at the Holiday Inn in Bothell, WA (Fig. D1), with an observed gravity of 980762.92 mGal, established during more than three round-trip base ties to base station Seattle Q on the University of Washington campus. We assumed a linear drift between base ties, resulting in a maximum error of 0.05 mGal for both base and subsequent roving stations. Horizontal and vertical position of each station comes from differentially corrected Trimble GeoXH data, using base stations within 50 km (31 mi) of the quadrangle. To obtain observed gravity values, we applied factory calibration constants for each meter augmented by correction factors obtained from the Mount Hamilton calibration loop east of San Jose, CA (Barnes and others, 1969) and corrected for meter drift and Earth tides. Our data are referenced to the International Gravity Standardization Net of 1971 (Morelli, 1974), and the reference ellipsoid is the Geodetic Reference System of 1967 (International Union of Geodesy and Geophysics, 1971).

Gravity data reduction formulas for the free-air anomaly are standard (for example, Swick, 1942; Telford and others, 1990), and we produced complete Bouguer anomalies by applying Bouguer, Earth curvature, and terrain corrections to 166.7 km (103.6 mi). Terrain corrections are a combination of field-based (to a radius of 68 m [223 ft] using the Hayford system; Plouff, 2000) and computer generated (using 30-m DEM and larger grids; Plouff, 1977) components. To assist in the interpretation of mid- to upper-crustal density contrast, we further reduce the complete Bouguer anomaly to isostatic by applying formulas that adjust for long-wavelength variations, such as those due to the existence of a crustal root and (or) upper mantle density contrasts. We use an Airy-Heiskanen model (Heiskanen and Vening-Meinesz, 1958) through the computer program ISOCOMP (Jachens and Roberts, 1981) to produce the isostatic correction, assuming a 25 km (15.5 mi)-thick crust at sea level and a crust–mantle density contrast of 400 kg/m^3. For all parts of the data reduction process, we used the standard reduction density of 2,670 kg/m^3.

The computed anomalies for the newer data are accurate to within 0.21 mGal on average, with the error arising predominantly from error in vertical position and terrain correction. Our elevations are accurate to a maximum of ~1.3 m (4.3 ft) and on average 0.3 m (0.98 ft), resulting in a maximum error of 0.26 mGal, but 0.06 mGal on average. Terrain correction error is generally 5 to 10 percent of the terrain correction; therefore the average uncertainty in terrain correction is 0.08 to 0.15 mGal, with average error in mountainous regions of the Cascades foothills of 0.12 to 0.23 mGal and in the flatter regions of 0.05 to 0.1 mGal. Error due to contrast between our newer data and that of Finn and others (1991) is 0.4 mGal on average within and adjacent to the Maltby quadrangle, from an analysis of reoccupied stations. Therefore, we consider anomalies of 0.5 to 1 mGal and greater to be interpretable within the region.

We created gridded surfaces of the isostatic gravity anomaly using the minimum curvature algorithm in the GIS software package Oasis Montaj. To quantify our interpretation of map-view gravity anomalies, we computed the maximum horizontal gradient and utilized curvature analysis (Phillips and others, 2007; we refer to these as 'max-spots') to pinpoint strong and linear boundaries between rocks having significant density difference in the subsurface.

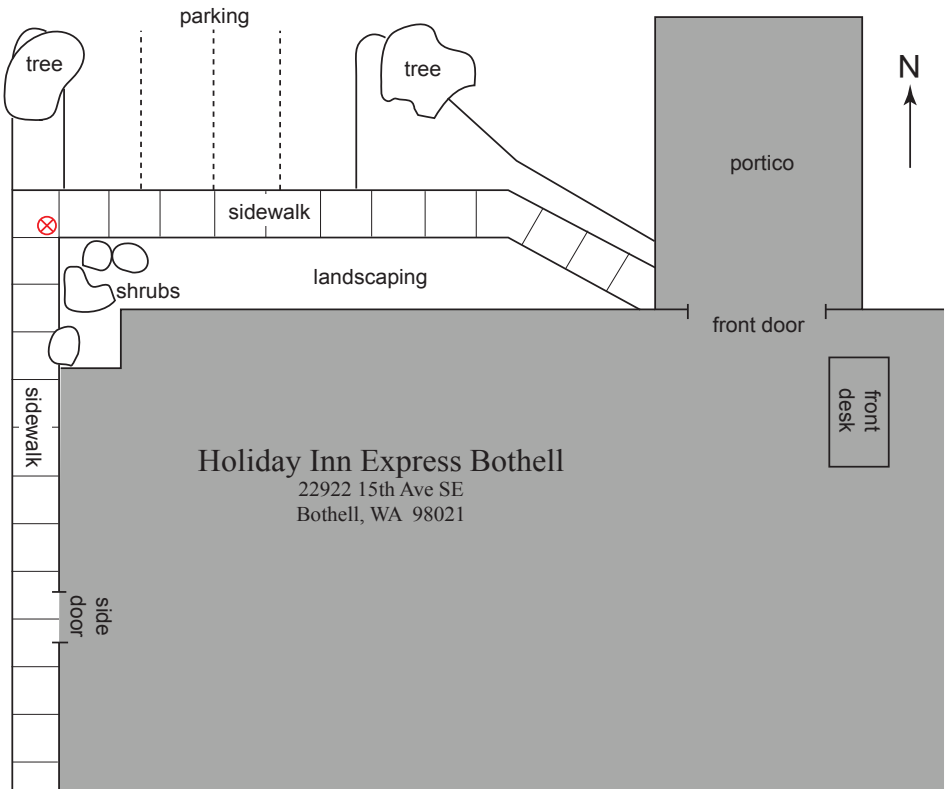

Figure D1. Schematic map showing the precise location of the temporary base station used to calibrate gravimeters during data collection. The red circle with an 'x' indicates the position of the gravimeter base plate on the sidewalk. The base plate was placed 2 in. from each edge of the edge of the corner concrete square and measurements were read facing the shrubs. The observed gravity value is 980762.92 mGal.

Appendix E. Seismicity in and near the Maltby Quadrangle

METHODS

We present earthquake epicenters and focal mechanisms reported by the Pacific Northwest Seismic Network (PNSN, downloaded on May 18, 2017) around the Maltby quadrangle to provide a sense of fault movements at depth. The focal mechanisms are plotted using the RFOC software package of Lees (1999, 2007, and 2008)(Fig. E1; DS9). The selected area (Fig. E1) contains 51 epicenters with focal mechanisms. We selected hypocenters at depths less than 25 km (16 mi) that lie above the subducting slab. Figure D1 excludes 449 earthquake epicenters that did not have calculated focal mechanisms.

OBSERVATIONS

Seismicity near the Maltby quadrangle does not appear to conform to any strong linear or clustered geographic trends. Most events (86%) with calculated focal mechanisms are at depths of more than 10 km (6 mi), and nearly half (49%) are at depths greater than 20 km (12 mi). Focal mechanism solutions show a range of possible failure planes and kinematic styles. We observed that the majority of focal mechanism solutions (~63%) indicate reverse or oblique-reverse sense of faulting. In the quadrangle, these solutions often have east-west-striking failure planes.

INTERPRETATIONS

Heterogeneous geographic distribution and orientation of epicenters and failure planes observed in focal mechanisms support structural complexity within the map area. There is no clear pattern of failure-plane orientations, suggesting that seismicity in the quadrangle reflects a complex interaction of structures and the multi-strand nature of the major fault systems. We believe that the higher proportion of reverse solutions reflects the overall compressional tectonic regime (with some solutions indicating north-south contractional strain), similar to conceptual models proposed to explain the complex interaction of the SWIF, RMFZ, and MF by Dragovich and others (2014). We suggest that the relatively deep hypocenters for seismic events cannot be definitively tied to specific fault strands, due to poor constraints of dipping fault planes within the quadrangle and the uncertainty of the deeper hypocenter locations.

Several of the shallowest events with calculated focal mechanisms are spatially associated with the geophysical traces of the vertically dipping Snoqualmie Valley faults and the RMFZ (southeast of the Maltby quadrangle). However, the focal mechanism solutions do not reflect a clear pattern of fault orientation or rupture kinematics, and we hesitate to ascribe these events to any single structure.

Figure E1. *(facing page)* Earthquake epicenters and focal mechanisms for selected earthquakes in the Maltby quadrangle and surrounding area. Southern Whidbey Island fault (SWIF) strands are simplified from Sherrod and others (2008); Rattlesnake Mountain fault zone (RMFZ) strands are simplified from Dragovich and others (2010b, 2011a). The Monroe fault (MF), anticline (MA), and syncline (MS) are modified from Dragovich and others (2015, fig. 1) with insights from this study. Geophysical lineaments and the Fiddlers Bluff anticline (FBA) are from this study. Numbered focal mechanisms correspond to solutions given in the Data Supplement (DS9).

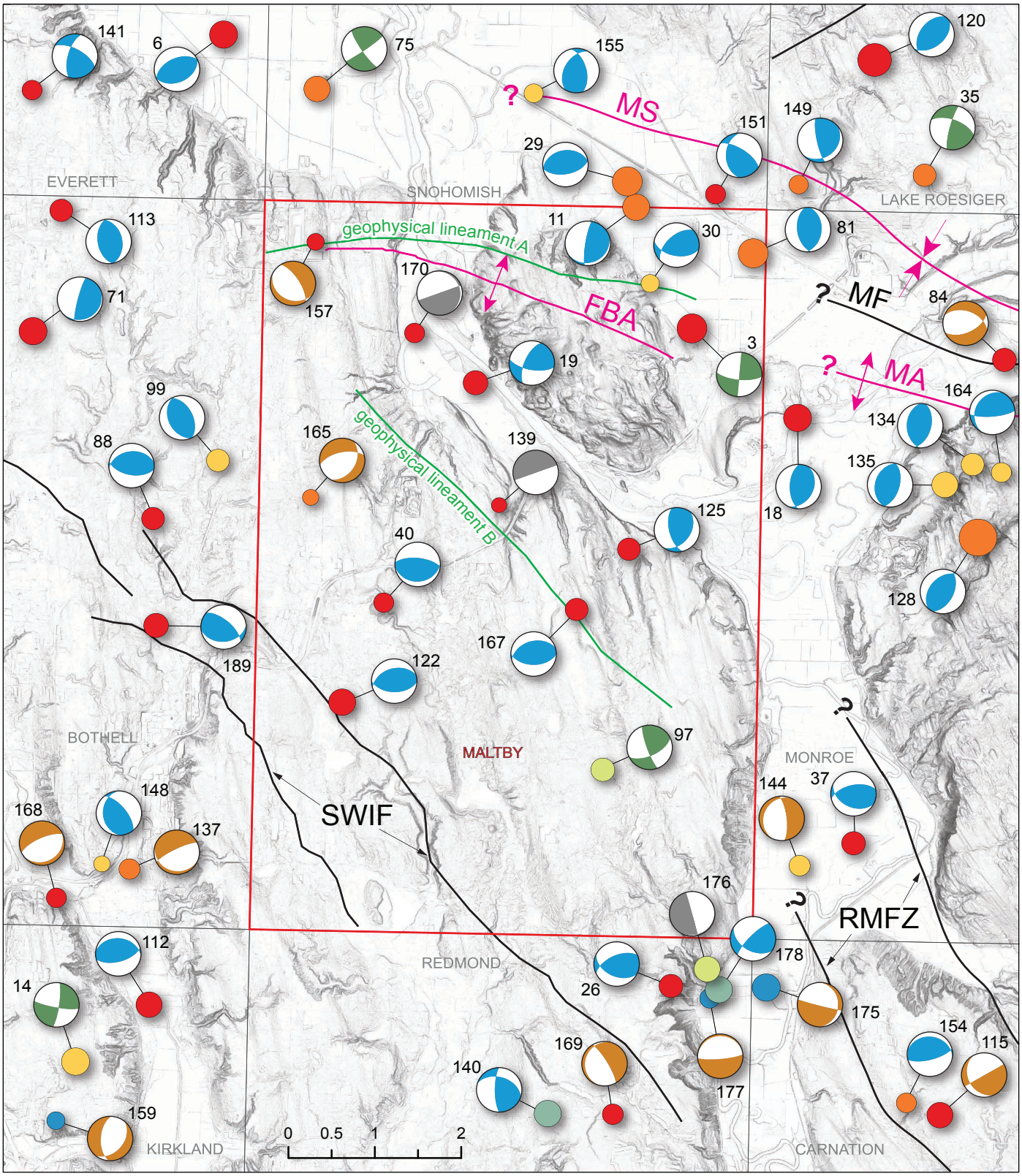

Earthquake depth (km)
- 1 to 2.5
- 2.6 to 5.0
- 5.1 to 10.0
- 10.1 to 15.0
- 15.1 to 20.0
- 20.1 to 24.9

Earthquake magnitude
1 — 3.3

Focal mechanism
88 colored by fault type
- Normal
- Reverse
- Strike slip
- Indeterminate

- Fault
- Anticline
- Syncline
- Geophysical lineament
- Maltby quadrangle